Measurement of the B_s lifetime

ACADEMISCH PROEFSCHRIFT

ter verkrijging van de graad van doctor
aan de Universiteit van Amsterdam
op gezag van de Rector Magnificus
Prof. Dr. P.W.M. de Meijer
ten overstaan van een door het college van dekanen
ingestelde commissie in het openbaar te verdedigen
in de Aula der Universiteit
op maandag 7 oktober 1996 te 10.30 uur

door

Ivar Siccama
geboren te Amsterdam

Promotor: *Prof. Dr. J.J. Engelen*
Co-promotor: *Dr. W. Ruckstuhl*

The work described in this thesis is part of the research program of 'het Nationaal Instituut voor Kernfysica en Hoge-Energie Fysica (NIKHEF)' in Amsterdam.
The author was financially supported by 'de Stichting voor Fundamenteel Onderzoek der Materie (FOM)'.

Cover design: Alan Tam, Text Perfection,
http://www.textperf.co.nz,
Wellington, New Zealand.

Contents

Introduction **3**

1 Theory **5**

1.1 Electroweak interactions of quarks and leptons 5
1.2 Strong interactions 6
1.3 B meson production from Z decays 7
1.4 B meson decay 9
1.5 B^0-$\overline{B^0}$ oscillations 13

2 LEP and DELPHI **17**

2.1 The LEP collider 17
2.2 The DELPHI detector 17
2.2.1 The tracking detectors 20
2.2.2 The calorimeters 23
2.2.3 The barrel RICH 23
2.3 Particle identification 26
2.3.1 Hadron identification 26
2.3.2 Lepton identification 27
2.4 Data analysis 29

3 Reconstruction of B_s decays **31**

3.1 Full B_s reconstruction 31
3.2 Partial B_s reconstruction 31
3.3 Background sources 33
3.4 Event selection 35
3.4.1 Track selection 36
3.4.2 D_s meson reconstruction 37
3.4.3 B_s meson reconstruction 39
3.4.4 Kaon identification 41
3.5 Time-dependence of the selection criteria 42
3.6 The selected event sample 42
3.7 Event sample composition 44

4 The B_s proper decay time measurement **51**
4.1 Momentum reconstruction 51
4.1.1 Momentum reconstruction for semi-leptonic B_s decays 51
4.1.2 Momentum reconstruction for hadronic B_s decays 53
4.1.3 The error on the reconstructed momentum 53
4.2 Flight distance reconstruction 55
4.2.1 Reconstruction of the interaction point 56
4.2.2 Reconstruction of the B_s decay vertex 57
4.3 Proper time reconstruction 59
4.4 D_s decay time reconstruction 62

5 Measurement of the average B_s decay time **65**
5.1 The decay time spectra 65
5.2 Result of the maximum likelihood fit 68
5.3 Study of the systematic error 70
5.4 Measurement of the D_s lifetime 73
5.5 Conclusions 74

A The neutral B meson system **75**
A.1 Time evolution 75
A.2 CP violation 77

B B_s branching fractions **81**

Bibliography **85**

Summary **89**

Samenvatting **91**

Acknowledgements **95**

Introduction

The Large Electron Positron collider located at CERN, the European Laboratory for Particle Physics at the French-Swiss border in Geneva, produces e^+e^- collisions at high energy and with high luminosity. Since the start of its operation in 1989, the LEP collider has been operated at the energy of the Z resonance until 1995. Currently, the acceleration power is being increased to allow the first production of W pairs in 1996. At the energy of the Z resonance the LEP collider has provided, among other things, an excellent laboratory for the study of beauty hadrons, which are produced abundantly through $\mathrm{Z} \to b\bar{b}$ decays.

The produced beauty hadrons are mostly mesons, that are formed by the combination of a heavy $\bar{b}$ quark with one lighter d, u or s quark, forming respectively $\mathrm{B_d}$, $\mathrm{B_u}$ or $\mathrm{B_s}$ mesons. The analysis presented in this thesis concentrates on the study of $\mathrm{B_s}$ mesons. Their production is suppressed relative to the $\mathrm{B_d}$ and $\mathrm{B_u}$ meson species, due to the s quark mass.

The analysis presented in this thesis uses data collected by the DELPHI detector between 1991 and 1994, which includes nearly all DELPHI data collected at the Z resonance. Since beauty hadrons are produced at large momenta in Z decays, they typically travel a distance of a few mm from the interaction point, before decaying inside the beampipe. Around the beampipe, their decay products are detected, which allows a reconstruction of the flight distance and momentum of the beauty hadrons. In this way the B meson proper decay times are reconstructed. The different species of B mesons are discriminated by the identification of their decay products, aided by the reconstruction of intermediate resonances. The DELPHI detector has been especially designed to provide optimal identification of pions and kaons.

By measuring the average decay times of the individual B hadron species the validity of the spectator model can be tested. This model predicts that the average decay times of all species of beauty hadrons are approximately equal. In particular the $\mathrm{B_s}$ lifetime is predicted to be equal to the $\mathrm{B_d}$ lifetime within 1 %. The reconstruction of $\mathrm{B_s}$ meson decay times is also an essential tool for the measurement of $\mathrm{B_s}$-$\overline{\mathrm{B}}_\mathrm{s}$ oscillations. The oscillation frequency x_s has not been measured yet, and is expected to be much higher than in the $\mathrm{B_d}$ system, where it has been measured. The measurement of the $\mathrm{B_s}$ lifetime and the oscillation frequency is further complicated by the suppressed production of $\mathrm{B_s}$ mesons compared to the other B meson species. These measurements therefore require a tagged sample of $\mathrm{B_s}$ decays that is accurately reconstructed, leading to a high resolution on the proper decay time.

In the analysis presented here such a sample of tagged $\mathrm{B_s}$ decays is collected, through the complete reconstruction of a D_s meson, in combination with a high momentum particle of opposite charge. Previously used methods mostly required this particle to be an identified lepton. Our analysis aims at obtaining an additional sample of high purity by including also hadrons as the additional particle. The proper decay time is accurately reconstructed, and is used for a measurement of the average B_s decay time. The selected event sample will also be used in the near future for a study of the B_s oscillation frequency.

The structure of this thesis is as follows. First, the motivation for a measurement of the B_s lifetime and its oscillation frequency are discussed. Chapter 2 then briefly describes the LEP collider and the DELPHI detector. The selection of B_s meson decays is explained in chapter 3, including a description of background and the event sample composition. Chapter 4 discusses the algorithm that is used to reconstruct the proper decay time for each B_s candidate, and finally chapter 5 presents the measurement of the average decay time.

Chapter 1

Theory

This chapter briefly introduces the electroweak and strong interactions as described by the Standard Model, and then discusses the production and decay of B mesons at the Z resonance. In this thesis we will concentrate on the B_s meson, a particle that is composed of a heavy $\bar{b}$ quark and an s quark, bound by the strong interaction. Its decay proceeds through the weak interaction. The main topic of this chapter is the average B_s meson decay time and the chapter ends with a short discussion of the B_s-$\overline{B}_s$ oscillation frequency.

1.1 Electroweak interactions of quarks and leptons

There are three families of fundamental fermions (particles of half integer spin), each containing an up-type quark, a down-type quark, a charged lepton and a neutrino, as listed in table 1.1. Each fermion is characterized by a specific *flavor*. Forces between the fermions are mediated by the exchange of bosons (particles of integer spin). In electromagnetic interactions and weak interactions these bosons are the photon and massive Z or $W^{\pm}$ bosons, respectively [1].

Here, we concentrate our discussion on the *charged current*, which is mediated by the exchange of $W^{\pm}$ bosons. The well-known parity violation in weak interactions is

fermions	family			Q/e
	1	2	3	
quarks	u	c	t	2/3
	d	s	b	-1/3
leptons	e	μ	τ	-1
	ν_e	ν_μ	ν_τ	0
gauge bosons		γ		0
		Z		0
		$W^{\pm}$		±1

Table 1.1: *The three known families of elementary fermions, the electroweak gauge bosons that act as their force carriers, and their respective charges.*

expressed in the Standard Model by the exclusive coupling of the $W^{\pm}$ boson to left-handed fermions (or right-handed anti-fermions). The hadronic current between the charge $\frac{2}{3}$ quarks (u, c and t) and the charge $-\frac{1}{3}$ quarks (d, s and b) takes the following form:

$$J_{\mu}^{CC} = (\bar{u}, \bar{c}, \bar{t})\, \gamma_{\mu}(1-\gamma_5) \mathrm{V}_{\mathrm{CKM}} \begin{pmatrix} d \\ s \\ b \end{pmatrix} \tag{1.1}$$

where γ_{μ} are the Dirac matrices and $(1-\gamma_5)$ is the projection operator to left-handed states. $\mathrm{V}_{\mathrm{CKM}}$ is the Cabibbo-Kobayashi-Maskawa matrix, which is a 3×3 unitary matrix in flavor space [2,3]:

$$\mathrm{V}_{\mathrm{CKM}} = \begin{pmatrix} V_{ud} & V_{us} & V_{ub} \\ V_{cd} & V_{cs} & V_{cb} \\ V_{td} & V_{ts} & V_{tb} \end{pmatrix} \tag{1.2}$$

The elements express the coupling strengths between charge $\frac{2}{3}$ quarks and charge $-\frac{1}{3}$ quarks. In its most general form, the CKM matrix contains 9 complex numbers, and thus 18 parameters. The condition of unitarity reduces this number to nine, three angles and six phases. Since five of these phases are arbitrary and unobservable, the matrix contains four independent parameters.

Interactions between quarks from the same family are strongly favored, while interactions between quarks from different families are referred to as *Cabibbo suppressed*. Elements along the diagonal of the matrix are therefore almost equal to one and off-diagonal elements are small, while elements furthest away from the diagonal are smallest. A representation of the CKM matrix in which this structure is clearly visible, is the Wolfenstein parameterization [4]. In this representation the matrix is expanded in powers of a parameter $\lambda \simeq 0.22$. To leading order the CKM matrix can be written as:

$$\mathrm{V}_{\mathrm{CKM}} = \begin{pmatrix} 1-\frac{1}{2}\lambda^2 & \lambda & A\lambda^3(\rho - i\eta) \\ -\lambda & 1-\frac{1}{2}\lambda^2 & A\lambda^2 \\ A\lambda^3(1-\rho-i\eta) & -A\lambda^2 & 1 \end{pmatrix} \tag{1.3}$$

The parameter A is currently measured to be 0.86 ± 0.10; the parameters ρ and η occur only in terms with λ^3 and are still largely unknown [5].

The b quark ("beauty" or "bottom" quark) is the down-type quark of the third family and only decays to fermions from lower families, e.g. $b \to c$. Since these decays are Cabibbo suppressed, they are intrinsically sensitive to higher order effects.

It is interesting to note that the mixing between different families as observed for quarks, can not occur for leptons, if the neutrinos are assumed to be massless.

1.2 Strong interactions

Only the quarks take part in the strong interactions. They are confined to bound states, called hadrons, which are composed of a quark-antiquark pair (mesons), or a combination of three quarks (baryons):

$$\begin{array}{lcl} \text{mesons} & \sim & q\bar{q} \\ \text{baryons} & \sim & qqq. \end{array}$$

Mesons and baryons are classified according to their quark flavor composition and the spin and angular momentum states of the quarks. In this way, the large hadronic spectrum of the Particle Data Tables [6] is successfully reproduced. Relevant for this thesis are the ground states of the beauty mesons:

$$\begin{array}{ccc} \mathrm{B_u^+} & \mathrm{B_d^0} & \mathrm{B_s^0} \\ (\bar{b}u) & (\bar{b}d) & (\bar{b}s) \end{array}$$

In the theory of strong interactions, Quantum Chromo Dynamics (QCD), the quarks carry a *color* charge, that is independent of the quark flavor. There are three different colors, which allows for the composition of hadrons as colorless objects.

In the theory of QCD, the strong interactions are mediated by gauge bosons called gluons. There are eight such bosons, associated to the SU(3) symmetry group of color. QCD is a non-abelian gauge theory which has the property that the gluons themselves carry a color charge, and therefore interact with each other. The strong interactions lead to a small effective coupling at short distances (large momenta). The quarks are therefore asymptotically free at short distances.

The aspects of asypmtotic freedom and confinement of quarks are described by a 'running' coupling constant that increases with the distance. Neglecting the dependence on quark masses, the QCD running coupling to first order is:

$$\alpha_s(Q^2) = \frac{12\pi}{(33 - 2N_f)\log(Q^2/\Lambda^2_{QCD})} \tag{1.4}$$

where Q is the transfer momentum in an interaction and N_f is the number of quark flavors. QCD has been very successful in the calculation of interactions at high energies. However, below a characteristic energy scale $\Lambda_{QCD} \approx 200$ MeV, calculations in QCD diverge. This region of non–perturbative QCD still leaves many questions open. The description of hadron decays belongs to this difficult region. Analytic calculations in this region may be possible in special cases, such as for hadrons containing quarks with a mass $\gg \Lambda_{QCD}$, where Heavy Quark Effective Theory can be used [7], as will be discussed later.

1.3 B meson production from Z decays

LEP provides an abundant production of heavy flavored hadrons containing a b quark, through decays of the Z into $b\bar{b}$ pairs. The two quarks move with a momentum of 45 GeV in opposite directions ("back to back"). They radiate gluons, that in turn radiate themselves, as shown in figure 1.1. Such high energy processes can be calculated quite accurately in perturbative QCD. During this first stage of high energy radiation, the average energy per quark/gluon decreases. At lower energies, the confinement of quarks and gluons into color singlets leads to the formation of hadrons. This stage is called the fragmentation process, which is indicated by the oval box in figure 1.1. It

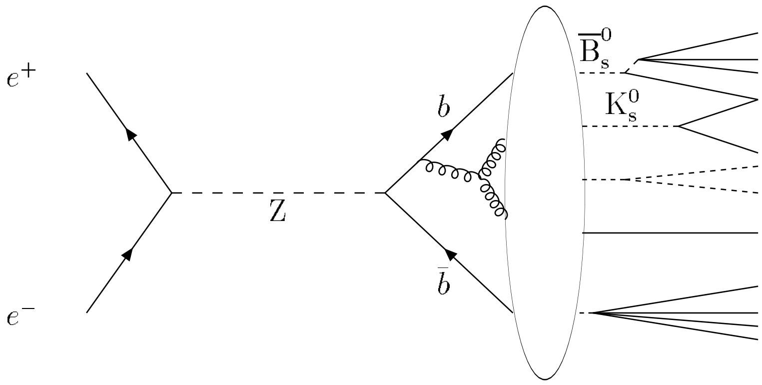

Figure 1.1: *Hadronic decay of the Z. This example shows an $e^+e^- \to \mathrm{Z} \to b\bar{b}$ transition.*

cannot be calculated exactly since low energy QCD processes are involved. Instead it is parametrized in multi–parameter models.

An example of such a model is the string fragmentation model, where the quarks are connected by string-like tubes made of the gluon field. As the distance between the quark and anti-quark becomes larger, the string is stretched and eventually breaks, producing a new quark anti-quark pair. This process repeats itself until all the available energy has been used, and all quarks and gluons have hadronized into colorless particles.

The quarks pass their energy and momentum to the final state hadrons. In the models, the energy E and longitudinal momentum p_L of the final state hadron are distributed according to a probability fragmentation function. Here, p_L is the momentum component of the final state hadron parallel to the direction of the original quark. The fraction $z = (E + p_L)_{hadron} \,/\, (E + p)_{quark}$, indicates the relative momentum of the original quark that is passed to the final state hadron. For light quarks the LUND fragmentation function is used:

$$f(z) \sim \frac{(1-z)^a}{z} \exp\left(-b\frac{m_T^2}{z}\right) \tag{1.5}$$

while for heavy quarks the Peterson fragmentation function is a better approximation:

$$f(z) \sim \frac{1}{z}\left(1 - \frac{1}{z} - \frac{\epsilon_q}{(1-z)}\right)^{-2} \tag{1.6}$$

The standard parameter values are: $a = 0.5$, $b = 0.9\ \mathrm{GeV}^{-2}$, $m_T^2 = 0.25\ \mathrm{GeV}^2$, $\epsilon_c \simeq 0.08$ and $\epsilon_b \simeq 0.006$. In hadronic Z decays, the "back-to-back" direction of the original quarks is experimentally observed in the form of two relatively narrow jets of hadrons, on opposite sides of the detector.

In this thesis, we are particularly interested in the production of $\mathrm{B_s}$ mesons. A $\mathrm{B_s}$ meson is formed when an original b quark from a Z decay combines with an $\bar{s}$ quark, created in the fragmentation process. The probability for a $q\bar{q}$ pair to be generated in this process depends strongly on the mass of the quark. Due to the large s quark mass,

(a) muon decay (b) b quark decay

Figure 1.2: *Analogy between muon decay and a "free" b quark decay.*

the production of the B_s mesons is therefore suppressed compared to the production of the lighter B_d and B_u mesons in an approximate ratio:

$$\begin{array}{ccccc} B_u & : & B_d & : & B_s \\ 3 & : & 3 & : & 1 \end{array} \tag{1.7}$$

About 92 % of the b quarks hadronize into beauty mesons[1] (the remaining 8 % hadronize into beauty baryons, mainly Λ_b baryons). Baryon production is suppressed since it requires the generation of a di-quark pair. In summary, 13 % of the b quarks hadronize into B_s mesons. It must be noted that the values of these production fractions are not well measured and that the predictions depend heavily on the fragmentation model that is used.

1.4 B meson decay

A beauty meson consists of a heavy b quark bound to a light quark by strong interactions. Its decay proceeds through the weak interaction. In the limit of an infinite mass m_b the presence of the light quark can be neglected and the decay width can be fully described by the decay of a "free" b quark. This so-called *spectator model* results in equal lifetimes for all B hadron species. The light quark plays only a spectator role and is assumed not to influence the decay. A free b quark decays analogous to a muon, as illustrated in figure 1.2, where the decay width is well known:

$$\Gamma(\mu \to e\nu_e\bar{\nu}_\mu) = \frac{G_F^2 m_\mu^5}{192\pi^3} \sim 5 \times 10^5 \ s^{-1} \tag{1.8}$$

Transitions of $b \to c$W are strongly Cabibbo favored compared to $b \to u$W. There is a large phase space available in b decays, which allows the virtual W boson to decay into a large range of final states, ranging from decays to a light $l\bar{\nu}_l$ pair to the heavy $c\bar{s}$ state. In the spectator model the decay width of $b \to c$W is obtained by summing over all final state fermion pairs:

$$\Gamma(b \to c\mathrm{W}^-) = \frac{G_F^2 m_b^5}{192\pi^3} f_{bc} \mid V_{cb} \mid^2 \sum \left(3 \mid V_{q_i q_j} \mid^2 \cdot f_{q_i q_j} + f_{l\nu_l}\right) \tag{1.9}$$

[1] Because the c quark mass is even larger than the s quark mass, the production of B_c mesons is extremely rare, and has sofar not been observed.

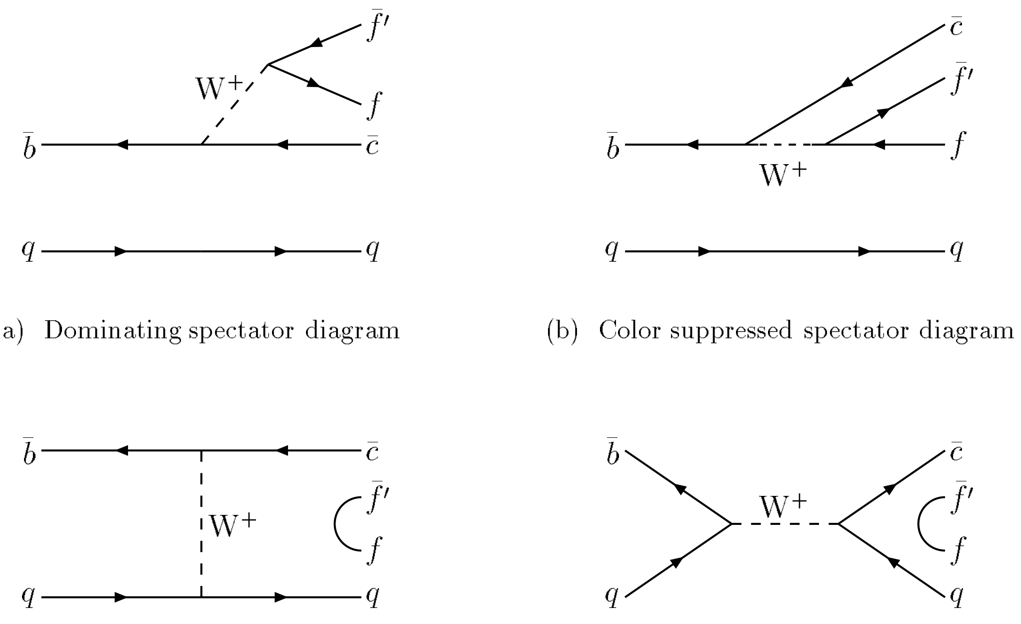

(a) Dominating spectator diagram

(b) Color suppressed spectator diagram

(c) W exchange diagram

(d) W annihilation diagram

Figure 1.3: *Examples of B meson decay diagrams.*

The factors f are phase space correction factors, and a factor 3 reflects the color freedom in decays to quark pairs. Since the b quark mass is large (~ 4.5 GeV/c^2 [6]) compared to the scale Λ_{QCD} of the strong interactions, the spectator model is expected to hold well in B meson decays.

Measurements of the average b lifetime are thus used to determine the matrix element V_{cb}. The first decay time measurements showed that B hadrons are long-lived, of the order of one picosecond. This was the first evidence for the small coupling between the third and second family: $V_{cb} \sim 0.04$. To extract a more precise value of V_{cb} more detailed measurements and more refined calculations are needed.

Significant progress has been made over the last years in the calculation of theoretical corrections to the spectator model. Detailed overviews of the current theoretical and experimental status in the study of B decays can be found in references [8] and [9]. The improved models aim at predicting the lifetime of each individual B hadron species. Lifetime measurements of the specific B hadrons: B_u, B_d, B_s mesons and B baryons are therefore needed to test the predictions of these models and to obtain a more precise value of V_{cb}.

The simple formula (1.9) is improved by including the decay diagrams shown in figure 1.3. There are two possible spectator decay diagrams. In the first diagram the c quark combines with the spectator quark into a D meson. This is the dominating diagram. In the second spectator diagram the fermion pair is "shared" between the final state c and the spectator quark. This diagram is color–suppressed by a factor 9, because the spectator quark has a definite color charge, and the final state must form color singlets.

Other possible decay diagrams proceed through W exchange or W annihilation. Note that the W exchange diagram contributes only for neutral B meson decays and that the W annihilation diagram contributes only for charged B meson decays. The decay rate contribution from these diagrams depends on the probability that the wave functions of the quarks in the meson overlap within the time necessary for the exchange of a virtual W. This probability requires the calculation of the hadronic matrix element:

$$< 0 \mid \bar{b}(0)\gamma_\mu\gamma_5 q(0) \mid \mathrm{B} >= i p_\mu f_B \tag{1.10}$$

where p_μ is the four-momentum of the B meson. Thus, the decay constant f_B is defined, which is proportional to $m_b^{-1/2}$ for $m_b \to \infty$ [1]. The decay width becomes:

$$\Gamma_{ann} \propto G^2 m_b^3 f_B^2 \propto G^2 m_b^2 \tag{1.11}$$

The strong dependence on the fifth power of m_b for the spectator diagram in equation (1.9), compared to the dependence on m_b^2 for the exchange and annihilation decays, ensures the dominance of the spectator diagram in B meson decays. In addition, the W exchange and annihilation diagrams are suppressed by the condition of helicity conservation.

In addition also interference effects between the different diagrams can cause lifetime differences. To illustrate this, figure 1.4 shows a color allowed and a color suppressed spectator decay that both contribute to the decay $\mathrm{B}^+ \to \overline{\mathrm{D}^0}\pi^+$. This interference has a destructive effect which would lead to a predicted charged B meson lifetime that is higher than that of a neutral B meson [10].

Sofar, the effect of strong interactions between the quarks has not been considered. In the semi-leptonic decay of a free b quark, as illustrated in figure 1.2(b), there can be interactions between the initial state b quark and the final state c quark. In a hadronic b quark decay there can even be interactions between any of the four quarks involved. These effects are common to all species of B hadrons and thus largely cancel in the calculation of lifetime ratios between the different B hadrons. We will therefore concentrate on the calculation of *relative* lifetime differences between the B hadron species.

Strong interactions involving the spectator quark contribute to these lifetime differences. Fortunately, an effective theory has recently been developed that allows the calculation of many of these corrections from non-perturbative effects, taking also the weak annihilation and interference effects into account. This theory has largely replaced previously existing phenomenological models. This Heavy Quark Effective Theory (HQET) is valid in the limit of $m_Q \gg \Lambda_{QCD} \sim 200$ MeV, where the four-momenta of the light quarks and of the gluons are small compared to the mass of the heavy quark [7]. In this limit, the exact mass of the heavy quark becomes irrelevant. This is analogous to the fact that different isotopes of the same elements have the same chemistry, since they have the same nuclear charge. In this case nuclear charge is replaced by a static source of color from the heavy quark. HQET uses this heavy mass limit to calculate matrix elements such as $B \to D$, which are important in the determination of the V_{cb} and V_{ub} matrix elements. The first correction to the decay of a free b quark (the effective heavy quark limit) is of the order of $(\Lambda_{QCD}/m_b)^2$.

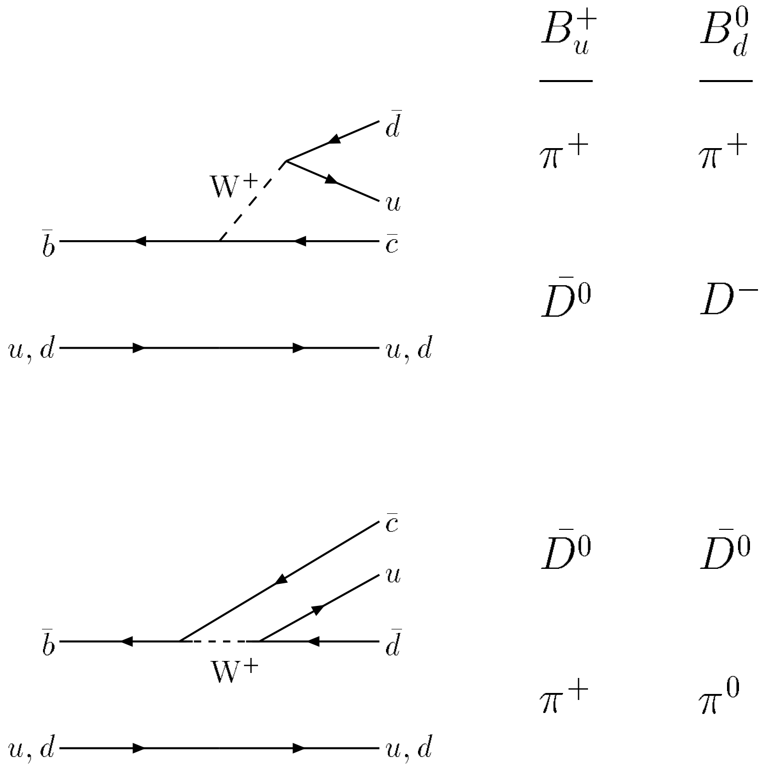

Figure 1.4: *Two decay diagrams which lead to the same final state for a charged B_u^+ meson decay, whereas a neutral B_d^0 meson decay produces different final states. Color allowed (top) and color suppressed (bottom) decays.*

Despite the success of HQET, calculations of the lifetime differences are still complex. A recent calculation estimates that the deviation of the ratio $\tau(\mathrm{B}^+)/\tau(\mathrm{B}^0)$ from unity could be as large as 20 % [11]. Even the sign of this deviation can not be predicted. Experimentally the difference is observed to be small ($<$ 5 %). A reliable prediction can be made for the ratio $\tau(\mathrm{B_s})/\tau(\mathrm{B_d})$, which is expected to be equal to one within 1 %. A measurement of $\tau(\mathrm{B_s})$ therefore presents a direct test of the validity of the spectator model.

In the charmed system, the corrections to the heavy quark limit are large, since they scale by a factor $m_b^2/m_c^2 \sim 10$. To date, the lifetimes of charmed mesons are measured with an accuracy of $\sim$ 1 %, yielding considerable lifetime differences [12]: $\tau(\mathrm{D}^+)/\tau(\mathrm{D}^0) \sim 2.5$.

An effect which has not been discussed sofar, are decay phase space differences between the two CP eigenstates of the $\mathrm{B_s}$ meson[2]. Such an effect is clearly visible in the neutral kaon system, where there is a large lifetime difference between the CP eigenstates, the $\mathrm{K_S}$ and $\mathrm{K_L}$. This lifetime difference is due to the large difference in phase space: the two CP eigenstates decay into two and three pions respectively (if CP is conserved).

[2] The CP symmetry operation is briefly introduced in appendix A.

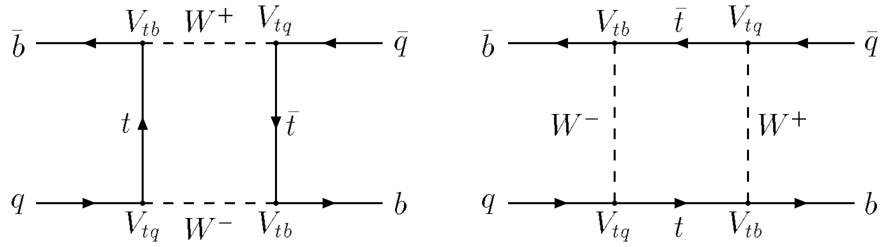

Figure 1.5: *Dominant box diagrams for the process* $B_q^0 \to \bar{B}_q^0$

In the B system the decays of the different CP eigenstates are not limited by phase space, and lifetime differences are therefore expected to be small. Recent calculations indeed predict a lifetime difference between the different CP eigenstates in the B_d system that is smaller than 1 %. However, the lifetime difference in the B_s system is expected to be larger, since here a few decay modes are limited by phase space [13]:

$$\Delta\Gamma(B_s) = \Gamma(B_1) - \Gamma(B_2) \sim 15\% \tag{1.12}$$

The largest contributions to $\Delta\Gamma$ come from decays to $D_s\overline{D_s}$, $D_s\overline{D_s^*}$, $D_s^*\overline{D_s}$ and $D_s^*\overline{D_s^*}$. This surprisingly large predicted difference follows from a study of all B_s decay modes, considering that some final states are specific to one CP eigenstate while others occur for both CP eigenstates.

1.5 B^0-$\overline{B^0}$ oscillations

The previous section introduced the use of lifetime measurements of the specific B mesons for an accurate determination of V_{cb}, and for tests of the spectator model. However, individual decay time measurements of the two neutral B meson species, the B_d and B_s mesons, are also an important tool in the study of neutral B meson oscillations. This section describes the object of oscillation measurements and their current status. The oscillation frequencies of B_d and B_s mesons are expected to be quite different, and an unexpected value could signal new physics processes. The index q will be used in the following to indicate that the B_q^0 meson may contain a d or an s quark.

B_q^0-$\overline{B_q^0}$ oscillations are transitions from a B_q^0 meson to its anti-particle $\overline{B_q^0}$, or vice versa. In the Standard Model such a $\Delta b = 2$ transition is only possible through the exchange of two W bosons. The dominant box diagrams in the Standard Model are shown in figure 1.5. In these diagrams two virtual W bosons are exchanged together with a pair of t quarks. The t quarks may be replaced by a pair of c or u quarks, but the exchange of the top quark is strongly Cabibbo favored, and is favored for its high mass (see equation(1.15)).

The existence of oscillations causes the state of a neutral B meson to be a superposition of $|\,B_q^0>$ and $|\,\overline{B_q^0}>$ states. The mass eigenstates form a light and a heavy state indicated by $|\mathrm{B_L}>$ and $|\mathrm{B_H}>$, which are combinations of $|\mathrm{B_q^0}>$ and $|\overline{\mathrm{B_q^0}}>$. The mass difference between these states is indicated by Δm_q.

Suppose a B meson is created in a pure $|\mathrm{B_q^0}>$ state at $t = 0$. The probability for it to decay at time $t > 0$ as a $|\mathrm{B_q^0}>$ state, or the probability for it to decay as a $|\overline{\mathrm{B_q^0}}>$ are then:

$$\begin{array}{rclcl} P(\mathrm{B_q^0} \to \mathrm{B_q^0}) & = & |< \mathrm{B_q^0}\,|\psi(t)>|^2 & = & e^{-t/\tau}\cos^2(x_q t/2\tau) \\ P(\mathrm{B_q^0} \to \overline{\mathrm{B_q^0}}) & = & |< \overline{\mathrm{B_q^0}}\,|\psi(t)>|^2 & = & e^{-t/\tau}\sin^2(x_q t/2\tau) \end{array} \tag{1.13}$$

where the effect of CP violation is neglected. This equation is derived in appendix A from basic quantum mechanical rules. The oscillation frequency x_q is proportional to the mass difference Δm_q multiplied by the lifetime:

$$x_q = \tau \Delta m_q \tag{1.14}$$

In the framework of the Standard Model, the diagrams of figure 1.5 can be calculated, which results in the following relation between the mass difference Δm_q and the CKM matrix elements V_{tb} and V_{tq}:

$$\Delta m_q = \frac{G_F^2}{6\pi^2} B_{B_q} f_{B_q}^2 M_{B_q}\, |V_{tb}^* V_{tq}\,|^2 M_t^2 \mathcal{F}\left(\frac{M_t^2}{M_W^2}\right) \eta_{QCD} \tag{1.15}$$

with

$$\mathcal{F}(x) = \frac{x}{4}\left(1 + \frac{3-9x}{(1-x)^2} + \frac{6x^2\ln(x)}{(1-x)^3}\right) \tag{1.16}$$

where $\eta_{QCD} \simeq 0.55$ is a QCD correction factor. An accurate calculation of Δm_q is limited by the uncertainty in the bag factor B and the decay constant f_B which are calculated in non-perturbative QCD: $Bf_B^2 = (1.0 \pm 0.2)(180 \pm 50)$ MeV^2. However, most of these uncertainties cancel for the ratio of the mass differences Δm_s and Δm_d:

$$\frac{\Delta m_s}{\Delta m_d} = \frac{(M_B\ \eta_{QCD} B f_B^2)_{B_s}}{(M_B\ \eta_{QCD} B f_B^2)_{B_d}} \left|\frac{V_{ts}}{V_{td}}\right|^2 \simeq \left|\frac{V_{ts}}{V_{td}}\right|^2 \tag{1.17}$$

The CKM matrix element V_{ts} is much larger than V_{td}. In the Wolfenstein parametrization the ratio is given by:

$$\left|\frac{V_{ts}}{V_{td}}\right|^2 \propto 1/\lambda^2 \approx 20. \tag{1.18}$$

The $\mathrm{B_s}$ oscillation frequency is thus expected to be much higher than the $\mathrm{B_d}$ oscillation frequency. An unexpectedly low value would signal the existence of new physics processes. One example that could cause a low value of the $\mathrm{B_s}$ oscillation frequency would be a new superweak interaction with much smaller coupling strength than the weak interaction [14]. Such an interaction would cause a transition $\Delta b = 2$ at tree level. The measurements of these CKM matrix elements are also an essential step towards the understanding of CP violation.

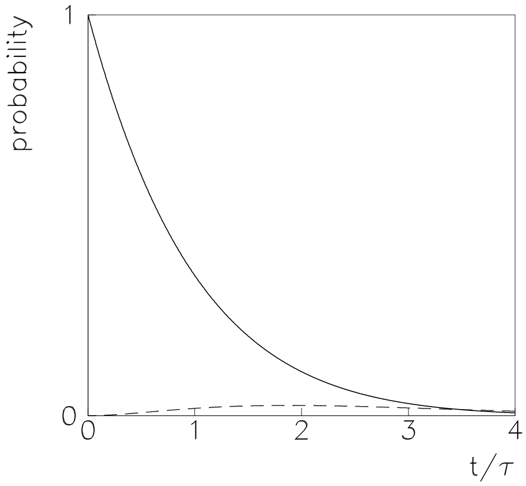

(a) B^0_d-$\overline{B}^0_d$ oscillation: $\Delta m = 0.45\ \hbar\mathrm{ps}^{-1}$

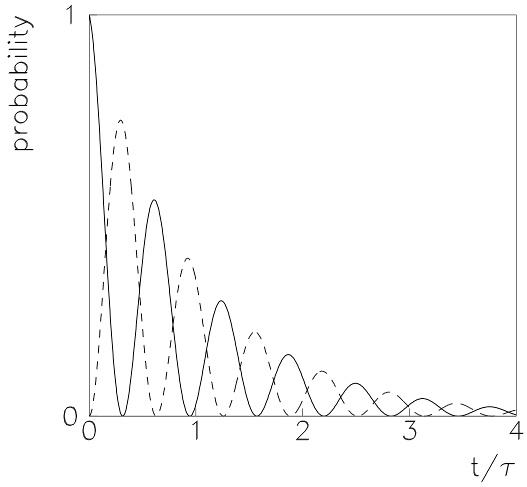

(b) B^0_s-$\overline{B}^0_s$ oscillation: for $\Delta m = 10\ \hbar\mathrm{ps}^{-1}$

Figure 1.6: *Time evolution of the oscillating* B^0-$\overline{B^0}$ *system. The probability that a created B^0 decays as a B^0* $P(B^0_q \rightarrow B^0_q)$ *(solid line), or as a $\overline{B^0}$* $P(B^0_q \rightarrow \overline{B^0_q})$ *(dashed line), as a function of time.*

$\Delta m_d = 0.465 \pm 0.024\ \hbar\mathrm{ps}^{-1}$
$\Delta m_s > 5.6\ \hbar\mathrm{ps}^{-1}$ or $x_s > 8.4$ at 95 % CL
$\mid V_{ts}/V_{td} \mid > 2.7$ at 95 % CL

Table 1.2: *Status of the B^0-$\bar{B}^0$ oscillation measurements.*

Measurements of B^0-$\overline{B^0}$ oscillation

Measurements of oscillations in the neutral B system have sofar been restricted to the B^0_d-$\overline{B}^0_d$ system, where the oscillation frequency is small compared to the lifetime: $x_d \simeq 0.7$ (or $\Delta m_d \simeq 0.46\ \hbar\mathrm{ps}^{-1}$), as illustrated in figure 1.6(a). It is therefore easier to observe than the high B_s oscillation frequency.

The large number of events that has been collected at LEP, has recently allowed direct measurements of the B_d oscillation frequency, making use of the reconstructed proper decay times. This has allowed an accurate determination of x_d. Since the fraction of B_s mesons in these measurements is low and the resolution of the measured decay time is also relatively low, they have not resulted in the observation of B_s oscillations. At the same time, they do imply that the B_s oscillations must be higher than a certain limit. Besides a measurement of x_d these measurements therefore also result in a lower limit on the oscillation frequency x_s.

Since the number of reconstructed B_s mesons is still relatively low, no measurements have yet been made with a significantly enriched sample of B_s mesons. The current status of the oscillation measurements as presented at the 1995 International Europhysics Conference on High Energy Physics in Brussels is shown in table 1.2.

Measurements of B_s^0-$\overline{B}_s^0$ oscillation

Within the Standard Model, the mass difference in the B_s^0-$\overline{B}_s^0$ system is predicted to be large. This follows from equation 1.18, using the value of λ as measured from the other matrix elements and requiring unitarity of the CKM matrix. The most likely value of Δm_s lies around 10 $\hbar \mathrm{ps}^{-1}$ (or $x_s \approx 15$) [5]. This is the value used in the illustration of figure 1.6(b).

To measure the fast B_s oscillation frequency, an enriched sample of reconstructed B_s decays is therefore needed, for which the proper decay time is reconstructed with high resolution for each event. The selection of such a sample is described in this thesis, where it is used for a lifetime measurement.

Chapter 2

LEP and DELPHI

2.1 The LEP collider

The Large Electron Positron Collider (LEP) produces e^+e^- collisions at the energy of the Z mass. It provides a laboratory to study physics at very high energies in a clean experimental environment. The main ring is built in an underground tunnel with a circumference of 26.7 kilometers near Geneva at CERN, and is in operation since 1989. Two beams consisting of bunches of electrons and positrons, respectively, move in opposite directions in one beampipe, which is kept at high vacuum. Before the particles are injected into the LEP ring they are accelerated to an energy of 20 GeV by a chain of pre-accelators, including the Super Proton Synchrotron (SPS).

After injection in the LEP main ring the beams are further accelerated to an energy of 45 GeV [1]. This acceleration is done in straight sections of the tunnel using radio frequency cavities, while dipole magnets guide the beams through the curved sections, and quadrupole and sextupole magnets are used to focus the beams. At four points in the ring the beams collide. At these interaction points detectors have been built, in large underground caverns, to record the products of the collisions. All four detectors ALEPH, OPAL, L3, and DELPHI are designed to measure the complete spectrum of physics at the Z resonance [15].

The data used in this thesis were collected with the DELPHI detector from 1991 to 1994. During these years the luminosity of LEP has been continuously improved, increasing the number of collisions considerably. Currently the luminosity has exceeded the design value of $1.3 \cdot 10^{31}\mathrm{cm}^{-2}\mathrm{s}^{-1}$. A complete description of the LEP collider can be found in the design reports [16] and [17].

2.2 The DELPHI detector

Figure 2.1 shows an outline of the LEP tunnel. The DELPHI detector is situated in an underground cavern in the south–east corner of the collider at the border of France and Switzerland, right at the edge of Geneva airport. DELPHI, a DEtector with

[1] Currently, the LEP acceleration power is being increased to allow the first production of W pairs in 1996. The final beam energy is expected to be around 96 GeV.

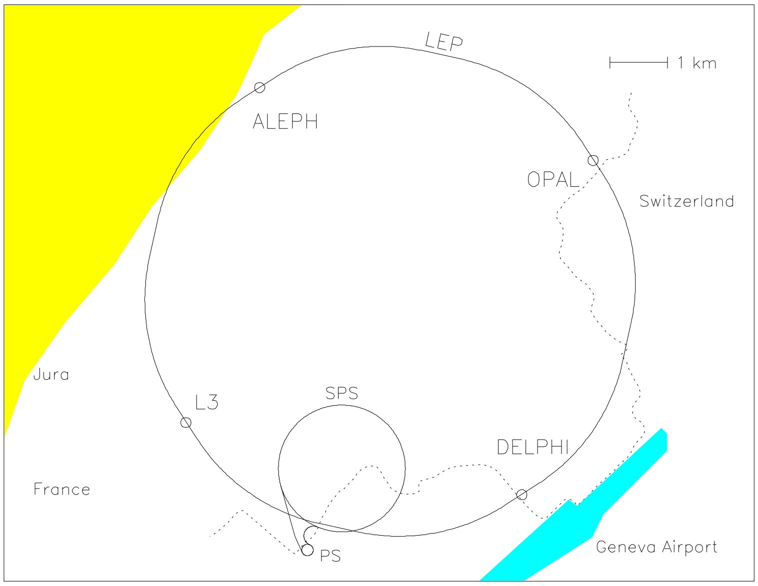

Figure 2.1: *Overview of the LEP collider*

Lepton, Photon and Hadron Identification, is designed as a general purpose detector for studying physics at LEP. The most outstanding feature of the DELPHI detector is the Ring Imaging CHerenkov detector (RICH), used for hadron identification. Other points of emphasis are the electromagnetic calorimeter with high granularity and the silicon detector close to the beam that allows for precise vertex reconstruction. All these detectors will prove to be of importance in this analysis.

The DELPHI detector consists of a cylindrical section, the barrel, and two endcaps. A perspective view of the detector is shown in figure 2.2. The short description given here is limited to the main part of the detector, the barrel region, where precise vertex reconstruction is available and the general detector performance is better. The endcap regions are not used in the present analysis. Reference [18] contains a complete description of the DELPHI detector. The recent performance of the detector is described in [19]. The coordinate system is defined with the z-axis running in the direction of the electron beam, the y-axis pointing vertically upwards, and the x-axis pointing to the center of the LEP ring. The polar angle θ is defined as the angle with the z-axis, the radius r and azimuthal angle ϕ are defined in the xy plane.

The various subdetectors of DELPHI can be divided into different groups. The first group consists of tracking detectors, in which charged particles are detected by the ionization traces they produce. The main tracking device is the Time Projection Chamber, which is supplemented closer to the beam pipe by the Inner Detector and the Vertex Detector. An additional measurement at larger radius is provided by the Outer Detector. All tracking detectors are placed inside a superconducting solenoid with an inner radius of 2.6 m and a length of 7.4 m, producing a magnetic field parallel to the z direction of 1.23 T. The resulting curvature of the charged particles in the xy plane allows an accurate momentum measurement, with an average resolution of $\sigma_p/p \approx 0.0008 \cdot p$ GeV/c.

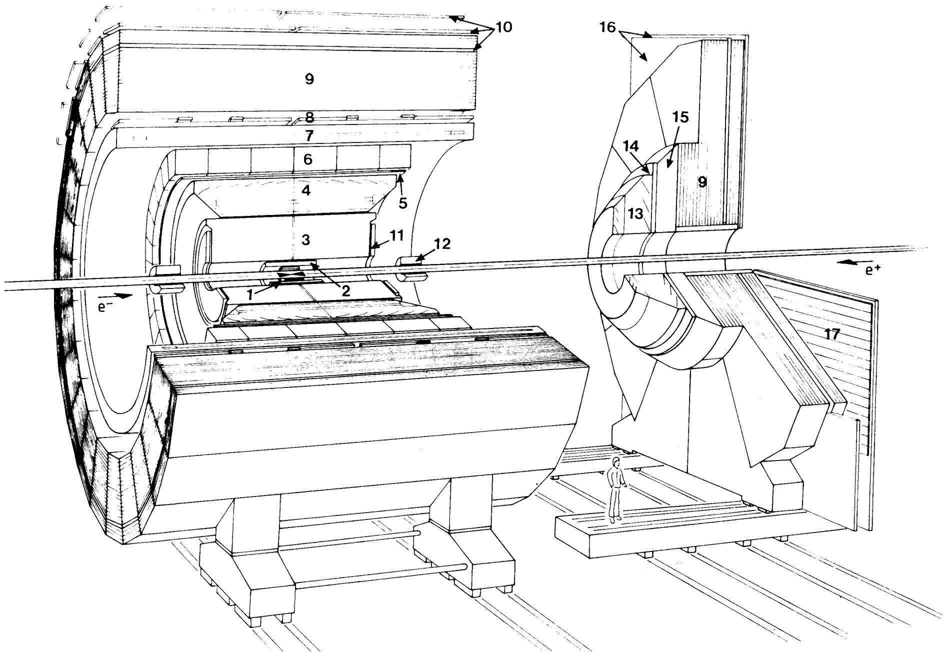

Figure 2.2: *A perspective view of the DELPHI detector; Vertex Detector (1), Inner Detector (2), Time Projection Chamber (3), Barrel RICH (4), Outer Detector (5), High density Projection Chamber (6), superconducting magnet (7), Time Of Flight (8), Hadron Calorimeters (9), Barrel Muon chambers (10), Forward Chambers A (11), Small Angle Tagger (12), Forward RICH (13), Forward Chambers B (14), Forward Electromagnetic Calorimeter (15), Forward Muon chambers (16), Forward Hodoscope (17).*

The second group of detectors, the calorimeters, measure the energy and position of charged and neutral particles. Both the electromagnetic calorimeter and the hadronic calorimeter contain high density materials in which most particles loose all their energy, producing showers of secondary particles. The position and energy of these showers are reconstructed using active materials placed between the layers of high density materials. Only the muons and neutrinos are not stopped. Muons are identified by a set of tracking chambers at the extreme outside of the detector, while neutrinos remain undetected.

The RICH detector uses the principle of Cherenkov radiation to measure the velocity of charged particles. This allows the identification of particles by combining the measured velocity with the measured momentum.

Additional calorimetric detectors are placed close to the beampipe at large distances from the interaction point to measure the luminosity through elastic e^+e^- scattering at low angles. These detectors are the Small Angle Tagger and the Very Small Angle Tagger. A single layer of scintillators placed on the inside of the return yoke provides a Time Of Flight measurement that is used as a fast trigger signal and to identify cosmic background events.

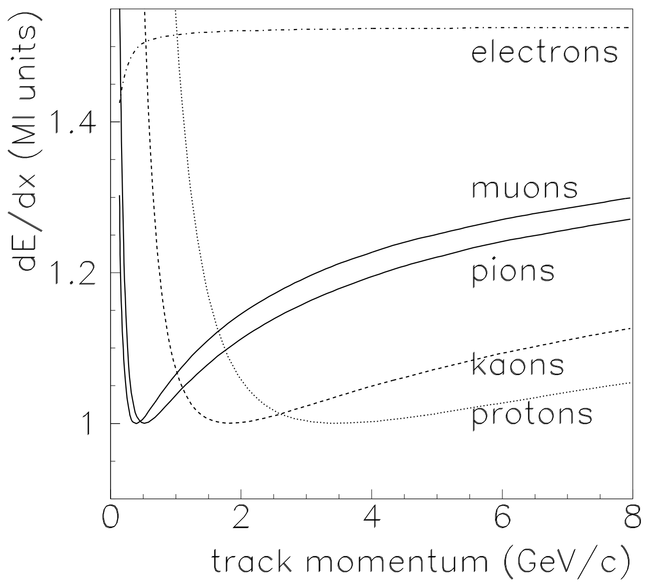

Figure 2.3: *Energy loss, dE/dx, versus momentum of the track*

2.2.1 The tracking detectors

The **Time Projection Chamber** (TPC) is the main tracking device of DELPHI. It is formed by a large cylinder with an inner radius of 35 cm and an outer radius of 111 cm, filled with an argon/methane mixture (80/20 %), at a pressure of 1 atm. In the middle of the detector, at $z = 0$, a high voltage plane divides the cylinder into two drift volumes that are both 130 cm long.

Charged particles traversing the gas volume produce ionization electrons, which drift in a strong electric field towards the end plates of the TPC, where they are detected. The z coordinate is measured by the drift time. The end plates are divided into 6 sectors of 192 sense wires and 16 circular pad rows, providing a maximum of 16 three dimensional space points per track.

Tracks are reconstructed at polar angles between 20^o and 160^o. Typical resolutions are 250 μm in $r\phi$ and 880 μm in z. The two-track separation is about 1 cm in both directions. In addition to the position measurement, the sense wires also provide an energy loss measurement. The energy loss dE/dx is typically measured with an uncertainty of 0.1 Minimum Ionizing units, providing a kaon/pion separation of 1.5 σ for particle momenta larger than 1.5 GeV/c, see figure 2.3. The dE/dx measurement is difficult when two charged tracks are at close distance and is therefore often missing in hadronic Z decays.

The **Vertex Detector** (VD) directly surrounds the beam pipe, and consists of three concentric layers of Si-strip detectors at distances of 6.3, 9 and 11 cm from the interaction point. The points provided by the Vertex Detector are essential for a precise reconstruction of the interaction point of the e^+e^- collision and for the reconstruction of B meson decay vertices. An example of an hadronic Z decay as recorded by the Vertex Detector is shown in figure 2.4. The upper plot shows the hits in the different VD layers. The lower plot shows an enlargement of the interaction area with the

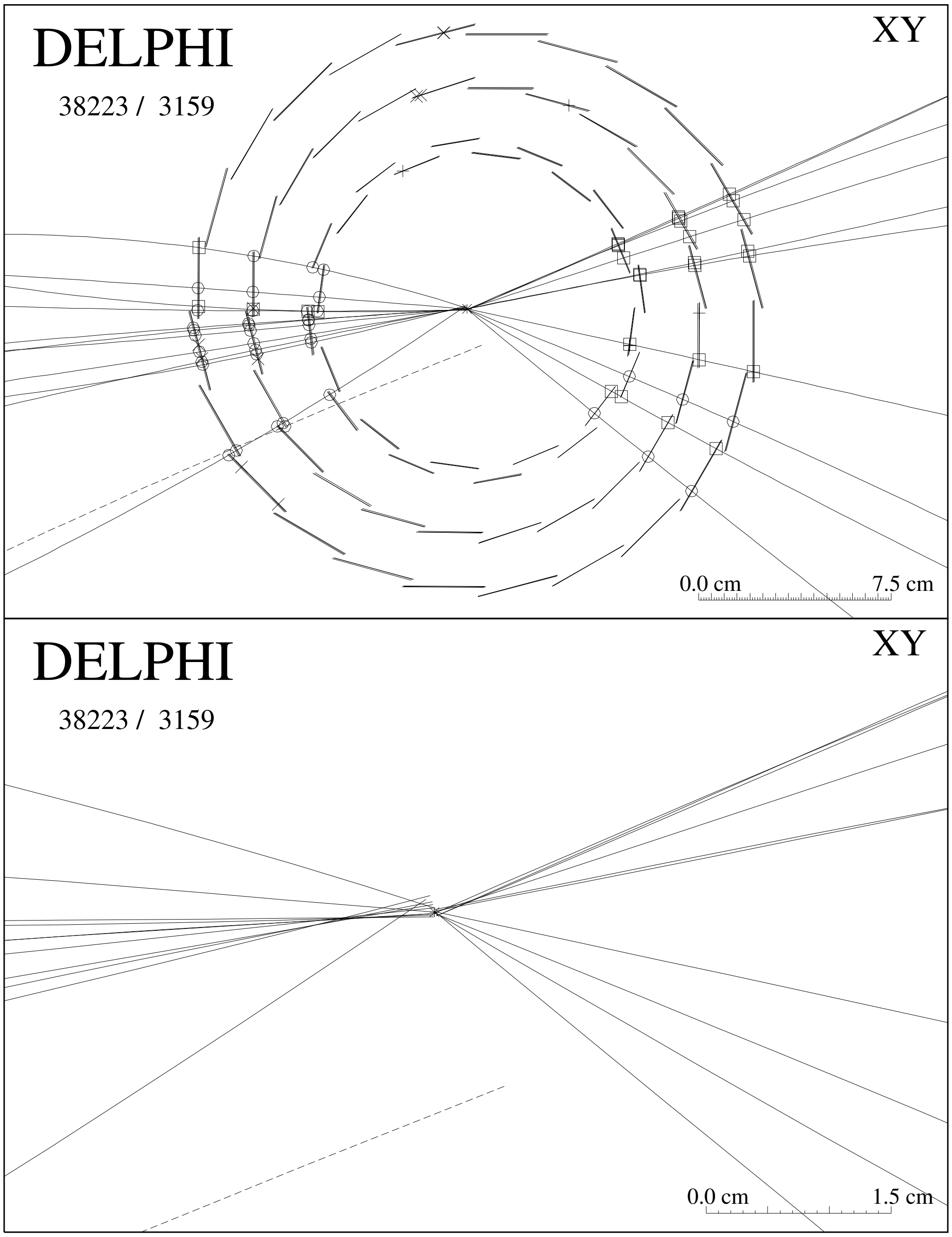

Figure 2.4: *Vertex Detector display of an hadronic Z decay, perpendicular to the beam. Full event display (top) and zoom-in of the interaction area (bottom). The decay vertices of short lived B and D mesons are clearly visible.*

interpolated tracks.

Each layer consists of 24 modules, which are composed of four detectors each, containing strips that run in parallel with the beam. Within one layer the modules overlap by about 10 % in ϕ to improve redundancy and facilitate internal alignment. In this way an average number of three and a maximum number of six hits is obtained for charged particles traversing the detector. In 1994 the detector was upgraded with strips on both inner and outer surfaces to provide also a measurement in z.

The intrinsic precision of each $r\phi$ measurement is 5 μm. The overall resolution is 8 μm, including residual internal alignment. The double track resolution is better than 100 μm. For polar angles between 44^o and 136^o, a particle crosses all three layers of the VD.

The **Inner Detector** provides an accurate reconstruction of charged tracks between the Vertex Detector and the TPC, from an inner radius of 12.0 cm to an outer radius of 28.0 cm. It consists of two components.

The first component, the Jet Chamber, is a cylinder filled with the drift gas CO_2. This cylinder contains planes of field wires parallel to the beam, thereby creating 24 separate azimuthal drift sectors. Centered in these sectors are additional planes of read-out wires, that run parallel to the field wires. The ionization electrons drift to these planes of read-out wires. Each plane contains 24 read-out wires. The drift field is constructed in such a way that a straight track coming from the interaction region will simultaneously give hits on all read-out wires, providing a fast trigger signal in a time window of $\sim$ 100 ns. The position of the track is reconstructed with a precision of 90 μm in $r\phi$ for each wire. The Jet Chamber covers polar angles from 23^o to 157^o and is 80 cm long.

The trigger signal from the Jet Chamber is used in coincidence with that of the second component: the Trigger Layers. These are five cylindrical layers of Multi Wire Proportional Chambers with read-out wires in $r\phi$ and read-out strips in z that are placed just outside the Jet Chamber. The z measurement has a resolution between 0.5 mm and 1 mm. The $r\phi$ measurement of the Trigger Layers is used to resolve the $r\phi$ ambiguity of the Jet Chamber.

An additional track measurement outside the RICH is provided by the **Outer Detector** at a distance of 1.98 to 2.06 m from the interaction point, thereby significantly improving the momentum resolution of high momentum tracks. Its position between the RICH and the electromagnetic calorimeter (HPC), strongly aids the particle identification of these two detectors. It also plays an important role in the trigger system.

Five layers of drift tubes precisely measure the position in $r\phi$, while three of the layers also provide a fast but crude z measurement, through a comparison of the signal timing on both ends. The detector is 4.7 m long, covering polar angles between 43^o and 137^o. The resolution is 110 μm in $r\phi$ and 4.4 cm in z.

The **Barrel muon detector** consists of three layers of drift chambers. Their aim is to identify muons, which penetrate through the iron of the hadron calorimeter. Each layer contains two staggered planes of drift tubes, which have a maximum drift distance of 10 cm to the central anode wire. The z coordinate is measured through a delay line, by comparing the time difference at both ends. The first layer is situated inside the return yoke after about 90 cm of iron, at 20 cm from the outer edge. The second layer is mounted on the outside of the iron. The third layer is positioned at 50 cm outside the return yoke and covers the regions that are left out by the first two layers, with a large overlap. The barrel muon chambers cover a polar region from 53^o to 127^o. Their resolution is approximately 3 mm in $r\phi$ and 2.5 cm in z.

2.2.2 The calorimeters

The High-density Projection Chamber (HPC)

The HPC is the barrel electromagnetic calorimeter and is positioned inside the magnetic coil. It is designed to reconstruct electromagnetic showers with high granularity while maintaining an adequate energy resolution. The HPC consists of many layers of lead, built from thick lead wires that produce an electric drift field. Secondary particles, which are created through conversions in the lead, produce ionization electrons in gas gaps between the layers. As in a TPC, these electrons drift in the z direction to a wire plane, where the $r\phi$ coordinates are measured. The drift time provides the z coordinate, allowing for a three dimensional shower reconstruction.

The high granularity enables an accurate spatial resolution of about 2 mrad in ϕ and in θ. This allows good separation between showers from electromagnetically interacting particles and hadrons. The high granularity is also important in the identification of the π^0 particle, as it decays into two nearly parallel photons. The energy of electromagnetic particles is measured with a resolution of $\sigma(E)/E = (32/\sqrt{E} + 4.3)$ % (E in GeV).

The hadron calorimeter (HAC)

The HAC is used for the detection of neutral particles. It is a sampling gas detector incorporated in the iron of the magnet return yoke. The detection layers consist of plastic tubes, each containing one anode wire, that are used in limited streamer mode [20]. The energy resolution is: $\sigma(E)/E = (112/\sqrt{E} + 21)$ % (E in GeV).

2.2.3 The barrel RICH

The barrel RICH provides a velocity measurement, that is used in combination with the momentum measurement to identify the mass of charged particles. It is designed to provide optimal pion–kaon–proton identification over the relevant momentum region at the Z resonance.

Charged particles that travel faster than the phase velocity of light in a medium produce Cherenkov radiation. The threshold velocity needed to produce Cherenkov light is $\beta = 1/n$ where n is the refractive index of the material. Above this threshold, photons are radiated at an angle Θ_c that is directly related to the velocity of the particle:

$$\cos\Theta_c = \frac{1}{\beta n}$$

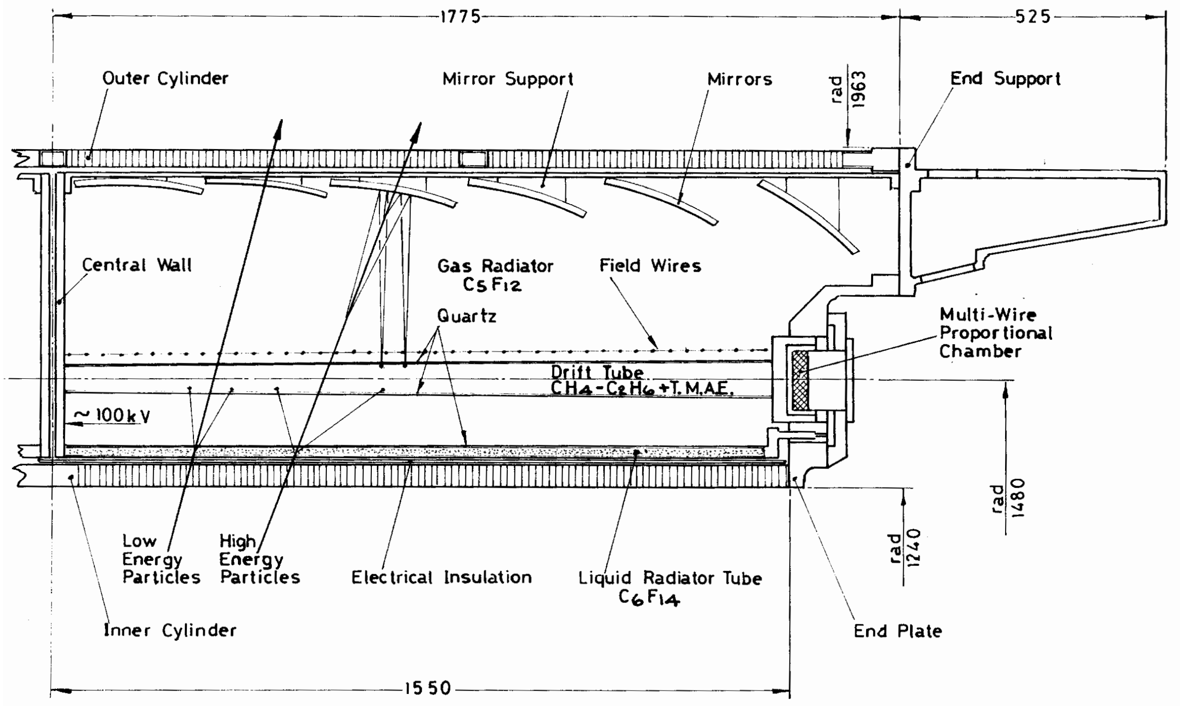

Figure 2.5: *Longitudinal cross section of a barrel RICH detector module.*

The number of emitted photons is proportional to $\sin^2 \Theta_c$.

The barrel RICH uses two different radiating media. A quartz drift tube is placed between the two media, as illustrated in figure 2.5. Coming from the interaction point, a particle first traverses the liquid radiating volume filled with C_6F_{14} ($n = 1.283$), where it may produce Cherenkov photons. These photons are projected directly onto the drift tube. The particle itself traverses the drift tube and enters the second radiating volume filled with the gas C_5F_{12} ($n = 1.00172$). Cherenkov photons that are produced in the gas are projected back onto the same photosensitive drift tube by focussing mirrors placed at the edge of the detector.

The drift tube is filled with the gases CH_4/C_2H_6 and the photosensitive gas TMAE [2]. The Cherenkov photons produce electrons by ionization of the TMAE gas. These electrons drift towards the end of the detector where their position is measured by a Multi Wire Proportional Chamber. The drift time provides a measurement of the z coordinate. Offline analysis combines these hits into a ring. The radius of the ring yields the Cherenkov angle of the emitted photons.

The total detector extends radially from 123 cm to 197 cm and is 3.5 m long, divided into two halves by a central support wall. It covers polar angles from 41.5^o to 138.5^o. Each half contains 144 mirrors.

Figure 2.6 shows the calculated Cherenkov angle as a function of momentum for the different particles. At momenta slightly above the threshold the Cherenkov angle increases rapidly until it saturates at higher momenta. The experimentally observed

[2] TMAE: tetrakis(dimethylamino)ethylene ($C_2[(CH_3)_2N]_4$)

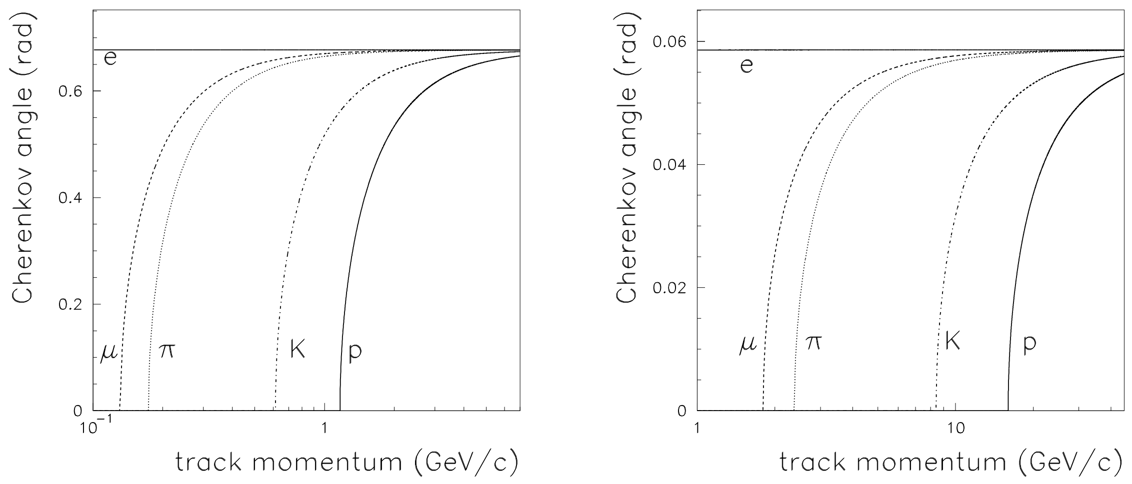

(a) Liquid radiator (b) Gas radiator

Figure 2.6: *Cherenkov angle as a function of the particle momentum for electrons, muons, pions, kaon and protons.*

	K/π	p/π	K/p
liquid ring	0.7–3.	1.5 –7.5	1.5–7.5
gas veto	2.5–8.5	2.5–16.	8.5–16.
gas ring	8.5–21.	16-25.	16–25.

Table 2.1: *Approximate momentum ranges for hadron identification in the barrel RICH (GeV/c)*

Cherenkov angles are distributed in bands around the calculated curves. There are two ways of identifying particles: the veto mode and the ring identification mode.

The veto mode is applied in the momentum range below the Cherenkov threshold. Heavy particles are then identified by the absence of photons. In the ring identification mode the Cherenkov angle can be measured. It is compared with the calculated Cherenkov angle for the different mass hypotheses. The particle of which the calculated angle corresponds best to the measured one, is the most likely hypothesis.

The approximate momentum ranges in which kaon–pion, proton-pion and kaon–proton separation are possible are shown in table 2.1. The liquid radiator covers the lower momentum region from 0.7 to 8 GeV/c whereas the gas radiator covers the higher momentum particles from 2.4 to 25 GeV/c. The RICH also contributes to electron identification below the pion threshold in the gas radiator of 2.5 GeV/c. Muon identification using the RICH is not possible, since the muon mass is too close to the pion mass to separate the two hypotheses.

2.3 Particle identification

2.3.1 Hadron identification

To distinguish between pions, kaons and protons the information from the RICH liquid radiator, the RICH gas radiator and the dE/dx measurement in the TPC are used. The combination of this information is a complicated task, since each detector provides identification in different momentum regions, that often overlap. To perform this task, the standard DELPHI software package for hadron identification HADIDENT is used [21]. HADIDENT produces flags that indicate the probability for each particle to be a pion, kaon or proton, using the information from the RICH or TPC only and also combining both. The values of these flags indicate confidence levels of identification that may be very loose, loose, standard, tight or very tight and an additional level that is reserved for cases in which both RICH and TPC lack sufficient information to identify the particle. Use of these flags depends largely on the physics subject under study, since each analysis sets its own specific requirements on the purity and efficiency of hadron identification.

The analysis described in this thesis requires kaons, of which the momentum is concentrated in the range from 1.0 to 8.5 GeV/c, to be identified with high efficiency, aiming to separate them from a large background of pions. To ensure this high effiency, the loose and very loose HADIDENT flags for kaon identification are used. No attempt is made to distinguish between kaons and protons.

Since the momenta of the kaon candidates in this analysis are mainly below the Cherenkov threshold of 8.5 GeV/c, the veto mode of the gas radiator is particularly important. Here, only one background photoelectron is allowed for kaon candidates. The liquid radiator provides additional useful information for momenta between 1 and 3 GeV/c. Here, loose kaon identification requires a Cherenkov ring of which the angle should correspond to the kaon hypothesis with a probability of more than 20 %.

Unfortunately the barrel RICH was not functioning at an optimal level for large parts of the data taken from 1991 to 1993. During this period the gas radiator was intermittently on and off while the liquid radiator recorded almost no data. In 1994 the RICH performance was optimal, adding also information from the liquid radiator over the whole year of data taking.

The identification power of the dE/dx measurement is limited. Below 1.5 GeV/c the kaon and pion bands overlap in such a way that the dE/dx measurement cannot be used to distinguish between kaons and pions, as can be seen in figure 2.3. At higher momenta, the dE/dx pion and kaon bands are separated by approximately 0.15 MI units, corresponding to 1.5 times the average error on the dE/dx measurement. Unfortunately, the dE/dx information is often missing in the high track multiplicity of hadronic decays. On average 60 % of the charged tracks in hadronic Z decays have sufficient dE/dx information.

Without hadron identification, a large background of pions overshadows the presence of kaons, since the production of kaons in hadronic Z decays is suppressed by a factor 7 compared to the production of pions [22]. This ratio is momentum dependent: at higher momenta the fraction of kaons increases. The number of pions and kaons as a

	kaon identification	
class	efficiency	probability of misid.
very loose	94 %	25 %
loose	80 %	10 %

Table 2.2: *Efficiency and misidentification probabilities of the very loose and loose kaon identification flags.*

function of momentum is shown in figure 2.7(a), for all charged particles in hadronic events. A sample of simulated hadronic Z decays is used, and the total number of particles is compared with a sample of real data events from 1994. When the very loose and loose kaon flags are applied, the fraction of kaons to the total number of particles increases, as shown in figure 2.7. The acceptance for kaons is summarized in table 2.2.

The performance of the particle identification is checked in the data by using particles for which the identity of the decay products is known, e.g. $K^0_S \rightarrow \pi^+\pi^-$, $\mathrm{D}^{*\pm} \rightarrow \mathrm{D}^0\pi^\pm$ and $\phi \rightarrow K^+K^-$ [23]. A more detailed description of the identification levels can be found in [24].

2.3.2 Lepton identification

Muon identification

Muons are identified by hits in the muon chambers, as hadrons have only a small probability to produce such hits. Hadrons are however much more abundant than muons and can still produce hits in the muon chambers when they fly through the iron of the hadron calorimeter without interacting (sail-through), or when they do interact and secondary particles cause hits (punch-through). Hits in the layers outside the return yoke suffer less from these backgrounds, and therefore carry more weight in the muon identification. Misidentifications also originate from the decay of pions or kaons to muons.

To reduce these backgrounds, a charged track in the TPC is required to form a good match with the muon chamber hits. For this purpose, each candidate muon track is refitted, and a χ^2 is calculated using the position of the track segment in the muon chambers and the extrapolated position, where hits are expected to be found.

The standard DELPHI muon idenfication package distinguishes three different classes of increasing purity: loose, standard and tight muons. Standard and tight muons are required to have at least one hit outside the return yoke. The efficiency and misidentification probabilities of the different classes are shown in table 2.3 [19].

Electron identification

The electron identification uses information from the electromagnetic calorimeter, the HPC, and information from the main tracking volume, the TPC. An electromagnetic energy deposition produces a characteristic shower profile in the HPC, since electrons loose all their energy early, while hadrons pass through the HPC, depositing on average

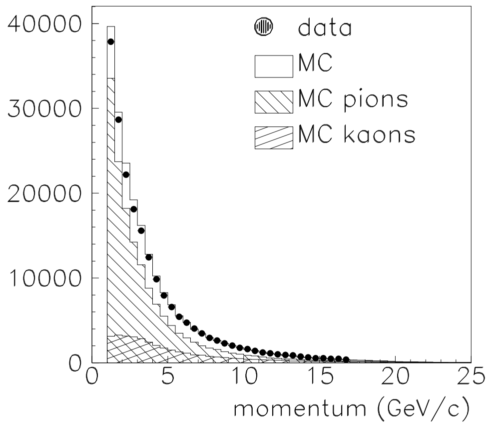

(a) momentum distribution of all tracks with information concerning hadron identification

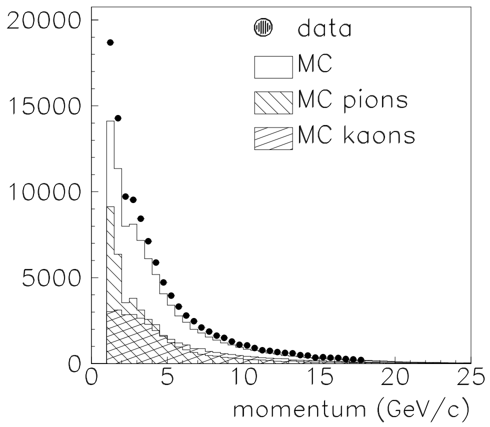

(b) momentum distribution of tracks with very loose kaon identification

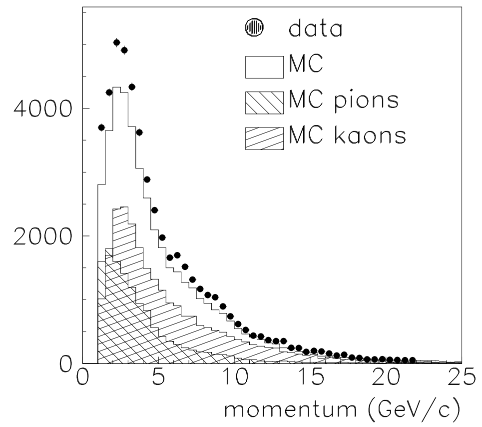

(c) momentum distribution of tracks with loose kaon identification

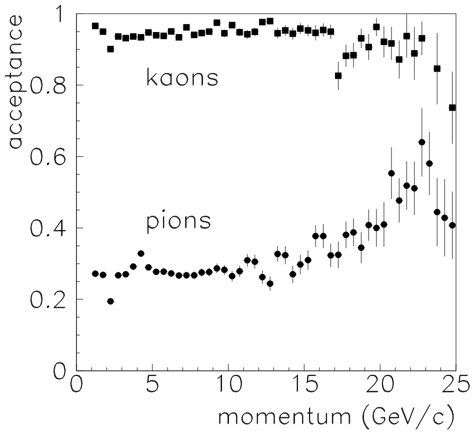

(d) acceptance as a function of momentum for kaons and pions demanding very loose kaon identification

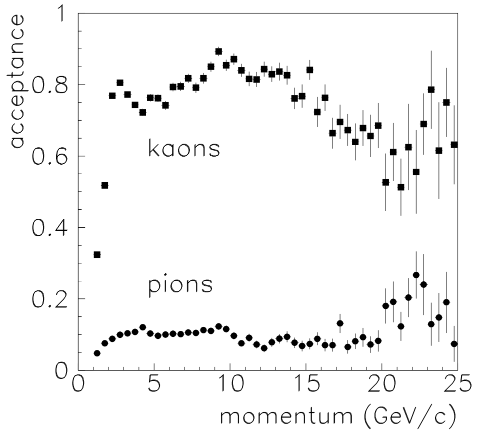

(e) acceptance as a function of momentum for kaons and pions demanding loose kaon identification

Figure 2.7: *Performance of the kaon identification.*

	muon identification		electron identification	
class	efficiency	probability of misid.	efficiency	probability of misid.
loose	$94.8 \pm 0.1\%$	$1.5 \pm 0.1\%$	80 %	$\simeq 1.6\%$
standard	$86.1 \pm 0.2\%$	$0.7 \pm 0.1\%$	55 %	$\simeq 0.4\%$
tight	$76.0 \pm 0.2\%$	$0.4 \pm 0.1\%$	45 %	$\simeq 0.2\%$

Table 2.3: *Efficiency and misidentification probabilities of the lepton identification ($p > 3$ GeV/c)*

an even amount of energy in all layers. The ratio of energy over momentum is therefore expected to be close to one for electrons, and small for hadrons. To further discriminate electron showers from photon showers, there must be a charged track pointing to the energy deposition. The dE/dx measurement in the TPC is also used, since electrons loose more ionization energy than charged hadrons, in the momentum range at LEP. In the momentum region below 2.5 GeV/c the gas RICH can be used, since at these momenta the pion rings are not yet saturated, contrary to the electron rings.

An additional search identifies electrons from photon conversions. The electrons are divided into three classes of increasing purity: loose, standard and tight. The efficiency and misidentification probabilities for these classes are shown in table 2.3 [19].

2.4 Data analysis

The time between two beam crossings at LEP is 11 μs (22 μs), when operating at 8 (4) bunches of electrons and positrons. Only a small fraction $\sim 10^{-5}$ of the beam crossings produces an e^+e^- annihilation. The DELPHI trigger and data aquisition system aims at selecting these events with high efficiency while operating at these high rates. Two trigger levels operate synchronously with the beam crossover gate, selecting candidate Z decays "online". These triggers use a combination of subdetector signals, thereby providing sufficient redundancy and geometrical overlap to achieve an efficiency close to one. After an additional third level of triggering the Z decay candidates are recorded on data tapes with a frequency of a few Hz.

The resulting raw data tapes are processed offline by the DELANA package [25]. DELANA performs local pattern recognition for every sub-detector to reconstruct valid track elements and energy clusters. It uses a database to provide calibration and alignment constants for each sub-detector. The individual track elements and energy clusters are then linked to form tracks.

To improve the calibration, a new processing of DELANA may be done, which uses the results of the first calibration and alignment. The resulting data are written to *data summary tapes* that are later reduced by a factor three in size by summarizing the information of individual detector components. The result is a shorter version of the data summary tapes, on which e.g. hadron identification flags are directly available.

Analysis of the Z decays begins at the DELPHI computer facility at SHIFT, which is a cluster of powerful workstations at CERN. There the events used in this thesis are preselected using the PHDST package that reads the data summary tapes. The selected events are stored in a compact form and transferred to NIKHEF Amsterdam. Here, the final data analysis takes place, the selection criteria are refined and the final measurement is done.

In this thesis Monte Carlo studies play an important role. They describe both the detector resolutions and simulate background processes, which allows tests of the statistical and systematical significance of the measurement. Simulated Z decays are generated through the LUND JETSET Monte Carlo programs [26]. The DELPHI detector is simulated by the DELSIM package [27], and the processing is done by DELANA in the same way as real data events.

Chapter 3

Reconstruction of B_s decays

3.1 Full B_s reconstruction

Only a very small fraction of the B_s decays can be fully reconstructed. Reconstruction requires decays to final states with charged particles only, since charged particles are measured more accurately than neutral particles, in DELPHI and in most other detectors. These rare, exclusively reconstructed decays such as $B_s \to D_s^+\pi^-$, allow the purest sample of B_s decays to be obtained. Here the D_s meson decays into three charged particles, and intermediate resonances help to select a pure signal.

In the clean experimental environment of the Z resonance there is almost no background to these fully reconstructed decays. Unfortunately, branching fractions to suitable final states are of the order 10^{-4}. The total number of reconstructed decays amounts to only a handful, with the current statistics of about three million collected hadronic Z decays. Some of these decays, such as $B_s \to J/\psi\phi$, cannot be used in an oscillation measurement, since they do not reveal the flavor of the B_s meson. Fully reconstructed decays at LEP allowed the first observation of the B_s meson and an accurate measurement of its mass [28]. However, to measure the average decay time and the oscillation frequency, larger event samples are needed. At LEP they can only be obtained through the use of partial reconstruction modes.

3.2 Partial B_s reconstruction

The decay of B mesons is well described by the spectator model, as introduced in section 1.4. The dominating spectator decay diagram is shown in figure 3.1(a). In this model all B_s meson decays produce a $\bar{c}s$ combination in the final state. This can be a D_s, D_s^* or a D_s^{**} meson. Most final states will contain a D_s meson, since all D_s^* decay to $D_s\gamma$ and only the radially excited D_s^{**}, produced in a small fraction of the B_s decays, decay to other D mesons. The inclusive branching ratio $BR(B_s \to D_sX)$ is estimated to be about 85 % [29], which makes the reconstruction of a D_s meson an efficient way of tagging B_s meson decays. A detailed discussion of the B_s meson and related branching fractions can be found in appendix B.

However, also other B hadron decays produce D_s mesons, dominantly through the

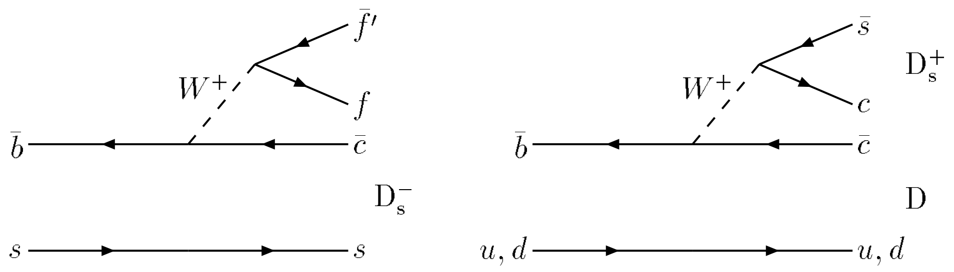

(a) $B_s \rightarrow D_s^- X$ (b) $B_{u,d} \rightarrow D_s^+ X$

Figure 3.1: *Dominating spectator diagrams of B_s meson and $B_{u,d}$ meson decays into D_s mesons.*

decay of a B_u or B_d meson into D_sD, as is shown in figure 3.1(b). The inclusive branching ratio $BR(B_{u,d} \rightarrow D_sX) \simeq 11\%$ is much smaller than the ratio $BR(B_s \rightarrow D_sX)$. However, only one out of seven B mesons produced in the fragmentation process is a B_s meson (relation 1.7). An event sample of reconstructed D_s mesons contains therefore approximately as many other B meson decays as B_s meson decays.

Our aim is to collect a sample of tagged B_s decays to measure the average B_s decay time. This requires an accurate reconstruction of the proper decay time of each B_s meson, which can only be achieved through a direct determination of the B_s decay vertex. D_s mesons have a long average lifetime of 0.47 ps, and are produced with sufficiently high momentum in the decay of B_s mesons to fly a considerable distance before decaying. For a direct reconstruction of the B_s decay vertex, an additional charged particle from the B_s decay vertex has to be included. This additional track can then be intersected with the line of flight of the D_s meson. The experimental situation is depicted in figure 3.2. The full lines indicate the final state tracks that are reconstructed in the detector, the dashed lines indicate the short lived B_s and D_s mesons which decay inside the beampipe (an example of a full Vertex Detector event display is shown in figure 2.4). Typical decay lengths are 2.5 mm and 1 mm, respectively. The resolution on the measured decay lengths is approximately 300 μm. In the majority of the B_s decays the additional track originates directly from the B_s decay vertex. However, in approximately 10 % of the decays the additional track comes from a longlived D meson or τ lepton, in which case the B_s vertex is reconstructed with less accuracy.

The additional particle often has opposite charge to the D_s meson, since it originates from the virtual W, see figure 3.1(a). In most analyses published sofar, this particle is a lepton. Here, a pure sample of semi-leptonic $B_s \rightarrow D_s l \nu X$ decays is obtained. However, only 20 % of the B_s mesons decay semi-leptonically. By allowing also pions or kaons as the additional track, a significant number of B_s decays can be added. The semi–exclusive reconstruction mode presented in this thesis thus aims at including also the hadronic decays $B_s \rightarrow D_s\pi X$ and $B_s \rightarrow D_sKX$. Throughout this thesis D_s-lepton combinations are indicated by D_sl, where the l stands for a muon or electron and D_s-hadron combinations are indicated by D_sh, where the h stands for a pion or kaon.

In order to collect an even larger number of B_s decays other inclusive reconstruction

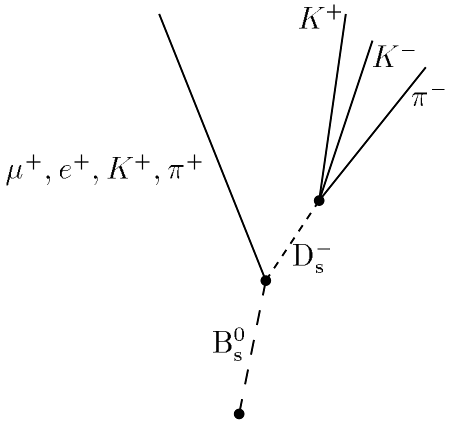

Figure 3.2: *Experimental view of a $B_s \to D_s$-lepton/hadron decay.*

modes are possible, which will not be used here. Examples of such reconstruction modes are decays in which only the D_s meson is reconstructed or decays to a ϕ meson accompanied by a high p_T lepton [30]. These reconstruction modes rely on a statistical separation between B_s meson and other B meson decays. The number of collected events is larger than for the reconstructed $D_s l$ and $D_s h$ decays but the background from other B meson decays is higher. In addition, the B_s meson decay vertex and its momentum are reconstructed less accurately.

In our analysis, the event selection will concentrate on a pure sample of tagged B_s meson decays. The semi-exclusive reconstruction mode $B_s \to D_s$-lepton/hadron used in this analysis, results in an event sample that is sufficiently large for a lifetime measurement, and that will be used for a direct measurement of the B_s oscillation frequency in the near future.

3.3 Background sources

This section describes the potential background in the event sample of selected B_s decay candidates. The suppression of this background is the main aim of the selection criteria described in the following sections. At this stage no experimental imperfections (e.g. in the lepton identification) are considered, but only the different types of "physics background" are discussed. The contribution of each background type is different in the $D_s l$ and $D_s h$ samples. Each type also produces a different decay time spectrum which is discussed in more detail in chapter 5, where the measurement of the B_s lifetime is described. There are three sources of background in our selected sample of B_s decay candidates, viz. two other sources of D_s mesons and the combinatorial background:

$B_{u,d,baryon} \to$ $\mathbf{D_s X}$ **:**
D_s mesons can originate from B hadron decays other than B_s mesons. This background type is dominated by B_u or B_d decays to $D_s D$, as described by the diagram of figure 3.1(b). Here, the additional particle originates from the second D meson. All B decay products are correctly reconstructed, but the source is not a B_s meson.

In B_u or B_d decays, D_s-lepton combinations are produced when the decay of the second D meson results in a lepton. The lepton then originates from the cascade decay $b \to c \to l$, which has a branching ratio of about 16 % when both muons and electrons are considered [31]. Direct semi-leptonic B_s decays occur with a branching ratio $b \to l$ of about 22 %. Since these ratios are approximately equal, the $D_s l$ sample would contain as many events from other B hadron decays as from B_s decays, without further discrimination.

However, in the direct semi-leptonic B_s decays only the neutrino remains undetected and a high invariant D_s-lepton mass is produced. In contrast, B_u and B_d decays produce additional particles besides the neutrino and will therefore result in a lower invariant D_s-lepton mass. The requirement of a high invariant mass can therefore be used to siginificantly reduce the background from other B hadron decays. Such a cut is equivalent to demanding a high p_T of the lepton with respect to the jet.

The same mass cut is also used for the D_s-hadron sample. Here, the requirement of a high invariant mass is less effective than for the semi-leptonic decays, since hadronic B_s meson decays tend to produce additional particles in the final state and thereby produce a relatively low D_s-hadron invariant mass.

The decay time spectrum of this background type is very similar to the signal from B_s decays.

D_s with an additional track from the fragmentation process:

These background events contain an additional track that originates from the fragmentation process, although the selection procedure aims at excluding such tracks. The main contribution is from $Z \to c\bar{c} \to D_s X$ decays, where the fragmentation process is the only possible source for the additional track. However, an additional track from the fragmentation may also be selected in $Z \to b\bar{b} \to D_s X$ decays.

This background type does not occur for decays to D_s-lepton combinations, since leptons are rarely produced directly in the fragmentation process. Hadronic B_s decay candidates contain a sizable background fraction of these events.

Since the additional track originates from the fragmentation process, the intersection with the line of flight of the D_s meson will be centered around the interaction point of the event. This results in a decay time spectrum that is concentrated at zero time.

Combinatorial background :

This is the largest source of background, and consists of events for which the selected tracks are not decay products of a D_s meson at all. Very often all or part of the particles originate from the fragmentation process. But combinatorial background can also originate from B decays. All selected tracks then originate from a B meson decay, even though no D_s meson decay is involved. This type of "flying combinatorial background" yields a decay time spectrum that is very similar to the signal from B_s decays. The decay time spectrum of the combinatorial background therefore contains mostly events that are centered at zero time, but also events from B hadron decays that contribute an exponential "flying background" tail.

The combinatorial background produces a continuous $KK\pi$ mass spectrum, while reconstructed $\mathrm{D_s}$ decays produce a resonance peak which is centered at the $\mathrm{D_s}$ mass. The background events in the $\mathrm{D_s}$ mass peak cannot be distinguished from $\mathrm{D_s}$ meson decays on an event-by-event basis. However, their number can be easily obtained from a fit to the mass spectrum.

To summarize, we note that the background level is lower in the $\mathrm{D_s}l$ sample than in the $\mathrm{D_s}h$ sample. In the search for an additional particle, which aims at including an additional track from the B meson, priority is therefore given to tracks that are identified as leptons.

3.4 Event selection

The total number of partially reconstructed $\mathrm{B_s}$ decays will be of the order of a hundred events. It is therefore important to keep the efficiency of the selection criteria high, while finding an optimal balance between statistics and purity of the final event sample.

As a first step, hadronic Z decays are selected by rejecting events with a low track multiplicity. In this way, leptonic Z decays into pairs of electrons, muons or tau leptons, and background from cosmic events are rejected. The standard DELPHI selection criteria for hadronic events are used:

- at least 5 charged tracks in the event with
  $p > 400$ MeV/c, $20^o < \theta < 160^o$ and a track length in the TPC > 30 cm
- total charged energy $\geq 0.12 \times$ center of mass energy
- thrust axis of the event $|\cos\theta_{thrust}| < 0.95$

These criteria are 95 % efficient for hadronic Z decays. A total of 3 million hadronic events are thus selected from data collected from 1991 to 1994. The summary in table 3.1 shows that a large fraction of these events was collected in 1994. Since also the full particle identification capability of DELPHI was available in this period, it dominates the lifetime measurement. The plots and comparisons between Monte Carlo and data presented in this section are therefore taken from 1994, unless stated otherwise.

The selection criteria described in the following sections exploit the high momenta of $\mathrm{B_s}$ decay products as compared to particles produced in the fragmentation process. In addition, the decay modes used to reconstruct $\mathrm{D_s}$ mesons offer kinematical features that are used to reject combinatorial background.

year	Number of hadronic Z decays
1991	255 k
1992	704 k
1993	710 k
1994	1,393 k
total	3,062 k

Table 3.1: *Number of hadronic Z^0 decays selected in the DELPHI detector from 1991 to 1994.*

Two decay modes are used for the full reconstruction of D_s mesons:

$$\begin{array}{lll} D_s^- \to \phi\pi^- & \text{with} & \phi \to K^+K^- \\ D_s^- \to K^{*0}K^- & \text{with} & K^{*0} \to K^+\pi^- \end{array}$$

The ϕ and K^{*0} resonances help to select a pure signal. The main difference between the two decay modes is the much smaller natural width of the ϕ resonance of 4.4 MeV compared to a width of 50 MeV for the K^{*0} resonance [6]. Experimentally, the observed width of the ϕ peak is dominated by the experimental resolution, while the width of the K^{*0} peak is determined by its natural width. Stricter selection criteria are therefore required for the $K^{*0}K$ decay channel, to reject more combinatorial background under the K^{*0} resonance.

The description of the event selection starts with the general selection of good quality tracks. Then the selection of D_s meson decays is discussed, followed by a description of the search algorithm for an additional track of opposite charge. Finally, the kaon identification is described.

To study the efficiency of the selection criteria, a Monte Carlo sample of 11802 simulated fully reconstructible D_s decays is used, of which the decay products all contain vertex detector hits. The generation was done by the LUND JETSET Monte Carlo programs [26], and the detector response was simulated by the DELSIM package [27]. The branching ratios of $D_s \to \phi\pi$ and $D_s \to K^{*0}K$ are approximately equal, yielding a sample of 5082 simulated D_s decays in the $\phi\pi$ channel and 6720 decays in the $K^{*0}K$ channel.

The absolute efficiency is only of secondary importance to the lifetime measurement. Differences in efficiency between the different sources of D_s mesons: B_s, $B_{u,d}$ and $Z \to c\bar{c}$ decays, are important. They originate mainly from the additional track finding algorithm and the applied kinematical criteria related to this track. These efficiencies are studied in detail in the discussion of the event sample composition at the end of this chapter.

3.4.1 Track selection

Rather loose selection criteria are applied to the tracks of all four charged particles from the B_s decay candidate. This eliminates badly measured tracks and allows an accurate

	$D_s \to \phi\pi$	$D_s \to K^{*0}K$
kinematical criteria	58 %	39 %
probability of the D_s vertex fit	84 %	84 %
kaon identification	84 %	49 %

Table 3.2: *Efficiency for selecting D_s meson decays.*

reconstruction of the B_s decay. Since Vertex Detector hits are needed to reconstruct the B_s decay vertex, all four tracks are required to have at least one VD hit. A minimum momentum is required, since at low momenta the vast majority of particles originates from the fragmentation process. The following track selection criteria are applied:

- TPC must be used in the track reconstruction
- closest distance of approach to the primary vertex < 2 cm in r and < 5 cm in z
- error on the measured momentum $< 10 \times$ the expected error for the corresponding kinematical conditions
- all tracks must have at least one Vertex Detector hit; and in addition their polar angles must be between 35^o and 145^o
- momentum > 1 GeV/c

3.4.2 D_s meson reconstruction

Both selected decay modes of the D_s meson produce two charged kaons and one charged pion in the final state. First, the $\phi \to K^+K^-$ or $K^{*0} \to K^+\pi^-$ resonance is reconstructed by combining two oppositely charged tracks. Then, a third particle is added to complete the reconstruction of the D_s meson decay. This last particle is called the *bachelor* particle, and is a pion for decays to $\phi\pi$ states and a kaon for decays to $K^{*0}K$ states. In both decay channels the two final state kaons are of opposite charge, which is explicitly required in the reconstruction. In this section, the kinematical selection criteria and the vertex fit for D_s decays are described, while the kaon identification criteria are discussed separately in section 3.4.4. The efficiencies of the selection criteria are summarized in table 3.2.

Slightly higher momenta than the standard cut at 1 GeV/c are required for the two kaon candidates from the $K^{*0}K$ channel, to ensure good quality for the particle identification:

- momenta of kaon candidates from $K^{*0}K$ decays > 1.5 GeV/c

The ϕ and K^{*0} mass resonances for the 1994 data are shown in figure 3.3. To select $\phi \to K^+K^-$ and $K^{*0} \to K^+\pi^-$ decay candidates the mass windows are set at approximately 2.5 standard deviations around the center resonance values:

- K^+K^- invariant mass within the ϕ selection interval of 1.019 ± 0.009 GeV/c^2

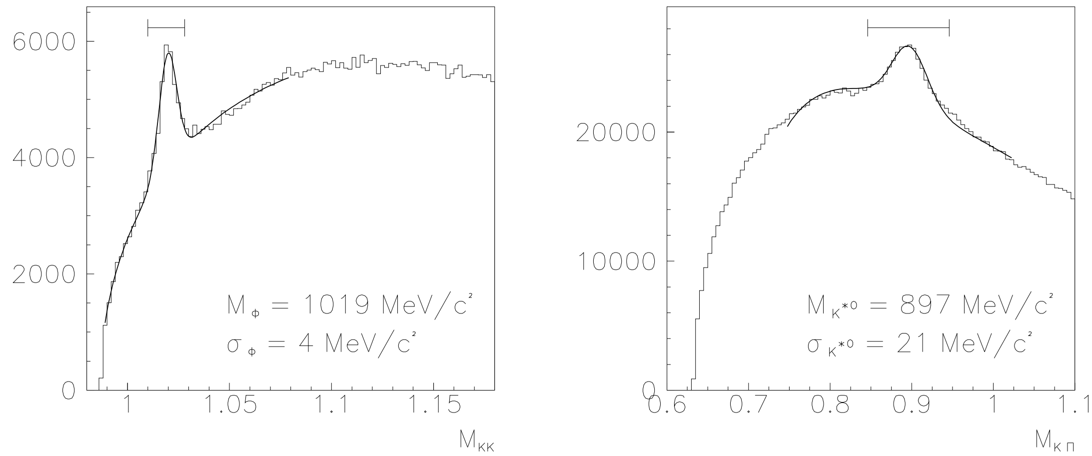

(a) KK invariant mass (b) $K\pi$ invariant mass

Figure 3.3: *Mass spectra of the ϕ and K^{*0} resonances. Kaon identification is used to enhance the resonance peaks.*

- $K^+\pi^-$ invariant mass within the K^{*0} selection interval of 0.897 ± 0.050 GeV/c^2

To reject low momentum combinatorial background from the fragmentation process the requirement of high momenta for the ϕ/K^{*0} resonance and the D_s meson are essential:

- ϕ/K^{*0} momentum > 4 GeV/c
- D_s momentum > 7 GeV/c

D_s mesons from $Z \to c\bar{c}$ decays tend to have higher momenta than D_s mesons from B decays. Therefore, the efficiency to accept D_s mesons from charm events is slightly higher at 86 % compared to an efficiency of 78 % for D_s mesons from B decays.

The helicity angle ψ related to the ϕ/K^{*0} decay is used to discriminate between D_s decays and combinatorial background. Since the ϕ/K^{*0} must have zero helicity in the D_s restframe, the angle between the direction of the ϕ/K^{*0} decay products with respect to the bachelor particle follows a $\cos^2\psi$ distribution [32]. Here, ψ is defined as the angle between one of the ϕ/K^{*0} decay products and the bachelor particle, when both are boosted to the ϕ/K^{*0} restframe. For the combinatorial background this angle is randomly distributed. The requirements for this decay angle and the corresponding efficiencies are:

- $D_s \to \phi\pi$: $|\cos\psi| > 0.4$, efficiency 91 %
  $D_s \to K^{*0}K$: $|\cos\psi| > 0.6$, efficiency 76 %

The reduction of combinatorial background is 40 % and 60 %, respectively.

If a triplet of tracks is found that fulfills the kinematical criteria a two-dimensional vertex fit is performed to determine the D_s vertex. Standard DELPHI vertex fitting software is used [33]. A minimum probability for the fitted vertex is required:

- probability of the three track vertex fit > 1 %

The distribution of this probability is expected to be flat for tracks originating from one common vertex, while tracks from different vertices cause a sharp peak at low probability. Unfortunately, the simulated data show that also 15 % of the selected D_s decays are concentrated at low probability and are thus lost by this cut. This occurs if one or more of the decay products is mismeasured, and the three tracks no longer point to one common vertex. Because of the large multiplicity of hadronic Z decays, tracks often lie close together and it is not surprising that such mismeasurements occur. Such tracks often miss Vertex Detector hits or are marked by a bad χ^2 of the track fit.

Although the requirement of a common vertex strongly reduces the combinatorial background, it must be noted that part of the background is expected to pass this cut. This occurs when all three particles originate from the fragmentation process, in which case they have the primary vertex as a common vertex, or when the combinatorial background tracks originate from one common B decay vertex.

Finally, the sample of D_s decay candidates is selected by applying a cut in the $KK\pi$ mass spectrum, around the center value of the D_s mass:

$$1940 \text{ MeV/c}^2 < \ KK\pi \text{ mass } < 1990 \text{ MeV/c}^2$$

This corresponds to a $\pm 2\sigma$ window, where $\sigma = 13$ MeV/c^2 is the width of the D_s mass peak. The $KK\pi$ mass spectrum of the selected $B_s \rightarrow D_s$-lepton/hadron decay candidates will be shown in section 3.6.

3.4.3 B_s meson reconstruction

The partial B_s meson reconstruction is completed by adding one track of opposite charge to the D_s meson.

The additional track must have a reconstructed invariant mass with the D_s meson that is lower than 5.6 GeV/c^2, a limit that is determined by the B_s mass of 5.38 GeV/c^2 plus a safe addition of about four times the mass resolution. The momentum of the additional track is required to be more than 3 GeV/c, which guarantees a good quality of the lepton identification, and decreases the probability of selecting a track from the fragmentation process, as illustrated in figure 3.4.

When more track candidates are present, the highest momentum track is selected to increase the probability that the additional particle originates from a B_s meson decay. An exception is made when one of the tracks is an identified lepton (loose, standard or tight, see section 2.3.2), in which case this track is preferred above all other candidates.

After the selection of the additional lepton or hadron track, several cuts are applied to ensure the quality of the event and to reduce the background. The reconstructed invariant D_s-lepton/hadron mass is demanded to be more than 3 GeV/c^2. This reduces the background from other B meson decays considerably, and is especially effective for semi-leptonic B_s decays. For hadronic B_s decays this cut is less effective since also about 50 % of the B_s decays are lost, see figure 3.5(a). This requirement also reduces the combinatorial background which is mostly concentrated at low masses, see figure 3.5(b).

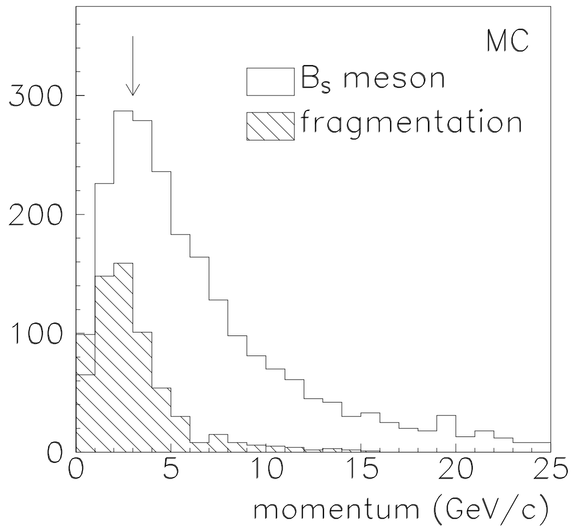

Figure 3.4: *Momentum distribution of additional track candidates, in simulated $B_s \rightarrow D_s X$ decays. The cut value is indicated by the arrow.*

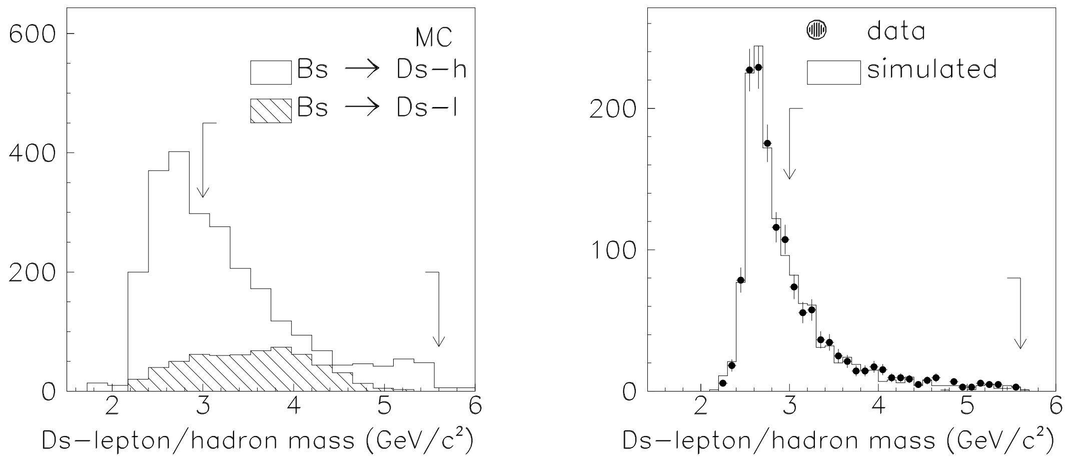

(a) Reconstructed invariant D_s-lepton/hadron mass for simulated B_s decays.

(b) Reconstructed invariant D_s-lepton/hadron mass for combinatorial background from data and simulation.

Figure 3.5: *Invariant* D_s*-lepton/hadron mass.*

In addition, the combined D_s-lepton/hadron momentum is required to be more than 15 GeV/c.

The probability of finding an additional track of opposite charge within the B_s mass window is high for all sources of D_s mesons. However, the requirement of a high momentum and a high invariant mass reduces this probability considerably. For B_s decays to a D_s meson the probability of finding an additional track that corresponds to the kinematical criteria is approximately 60 %. When an additional track is found, it has a probability of 85 % to originate from the B_s meson. The remaining tracks originate from the fragmentation process. The largest differences in efficiencies between the various sources of D_s mesons arise from the requirement of a high invariant D_s-

lepton/hadron mass. This is discussed in more detail in section 3.7 where the event sample composition is determined.

The selected additional track is intersected with the line of flight of the D_s meson, to obtain the B_s decay vertex. This vertex is required to be closer to the interaction point than the D_s vertex. In other words the apparent D_s flight distance is required to be positive. This requirement rejects 45 % of the combinatorial background, while accepting 75 % of the signal events from $B_s \to D_sX$ decays. In the rejected signal events, the B_s vertex is mistakenly reconstructed at a larger distance from the primary vertex than the D_s vertex, which can occur due the experimental uncertainty in the vertex determination, in combination with small D_s flight distances. The effect of this cut is different for other B hadron decays where the additional track is often produced through a second, long-lived D meson. In these decays the reconstruction of the D_s flight distance is less accurate and slightly more decays are removed.

3.4.4 Kaon identification

The kaon identification used in this analysis aims at maintaining a high efficiency for kaons, while reducing the large background of pions. All tracks that are incompatible with the kaon hypothesis are rejected. This implies that particles without particle identification are in general accepted. The HADIDENT kaon flags are used that combine both RICH and dE/dx information [21], see section 2.3.1. No attempt is made to distinguish kaons from protons, and no particle identification is required for the pion track candidate.

For decays in the $\phi\pi$ channel that belong to the D_sh sample, at least one of the kaon candidates is required to have very loose kaon identification. In the $K^{*0}K$ channel both kaon candidates are required to have positive kaon identification. A slight distinction is made between the kaon from the K^{*0} decay compared to the bachelor kaon:

- kaon from K^{*0} identified as loose

- bachelor kaon:
  if $p > 3$ GeV/c then very loose identification is required
  if $p < 3$ GeV/c then loose identification is required

The last condition reflects a higher background for low momentum tracks, which requires stricter kaon identification. Decays recorded in 1994 can benefit from data taken with the liquid RICH, which provides ring identification in this low momentum region.

The acceptance of the particle identification criteria is studied on Monte Carlo data to be 84 % for $D_s \to \phi\pi$ decays and 49 % for $D_s \to K^{*0}K$ decays. These acceptances were calculated after all kinematical cuts were applied. The effect of the kaon identification is illustrated for simulated decays in the $\phi\pi$ channel in figure 3.6. The background is reduced by a factor 4, while the loss in signal is minimal. Since the criteria require only a loose form of kaon identification, about 50 % of the combinatorial background in the final event sample is still composed of pions.

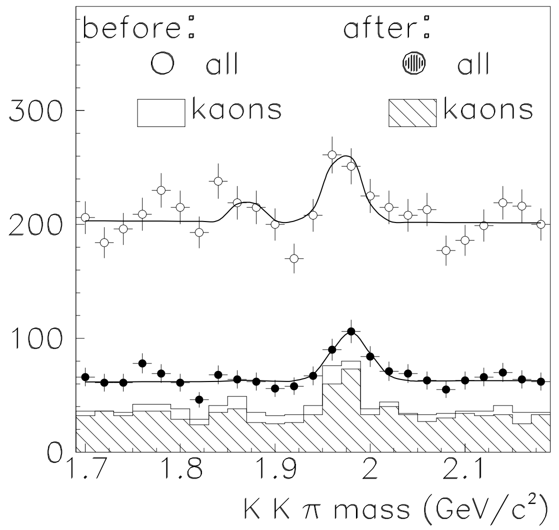

Figure 3.6: *Effect of the kaon identification. The $KK\pi$ mass spectrum is shown for simulated B_s decay candidates in the $\phi\pi$ channel. The points show the mass spectra for all decay candidates before and after the use of kaon identification. The histograms show the mass distributions of the events for which both particles are known to be kaons (or protons).*

3.5 Time-dependence of the selection criteria

Selection criteria might introduce systematic effects in the decay time distribution, by e.g. favoring high decay times. To check if any such biases are present, the time-dependence of the selection criteria is studied using simulated events.

In figure 3.7(a) the effect of requiring a positive D_s flight distance is shown. Such a cut does not bias the generated B_s flight distance nor the generated B_s proper decay time. The total efficiency of all cuts is shown as a function of the generated decay time for B_s and other B hadron decays in figures 3.7(b) and 3.7(c). Although statistics is low, there are no indications of a systematic effect.

3.6 The selected event sample

The $KK\pi$ mass spectrum of the B_s candidates, after all selection criteria are applied, is shown in figure 3.8, where the 2σ selection window is indicated by dashed lines. All data from 1991 to 1994 are used. The mass resonance from D_s meson decays is visible as a Gaussian peak above a linear spectrum of combinatorial background events. The peak is centered at 1965 ± 2 MeV/c^2, and has a width σ of 13 ± 2 MeV/c^2. The center and width will be fixed at these values in subsequent plots.

The total number of events found in the selection window is indicated by N_T. The number of D_s decays (including all sources of D_s mesons), and the number of combinatorial background events are indicated by N_S and N_B, respectively, where $N_S + N_B = N_T$. They are determined from a fit to the $KK\pi$ mass spectrum. The fitted function that is used to describe the mass spectrum consists of a linear function for the combinatorial background events and two Gaussian peaks, one for the D_s mass peak and one smaller peak for the D^+ resonance at 1.87 GeV/c^2.

The event sample is divided into D_s-lepton and D_s-hadron decay candidates, which are further subdivided into decays of the D_s meson into $\phi\pi$ and $K^{*0}K$ states. The num-

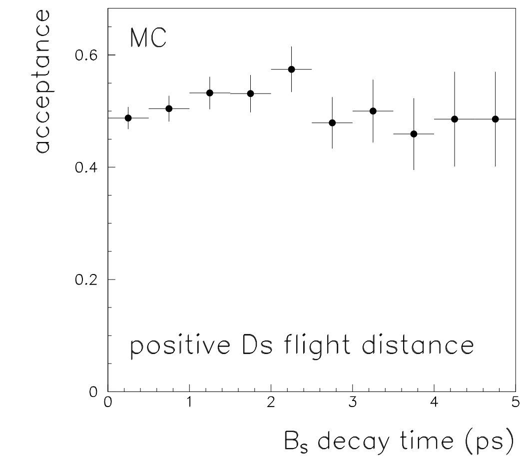

(a) Effect of a positive D_s flight on generated B_s decay time

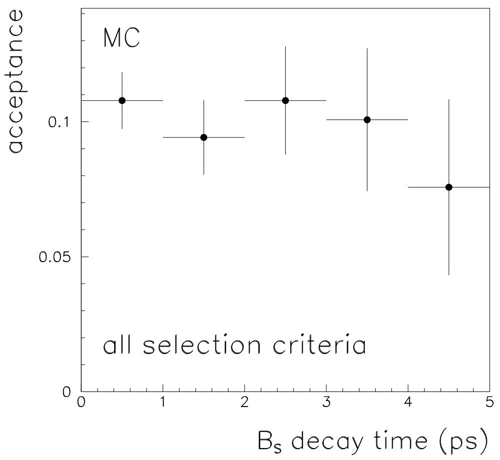

(b) Effect of all criteria on generated B_s decay time

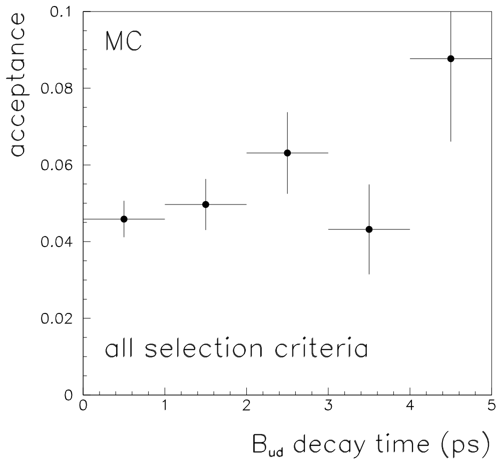

(c) Effect of all criteria on generated other B decay time.

Figure 3.7: *Efficiency versus generated decay time.*

	event class		N_T	N_S/N_T
(1)	$\phi\pi$	lepton	48	0.78 ± 0.07
(2)	$K^{*0}K$	lepton	35	0.69 ± 0.10
(3)	$\phi\pi$	hadron	226	0.32 ± 0.06
(4)	$K^{*0}K$	hadron	274	0.36 ± 0.05
	$\phi\pi$	hadron ($t > 0.5$ ps)	48	0.77 ± 0.07
	$K^{*0}K$	hadron ($t > 0.5$ ps)	55	0.65 ± 0.08

Table 3.3: *Size of the collected D_sl and D_sh final event samples.*

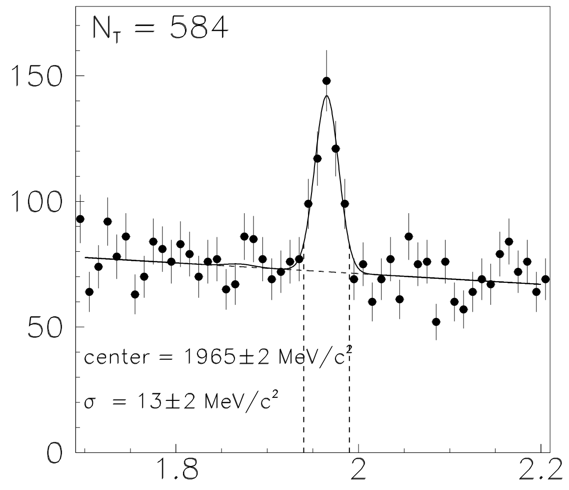

Figure 3.8: *$KK\pi$ invariant mass spectrum of all selected semi-exclusive* $\mathrm{B_s}$ *decay candidates. This figure is the sum of the mass spectra of the individual event classes shown in figures 3.9(a), 3.9(b), 3.9(c), and 3.9(d). N_T is the total number of events found in the D_s selection window.*

ber of selected candidates, for all four classes, is shown in table 3.3. The corresponding $KK\pi$ invariant mass spectra are shown in figure 3.9.

The $\mathrm{D_s}$-hadron event samples are seen to have a larger combinatorial background than decays to $\mathrm{D_s}$-lepton combinations. Most of this background is concentrated at small reconstructed decay times. To illustrate this, the $\mathrm{D_s}$-hadron mass spectra are shown in the bottom plots of figures 3.9(c) and 3.9(d), for those events that have a reconstructed decay time larger than 0.5 ps. The combinatorial background is strongly reduced above this time, which is small compared to the average B lifetime of 1.5 ps.

Fully reconstructed $\mathrm{B_s}$ decay candidates

The selected sample of hadronic $\mathrm{B_s}$ decay candidates may include fully reconstructed $\mathrm{B_s} \to \mathrm{D_s}\pi$ decays. These events would be seen as a peak in the tail of the invariant $\mathrm{D_s}$-hadron mass spectrum, shown in figure 3.10(a). In the same figure, the mass distribution is shown for a sample of simulated hadronic Z decays, and is found to match the data well.

The combinatorial background is still relatively high in the tail of the spectrum, where fully reconstructed $\mathrm{B_s}$ decays are to be found. Therefore, to check if any such decays are present, the tail of the mass spectrum is shown in figure 3.10(b), for those events of which the reconstructed decay time is larger than 0.5 ps. This reduces the background considerably. One candidate is found at the $\mathrm{B_s}$ mass of 5.4 GeV/c^2.

3.7 Event sample composition

The previous section presented the number of collected $\mathrm{D_s}$-lepton/hadron decays and the number of combinatorial background events. The collected sample, however, still consists of various sources of $\mathrm{D_s}$ mesons. The relative contributions of these sources are described in this section. With the efficiencies, obtained from a study of simulated decays, the composition of the $\mathrm{D_s}$-lepton and $\mathrm{D_s}$-hadron event samples are calculated.

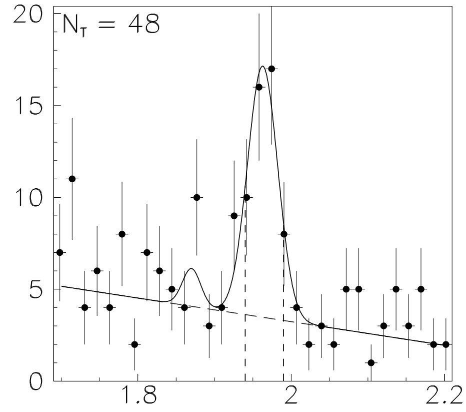

(a) $\phi\pi$-lepton

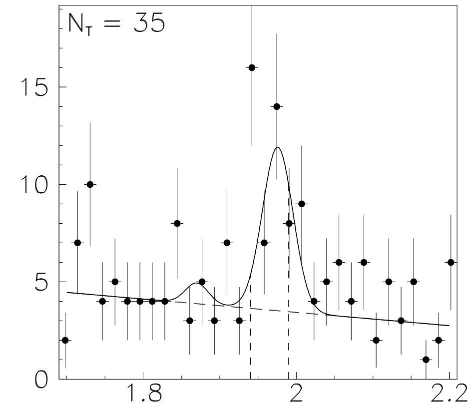

(b) $K^{*0}K$-lepton

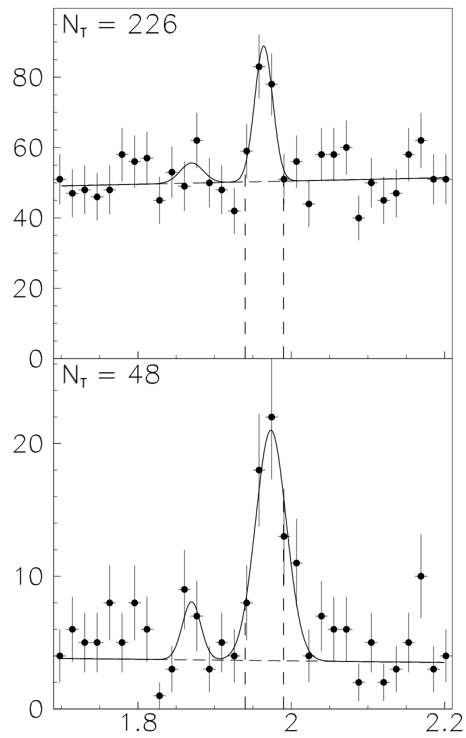

(c) $\phi\pi$-hadron, **top:** all events
bottom: reconstructed decay time > 0.5 ps

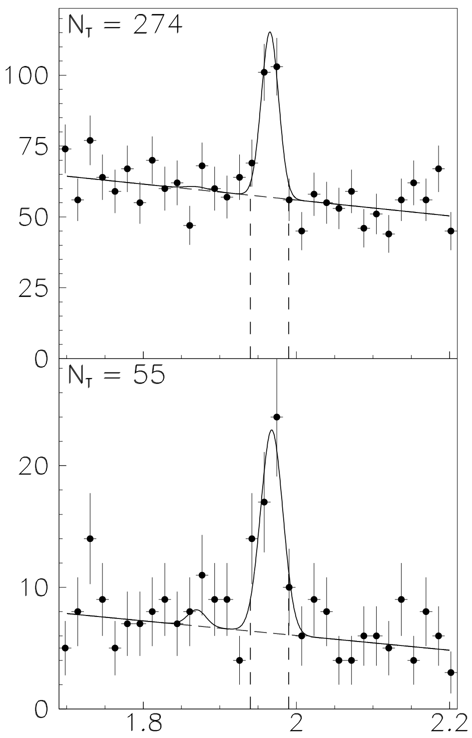

(d) $K^{*0}K$-hadron, **top:** all events
bottom: reconstructed decay time > 0.5 ps

Figure 3.9: *Invariant $KK\pi$ mass spectra of the selected B_s decay candidates, divided into four different event classes.*

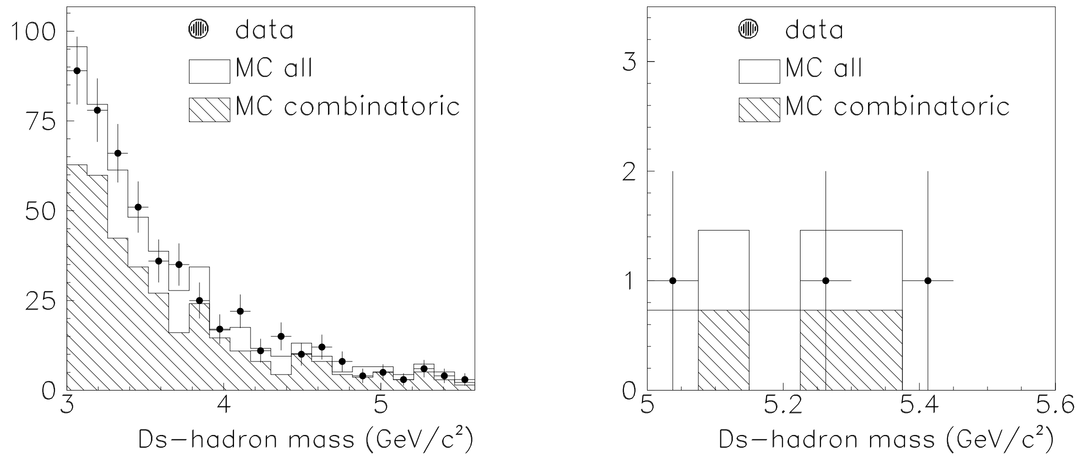

(a) D$_s$-hadron mass spectrum, all decay times

(b) Tail of the D$_s$-hadron mass spectrum, for events with a reconstructed decay time > 0.5 ps

Figure 3.10: *Fully reconstructed B_s decay candidates.*

$B1 =$	$2 \times \mathrm{BR}(b \to \mathrm{B_s} \to \mathrm{D_s} l) \times \mathrm{BR}(\mathrm{D_s} \to \phi\pi)$	$= 2 \times (0.031 \pm 0.005) \times 10^{-2}$
$B2 =$	$\mathrm{BR}(\mathrm{B_{u,d}} \to \mathrm{D_s} X) \times \mathrm{BR}(\mathrm{D_s} \to \phi\pi)$	$= (0.366 \pm 0.022) \times 10^{-2}$
$B3 =$	$\mathrm{BR}(b \to \mathrm{B_s} \to \mathrm{D_s} X) \times \mathrm{BR}(\mathrm{D_s} \to \phi\pi)$	$= (0.39 \pm 0.09) \times 10^{-2}$
$B4 =$	$\mathrm{BR}(c \to \mathrm{D_s} X) \times \mathrm{BR}(\mathrm{D_s} \to \phi\pi)$	$= (0.32 \pm 0.04) \times 10^{-2}$

Table 3.4: *Measured branching ratios of processes that produce D_s mesons, where* $\mathrm{BR}(\mathrm{D_s} \to \phi\pi) = 3.5 \pm 0.4$ %. *The complete listing is given in table B.2.*

Branching fractions

D$_s$ mesons originate from $\mathrm{Z} \to b\bar{b}$ decays and from $\mathrm{Z} \to c\bar{c}$ decays. The branching ratios of these decays relative to the total hadronic Z decay width are measured accurately at LEP [31]:

$$R_{b\bar{b}} \equiv \Gamma(\mathrm{Z} \to b\bar{b})/\Gamma(\mathrm{Z} \to \mathrm{hadrons}) = 0.2219 \pm 0.0017$$
$$R_{c\bar{c}} \equiv \Gamma(\mathrm{Z} \to c\bar{c})/\Gamma(\mathrm{Z} \to \mathrm{hadrons}) = 0.1543 \pm 0.0074$$

The measured branching ratios of processes that produce D$_s$ mesons are shown in table 3.4 (the complete list of measurements is given in appendix B). The ratios that are related to B$_s$ meson decays are measured by the LEP experiments, and ratios of B$_u$ and B$_d$ meson decays to D$_s$ mesons are measured at the $\Upsilon(4S)$ resonance.

These values, labelled $B1$–$B4$, are used to determine the production of D$_s$ mesons before any selection criteria are applied. The distribution between the various sources of D$_s$ mesons in Z decays is shown in table 3.5, where $P_s = \mathrm{BR}(b \to \mathrm{B_s}) = 0.102 \pm 0.023$ is used. This table shows that other B hadron decays produce as many D$_s$ mesons as B$_s$ decays, and that a significant fraction of the D$_s$ mesons originates from $\mathrm{Z} \to c\bar{c}$ decays.

$f(\mathrm{Z} \to b \to \mathrm{B_s} \to \mathrm{D_s} l)$	$= 2 \times R_{b\bar{b}} \times B1$	$= .028 \pm .004$ (7 %)
$f(\mathrm{Z} \to b \to \mathrm{B_s} \to \mathrm{D_s} h)$	$= 2 \times R_{b\bar{b}} \times (B3 - B1)$	$= .146 \pm .040$ (35 %)
$f(\mathrm{Z} \to b \to \mathrm{B_{u,d,baryon}} \to \mathrm{D_s} X)$	$= 2 \times R_{b\bar{b}} \times (1 - P_s) \times B2$	$= .146 \pm .010$ (35 %)
$f(\mathrm{Z} \to c \to \mathrm{D_s} h)$	$= 2 \times R_{c\bar{c}} \times B4$	$= .099 \pm .013$ (24 %)
$f(\mathrm{Z} \to \mathrm{D_s} X)$		$= .418 \pm .044$ (100 %)

Table 3.5: *Branching ratios for all sources of D_s mesons in Z decays, before any selection criteria are applied.*

source	N_{sim}	N_{pass}	efficiency
$\mathrm{B_s} \to \mathrm{D_s} l$	1709	139	$8.1 \pm .7$ %
$\mathrm{B_s} \to \mathrm{D_s} h$	3667	122	$3.3 \pm .3$ %
$\mathrm{B_{u,d,baryon}} \to \mathrm{D_s} X$	11698	238	$2.0 \pm .1$ %
$c \to \mathrm{D_s} h$	8945	136	$1.5 \pm .1$ %

Table 3.6: *Efficiencies for all sources of D_s mesons.*

Efficiencies

To determine the event sample composition after the selection criteria are applied, the efficiencies for the different sources are studied. A sample of $\mathrm{D_s}$ meson decays is used, which are generated in $Z \to q\bar{q}$ events. The result is shown in table 3.6. These efficiencies are combined with the branching fractions of the various sources as given above, to determine the event sample composition. Before this can be done the contribution of each source to the $\mathrm{D_s}$-lepton and $\mathrm{D_s}$-hadron event samples has to be studied. For this, the events passing all selection criteria are used, which are listed in the corresponding column "N_{pass}" of table 3.6.

Contributions to the $\mathrm{D_s}$-lepton and $\mathrm{D_s}$-hadron samples

Other B hadron decays produce both leptons and hadrons through the decay of the second D meson, and can therefore contribute both to the $\mathrm{D_s}$-lepton and to the $\mathrm{D_s}$-hadron event samples. In general each source may contribute both to the $\mathrm{D_s}$-lepton sample and the $\mathrm{D_s}$-hadron sample. Even a semi-leptonic $\mathrm{B_s}$ decay may contribute to the $\mathrm{D_s}$-hadron event sample, when the lepton is not identified as such. Therefore, two contribution fractions are assigned to each source: r_{lep} indicates the fraction of decays that contributes to the $\mathrm{D_s}$-lepton event sample and r_{had} indicates the fraction that contributes to the $\mathrm{D_s}$-hadron event sample. These fractions add up to one. The fraction r_{lep} is high for semi-leptonic $\mathrm{B_s}$ decays and is low for hadronic decays, where it is determined by the hadron misidentification rate. Table 3.7 shows the contributions of all sources.

The probability of selecting an additional track from the fragmentation process still has to be taken into account. In $\mathrm{Z} \to c\bar{c} \to \mathrm{D_s} X$ decays the fragmentation process is the only source of additional tracks and the mistake cannot be prevented, but also in $\mathrm{Z} \to b\bar{b} \to \mathrm{D_s} X$ events these mistakes do occur. The probabilities p_{lep} and p_{had} are assigned to each source, to indicate the fraction of decays for which the selected

sources	r_{lep}	p_{lep}	r_{had}	p_{had}
$B_s \to D_s l$	$.784 \pm .035$	$1.000 \pm .000$	$.216 \pm .035$	$.900 \pm .055$
$B_s \to D_s h$	$.049 \pm .020$	$.833 \pm .152$	$.951 \pm .020$	$.879 \pm .030$
$B_{u,d,baryon} \to D_s X$	$.118 \pm .021$	$.893 \pm .058$	$.882 \pm .021$	$.814 \pm .027$
$c \to D_s h$	$.022 \pm .013$	$.000 \pm .000$	$.978 \pm .013$	$.000 \pm .000$

Table 3.7: *Contributions of all sources of D_s mesons to the D_s-lepton and D_s-hadron event samples.*

additional lepton or hadron originates from a B decay. For B_s decays and other B hadron decays this probability is about 85 %, or as high as 100 % when the additional track is a lepton. The values for the different sources are given in table 3.7.

Composition of the D_s-lepton and D_s-hadron event samples

The resulting compositions of the D_s-lepton and D_s-hadron event samples are shown in table 3.8. From each of these tables two parameters are extracted.

The first parameter is the total fraction of decays in which the additional track originates from the fragmentation process, which corresponds to the sum of the numbers in the second column of table 3.8. This background fraction is small for the D_s-lepton event sample (4.6 ± 2.1%), and relatively large for the D_s-hadron event sample (27.9 ± 3.4 %).

The second parameter is defined as the ratio of B_s decays to $B_{u,d,baryon}$ decays:

$$R = \frac{N(B_s \to D_s l) + N(B_s \to D_s h)}{N(B_{u,d,baryon} \to D_s X)}$$

with the condition that the additional track must come from the B hadron, i.e. only the numbers from the first column are used. For the D_s-lepton event sample $R = 6.3 \pm 1.7$, and for the D_s-hadron event sample $R = 2.1 \pm 0.6$. In the D_s-hadron sample, the background from other B decays is higher, since the requirement of a high invariant D_s-hadron mass is not as efficient for hadronic B_s decays. The errors quoted here include uncertainties on the measured branching fractions and Monte Carlo statistics.

Summary of the collected event sample

From the collected event sample (table 3.3) and its composition (table 3.8), the following may be concluded: an approximately equal number of D_s-lepton and D_s-hadron candidates is selected. The addition of hadronic B_s decays to a sample of semi-leptonic B_s decays therefore increases the number of decay candidates by a factor two.

There are three types of background. The first background originates from other B hadron decays to D_s mesons. The contribution of this background is expected to be 13.1 % for the D_s-lepton sample and 23.2 % for the D_s-hadron sample. The second type of background combines a D_s meson with an additional track from the fragmentation process. This fraction is expected to be 4.6 % for the D_s-lepton sample and 27.9 % for the D_s-hadron sample. These events are concentrated at small times. The third background is the combinatorial background, which is also mainly concentrated at small

source	lepton from B	lepton from fragmentation
$B_s \rightarrow D_s l$	73.9 ± 3.6 %	$.0 \pm .0$ %
$B_s \rightarrow D_s h$	8.4 ± 4.0 %	1.7 ± 1.7 %
$B_{u,d,baryon} \rightarrow D_s X$	13.1 ± 2.4 %	$1.6 \pm .9$ %
$c \rightarrow D_s h$		$1.4 \pm .8$ %
total	95.4 ± 2.1 %	4.6 ± 2.1 %

source	hadron from B	hadron from fragmentation
$B_s \rightarrow D_s l$	4.7 ± 1.1 %	$.5 \pm .3$ %
$B_s \rightarrow D_s h$	44.1 ± 7.2 %	6.1 ± 2.2 %
$B_{u,d,baryon} \rightarrow D_s X$	23.2 ± 1.8 %	$5.3 \pm .9$ %
$c \rightarrow D_s h$		16.0 ± 2.1 %
total	72.1 ± 3.4 %	27.9 ± 3.4 %

Table 3.8: *Event sample composition for D_s-lepton candidates (top) and D_s-hadron candidates (bottom).*

times. Although the D_s-hadron sample contains more combinatorial background, a sample of similar high purity ($\sim$ 75 %) to the D_s-lepton sample is achieved at higher times, as shown in table 3.3.

The second and third background types are relatively harmless to the lifetime measurement and the measurement of the oscillation frequency, since they are mainly concentrated at zero decay time. However, the additional background from other B mesons in the D_s-hadron sample (compared to the D_s-lepton sample) does complicate the B_s lifetime measurement, since other B mesons have approximately the same lifetime. In contrast to this, the B_s oscillation frequency is much higher than that of B_d mesons, which would allow the signal to be observed above a relatively constant background spectrum. The additional sample of hadronic B_s decays will therefore carry more weight in a measurement of the oscillation frequency.

The next chapter describes the method that is used to reconstruct the proper decay time of each individual B_s decay candidate.

Chapter 4

The B_s proper decay time measurement

This chapter describes the algorithm used to obtain the proper decay time of each B_s meson candidate. Both B_s momentum and flight distance need to be reconstructed. In addition, an error on the reconstructed time is calculated for each decay, which will be used as a weight in the measurement of the average decay time. The performance is tested on a sample of simulated B_s decays.

4.1 Momentum reconstruction

As explained in the previous chapter, B_s meson decays are partially reconstructed by combining a D_s meson with an additional track of opposite charge. The combined momentum of these particles already constitutes a large fraction of the total B_s momentum. However, a significant fraction is generally missing. Here, the methods used to reconstruct the complete momentum are described. Separate methods are used for semi-leptonic and hadronic B_s meson decays.

4.1.1 Momentum reconstruction for semi-leptonic B_s decays

In semi-leptonic B_s decays all visible momentum is contained in the D_s and the lepton, as the neutrino escapes detection. An indication of the neutrino momentum is however provided by the missing energy in the hemisphere of the D_s-lepton combination. If no neutrino were present this total "hemisphere energy" would be equal to the LEP beam energy. Thus any missing energy originates from neutrinos.

To calculate the hemisphere energy, all charged tracks are included, as well as all energy depositions of neutral particles in the calorimeters. Pion masses are assumed for charged particles. Neutral particles are assigned a zero mass when identified as a photon or the mass of a neutron when identified by an energy deposition in the hadronic calorimeter.

Useful information on the missing momentum is also provided by the invariant mass of the D_s-lepton system, since a low invariant mass indicates that a large fraction of the

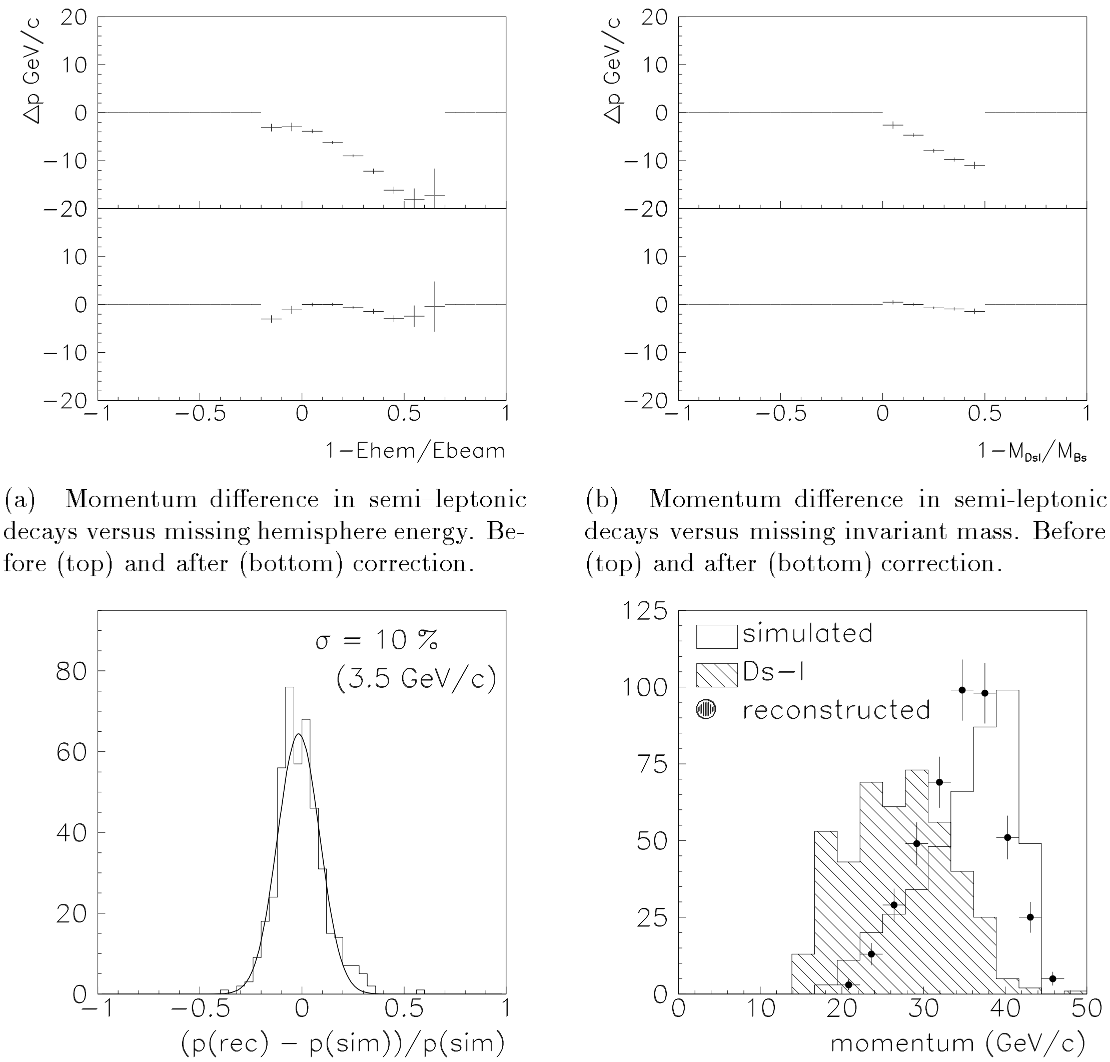

(a) Momentum difference in semi–leptonic decays versus missing hemisphere energy. Before (top) and after (bottom) correction.

(b) Momentum difference in semi-leptonic decays versus missing invariant mass. Before (top) and after (bottom) correction.

(c) Relative resolution of the reconstructed momentum for semi-leptonic B_s decays.

(d) Distribution of the simulated momentum, D_s-lepton momentum, and reconstructed momentum.

Figure 4.1: *Difference between reconstructed and simulated momentum and quality of the resulting reconstructed momentum for semi-leptonic B_s decays.*

B_s momentum is missing. Both hemisphere energy and the D_s-lepton invariant mass are therefore used to correct the combined D_s-lepton momentum $p_{D_s l}$, in order to obtain the reconstructed B_s momentum p(rec):

$$\mathrm{p(rec)} = \mathrm{p}_{\mathrm{D_s l}} + 0.4 + 21.6\,(1 - \mathrm{E_{hem}}/\mathrm{E_{beam}}) + 9.3\,(1 - \mathrm{M_{D_s l}}/\mathrm{M_{B_s}}) \qquad (4.1)$$

where the hemisphere energy is normalized to the beam energy, E_{beam}, and the invariant mass of the D_s-lepton combination is normalized to the B_s mass, M_{B_s}. Since E_{hem} and $M_{D_s l}$ are correlated, the parameter values in relation 4.1 are simultaneously determined. This is done by minimizing the average difference between reconstructed and simulated

B_s momentum using simulated B_s decays. Before the correction the difference $p(D_s l)$–p(sim) shows a clear dependence on missing hemisphere energy as well as on missing invariant mass; after the correction (for the difference p(rec)–p(sim)) the dependence has disappeared, as illustrated in figures 4.1(a) and 4.1(b).

The resulting reconstructed momentum has an absolute resolution of 3.5 GeV/c corresponding to a relative momentum resolution of 10 %, see figure 4.1(c). Figure 4.1(d) shows the momentum spectrum before and after correction, giving an indication of the size of the correction.

4.1.2 Momentum reconstruction for hadronic B_s decays

Hadronic B_s decays often produce additional particles besides the observed D_s-hadron combination. An attempt is made to include these particles in the reconstructed momentum. Both charged tracks and energy depositions of neutral particles are considered. The momenta of these particles, if found close to the combined D_s-hadron momentum direction, are added to the momentum vector. To quantify the vicinity to this axis, the rapidity y is used, which is defined as:

$$y = \frac{1}{2}\log\left(\frac{E + p_{long}}{E - p_{long}}\right) \tag{4.2}$$

where p_{long} is the longitudinal momentum of the track with respect to the D_s-hadron direction and E is the energy of the track. Individual particles are included in the reconstructed momentum if they have a rapidity $y > 1.5$ and an invariant mass with the $D_s h$ system below 5.6 GeV/c^2. On average, a momentum of 14 GeV/c is added in this way. The resulting momentum p(raw) is the sum of all selected tracks, including the D_s meson and the additional hadron.

The raw momentum is further improved by using the "hemisphere energy" and the total invariant mass of all tracks used in the raw reconstructed momentum:

$$p(rec) = p(raw) - 1.0 + 15.4\,(1 - E_{hem}/E_{beam}) + 16.6\,(1 - M_{raw}/M_{B_s}) \tag{4.3}$$

where M_{raw} is the total invariant mass of the D_s-hadron system including all additional tracks. Ideally this total mass would be equal to the B_s mass, in practice however also tracks from the fragmentation may be added and decay products from the B_s meson may be missed. This leads to a higher or lower invariant mass, respectively. Before the correction p(raw)–p(sim) depends strongly on the missing hemisphere energy and missing invariant mass. The performance of the reconstructed momentum is shown in figure 4.2. The resulting resolution is comparable to the resolution for semi-leptonic B_s decays.

4.1.3 The error on the reconstructed momentum

The error on the reconstructed momentum depends on the hemisphere energy. When there is a large missing hemisphere energy, the difference between reconstructed and

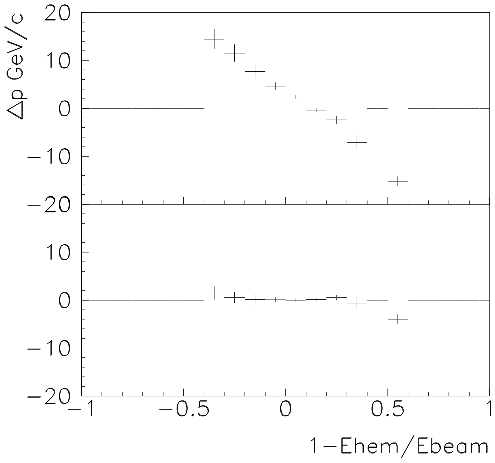

(a) Momentum difference in hadronic decays versus missing hemisphere energy. Before (top) and after (bottom) correction.

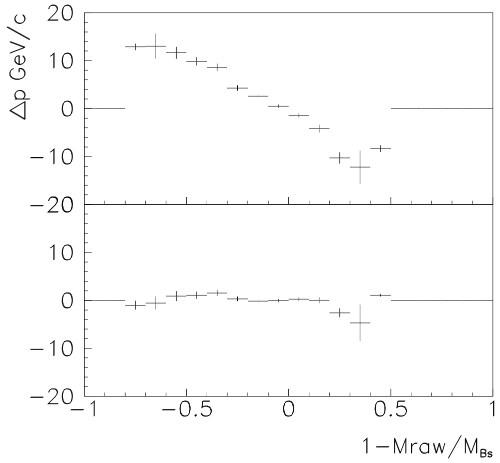

(b) Momentum difference in hadronic decays versus missing invariant mass. Before (top) and after (bottom) correction.

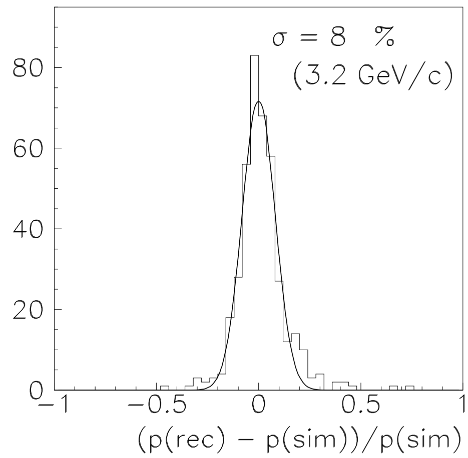

(c) Relative resolution of the reconstructed momentum for hadronic $\mathrm{B_s}$ decays.

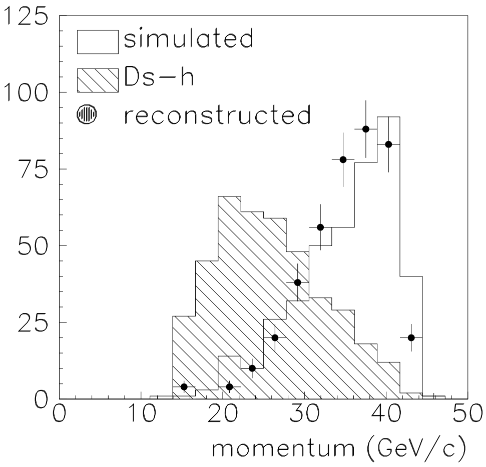

(d) Distribution of the simulated momentum, raw reconstructed momentum, and reconstructed momentum.

Figure 4.2: *Difference between reconstructed and simulated momentum and quality of the resulting reconstructed momentum for hadronic B_s decays.*

simulated $\mathrm{B_s}$ momentum tends to be large, as is shown in figure 4.3(a). The error is parameterized as follows:

$$\begin{array}{lcl} 1 - \mathrm{E_{hem}/E_{beam}} < 0 & : & \sigma_p = 2.4 - 19.7 \cdot (\, 1 - \mathrm{E_{hem}/E_{beam}}\,) \\ 1 - \mathrm{E_{hem}/E_{beam}} > 0 & : & \sigma_p = 2.4 + 5.4 \cdot (\, 1 - \mathrm{E_{hem}/E_{beam}}\,) \end{array} \tag{4.4}$$

The dependence is identical for semi-leptonic and hadronic $\mathrm{B_s}$ decays.

The pull of a quantity can be calculated on simulated data. It is defined as the difference between the reconstructed and simulated quantity, divided by the error, in this case: (p(rec)–p(sim))/σ_p. The pull distribution should be centered at zero, of Gaussian shape, and of width one. This is the case for the reconstructed momentum

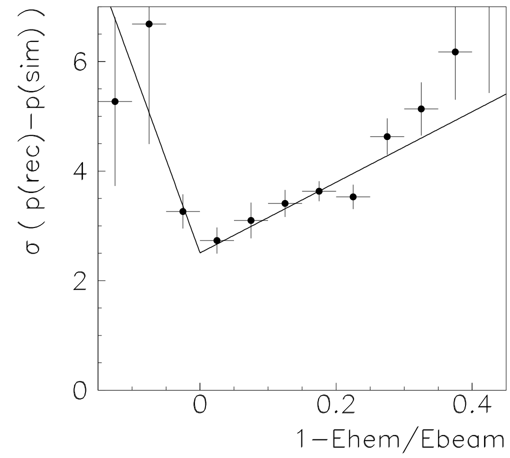

(a) Error on the reconstructed momentum as a function of the missing hemisphere energy.

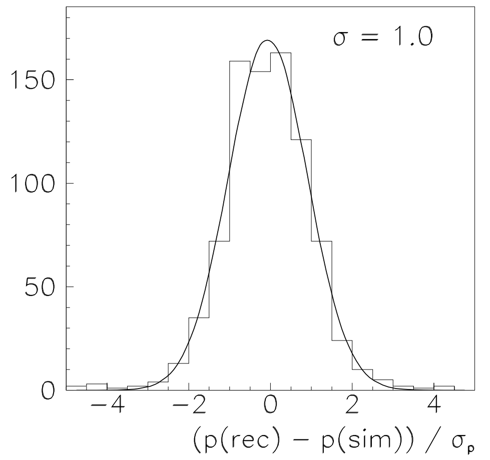

(b) Pull distribution of the reconstructed momentum.

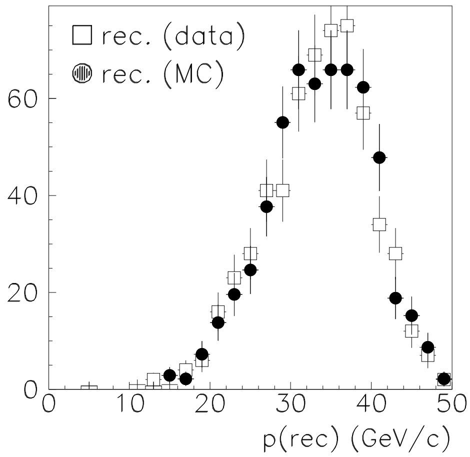

(c) Reconstructed momentum in real and simulated data.

Figure 4.3: *Determination and quality of the error on the reconstructed momentum.*

as shown in figure 4.3(b). A larger width would indicate a systematic underestimation of the error.

Figure 4.3(c) shows that there is a good agreement between the reconstructed momentum in simulated events and in "real" data events (the selected events as discussed in the previous chapter, including the combinatorial background events in the D_s peak). The difference between the mean values of these distributions in real and simulated data is 0.2 GeV, while the uncertainty on this difference is 0.4 GeV/c. The latter value will be used as the uncertainty between the reconstructed momentum in real and simulated data.

4.2 Flight distance reconstruction

Three ingredients are used to reconstruct the flight distance of the B_s meson:

1. the production vertex of the B_s meson in xy,
2. the decay vertex of the B_s meson in xy,
3. the polar angle θ of the B_s meson.

The production vertex of the B_s meson corresponds to the interaction point of the e^+e^- collision. Many charged particles in hadronic Z decays are created in the fragmentation process and originate from this interaction point. The tracks of these particles allow an accurate event-by-event reconstruction of the interaction point, which is aided by the constraint that this vertex should be within the LEP beamspot area. The interaction point is often referred to as the primary vertex of the event, in contrast to secondary decay vertices from long-lived D and B mesons.

The decay vertex of the B_s meson is determined in two consecutive steps. First the tracks of the three D_s decay products are combined into one common decay vertex. Then, the B_s decay vertex is determined by intersecting the combined D_s meson "track" with the additional lepton or hadron.

The polar angle is needed to transform the two dimensional distance to a three dimensional distance, since both the production and the decay vertex of the B_s meson are determined in the xy plane. In 1994, the Vertex Detector was upgraded with double sided detectors, to provide also a measurement of the z-coordinate. In the present analysis this information is not used, since the errors on the z-coordinate are not yet well understood.

For semi-leptonic B_s decays, the polar angle of the B_s meson is approximated by the direction of the combined D_s-lepton momentum direction, which has an accuracy of 1.8 degrees, see figure 4.4(a). For hadronic B_s decays the angle is more accurately reconstructed by using the direction of the raw reconstructed momentum. The resolution of the θ angle is then 0.8 degrees, see figure 4.4(b). Since the relative error on $1/\sin\theta$ corresponds to only 1 %, the resolution of the polar angle measurement gives a negligible contribution to the error on the proper time. At very small polar angles the error would be large, but the measurement here is restricted to the barrel region ($35^o < \theta < 145^o$). The two following sections describe the reconstruction of the B_s flight distance in more detail.

4.2.1 Reconstruction of the interaction point

The position of the beam spot varies slightly per LEP fill and may even change during a fill. It is therefore determined on a regular basis by calculating an average position for each run of about 200 collected hadronic Z decays. The shape of the beams leads to an oval beam spot with high resolution in the y direction, $\sigma_y = 10$ μm and a larger spread in the x direction, $\sigma_x = 150$ μm. The relatively large spread in x is due to the effect of Bremsstrahlung in the horizontal plane.

To obtain the interaction point with better precision than the beamspot, it is determined for each individual event. The resolution of this event-by-event primary vertex fit will not improve the resolution in the y direction beyond the beamspot size, but in the x direction it can be significantly improved.

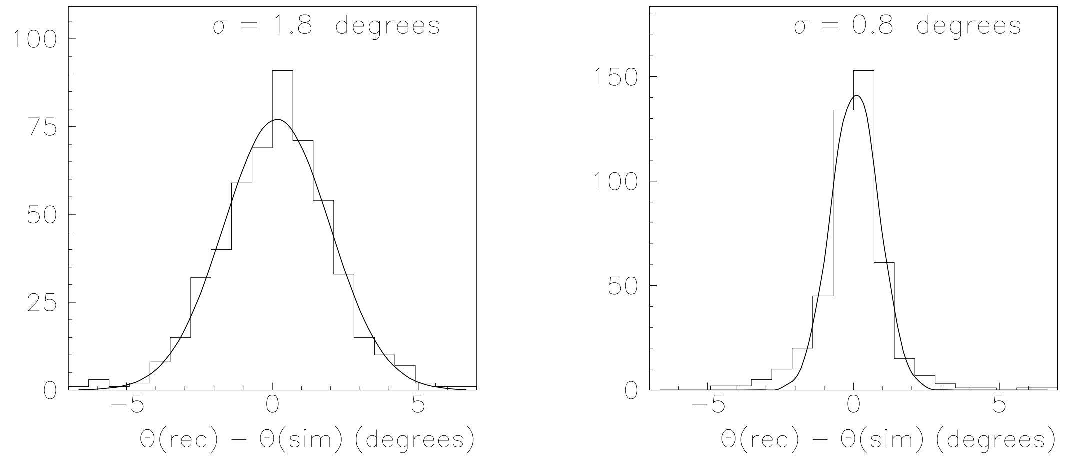

(a) Difference between reconstructed and simulated polar angle of semi-leptonically decayed B_s mesons

(b) Difference between reconstructed and simulated polar angle of hadronically decayed B_s mesons

Figure 4.4: *Resolution of the reconstructed polar angle of the B_s meson.*

In a first iteration the approximate position of the primary vertex is determined by using all charged tracks in the event. In the following iterations only tracks are used that have a distance of closest approach to the vertex position of less than 500 μm in the xy plane and 1 cm in the z direction. After each iteration the track with the largest chi–squared contribution is omitted. The iteration stops when there is no track left with a chi–squared contribution larger than 5. During this procedure the primary vertex is constrained to the beamspot area.

On average 7.6 tracks are used in the final iteration, while the procedure fails to obtain a primary vertex for 4 % of the hadronic Z decays. In these cases the average beamspot position is used. In Monte Carlo data the average number of tracks used is higher; 10.6 tracks per event. This leads to an optimistic estimate of the resolution, although the difference is expected to be negligible. As already mentioned, the result of the event-by-event primary vertex fit does not improve the resolution in the y direction beyond the beamspot resolution, see figure 4.5(a). The resulting resolution in the x direction is best described by a Cauchy distribution with Full Width at Half Maximum $\Gamma = 68$ μm, as shown in figure 4.5(b)[1]. The tails in the distribution are caused by badly measured tracks, and tracks from secondary vertices. The resolution in the x direction is: $\Gamma/2.35 = 29$ μm, a convention that shall be used throughout this thesis whenever the resolution of a Cauchy distribution is concerned[2].

4.2.2 Reconstruction of the B_s decay vertex

B_s meson decays produce D_s mesons with sufficiently high momentum to fly several hundred micrometers before decaying. Therefore, the position of the D_s meson decay

[1] The Cauchy function is defined as: $f(x) = \Gamma^2/((x-\bar{x})^2 + \Gamma^2/4)$.

[2] For a Gaussian distribution: FWHM $= 2.35 \cdot \sigma$.

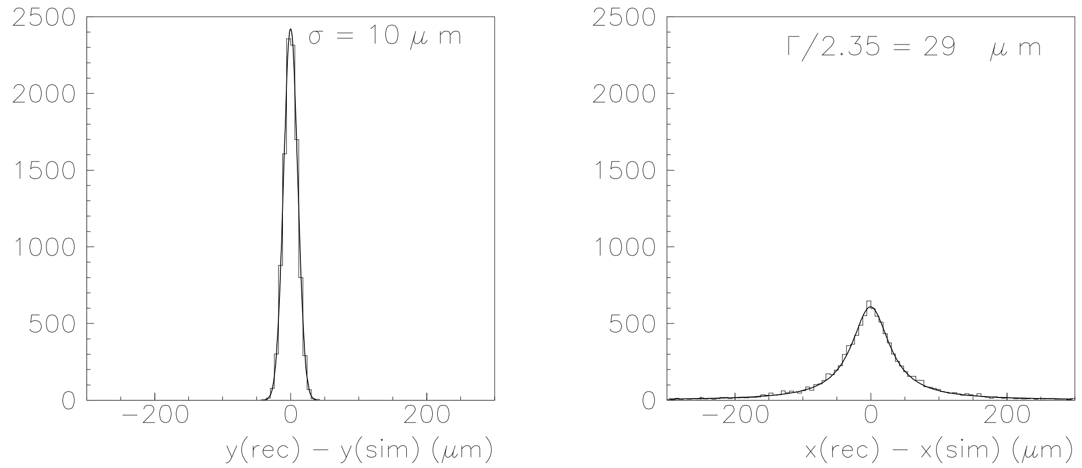

(a) Difference between reconstructed and simulated y coordinate of the primary vertex.

(b) Difference between reconstructed and simulated x coordinate of the primary vertex.

Figure 4.5: *Resolution in x and y of the primary vertex fit performed with beamspot constraint*

vertex is determined first, by fitting the three D_s decay products into one common vertex. The reconstruction of the D_s decay vertex in the xy plane has a resolution of 173 μm in the flight direction of the D_s meson (the r direction) and 13 μm in the transverse direction (the ϕ direction).

Then, a second vertex fit determines the intersection point of the D_s meson, which is now considered as one track, with the additional lepton or hadron. The B_s vertex in the xy plane is determined with a resolution of 150 μm in the flight direction and 11 μm in the transverse direction, the resolutions having Cauchy shapes.

The distance between the B_s decay vertex and the interaction point in the xy plane is determined with a resolution of 170 μm, as shown in figure 4.6(a), fitted with a Cauchy function. Based on the errors from the track reconstruction, the vertex fitting program calculates errors on the coordinates of the reconstructed vertices. These errors are used to calculate an error on the distance measurement. The pull distribution of the reconstructed B_s flight distance in the xy plane has a Gaussian distribution without tails. However, the width is 1.5 standard deviations, as shown in figure 4.6(b), which indicates an underestimation of the error. This is corrected for by multiplying the error by a factor 1.5.

The polar angle is used to transform the two dimensional B_s flight distance d(xy) and its calculated error σ(xy) to a three dimensional distance and error:

$$\begin{aligned} \mathrm{d(rec)} &= \mathrm{d(xy)}/\sin\theta \\ \sigma_d &= 1.5 \cdot \sigma(\mathrm{xy})/\sin\theta \end{aligned}$$

The resulting B_s flight distance d(rec) has a resolution of 199 μm, which has the shape of a Cauchy function, as illustrated in figure 4.6(c). It has a Gaussian pull distribution of width one. Furthermore, σ_d does not depend on the simulated flight distance, as

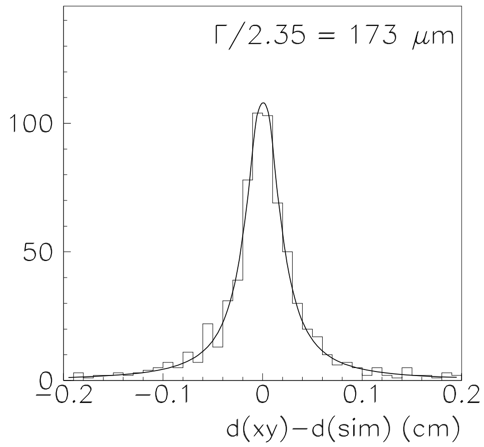

(a) Resolution of the reconstructed distance between the interaction point and the B_s vertex in xy

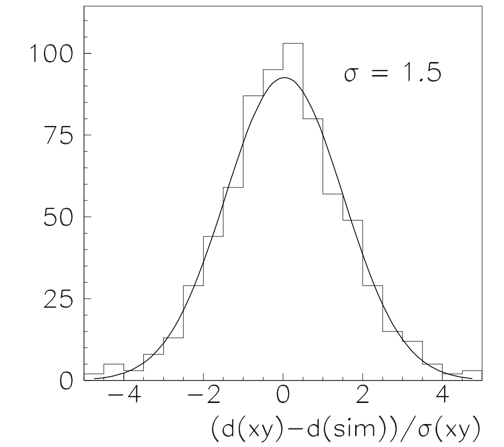

(b) Pull distribution of the distance between the interaction point and the B_s vertex in xy.

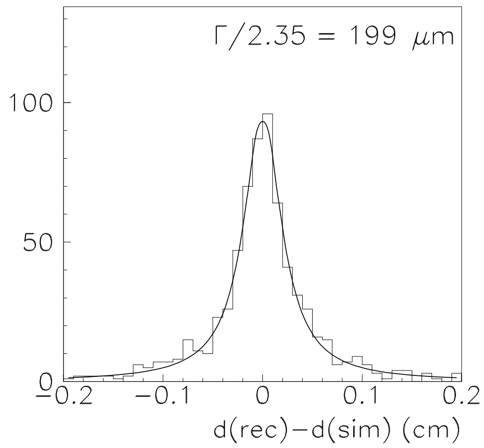

(c) Difference between reconstructed and simulated B_s flight distance in xyz

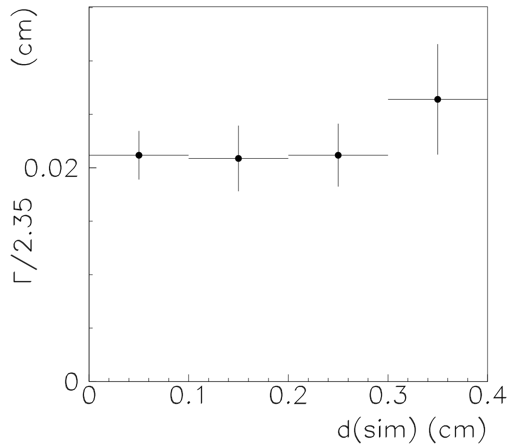

(d) Resolution of the reconstructed distance versus the simulated distance

Figure 4.6: *Quality of the reconstructed flight distance from the interaction point to the* B_s *vertex.*

shown in figure 4.6(d).

4.3 Proper time reconstruction

The reconstructed proper decay time t(rec) of the B_s meson is directly derived from the reconstructed momentum and flight distance:

$$t(rec) = \frac{M \cdot d(rec)}{c \cdot p(rec)} \tag{4.5}$$

with M in GeV/c^2 and p in GeV/c. Here, c is the speed of light, M is the B_s meson mass, p(rec) is the reconstructed momentum, and d(rec) is the reconstructed flight distance.

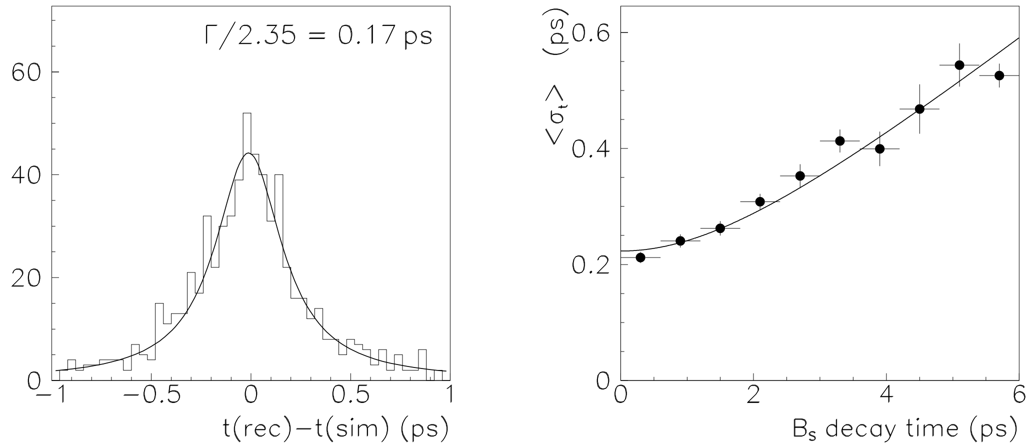

(a) Difference between reconstructed and simulated B_s proper time.

(b) The average error on the decay time as a function of the decay time.

Figure 4.7: *Quality of the reconstructed proper decay time.*

The mass of the B_s meson, as recently measured by several LEP experiments, is taken to be 5.374 ± 0.004 GeV/c^2 [28]. The difference between reconstructed and simulated proper time has a Cauchy shape with a resolution of 0.17 ps, as shown in figure 4.7(a).

The errors on the momentum, σ_p, and flight distance, σ_d, are used to calculate the error on the proper time σ_t of a B_s meson decay:

$$\sigma_t = \mathrm{t(rec)}\sqrt{\left(\frac{\sigma_d}{\mathrm{d(rec)}}\right)^2 + \left(\frac{\sigma_p}{\mathrm{p(rec)}}\right)^2} \tag{4.6}$$

This error will be used as a weight in the measurement of the average B_s decay time. The pull distribution of the reconstructed proper time is checked to be of Gaussian shape with width one, as shown in figure 4.8(a).

It should be noted that the error on the decay time increases with the decay time itself, as is shown in figure 4.7(b). This effect becomes clear when equation 4.6 is rewritten as:

$$\sigma_t = \mathrm{p(rec)}^{-1}\sqrt{M^2/c^2 \cdot \sigma_d^2 + \mathrm{t(rec)}^2 \cdot \sigma_p^2} \tag{4.7}$$

At small times the error on the proper decay time is dominated by the error on the flight distance, while at large times the momentum error dominates. The error on the proper time caused by the error on the polar angle is negligible.

The algorithm which is used to reconstruct the proper decay time of B_s decays is also used on background events from other B hadron decays and on events with an additional track from the fragmentation process. In the former case, the error on the proper time σ_t tends to underestimate the real error, because in these decays the additional track tends to originate from a second D meson. This leads to a larger error on the determined B decay vertex. The pull distribution for these decays has a width of 1.4, see figure 4.8(b). Events with an additional track from the fragmentation process have a pull distribution of width 1.3, as shown in figure 4.8(c).

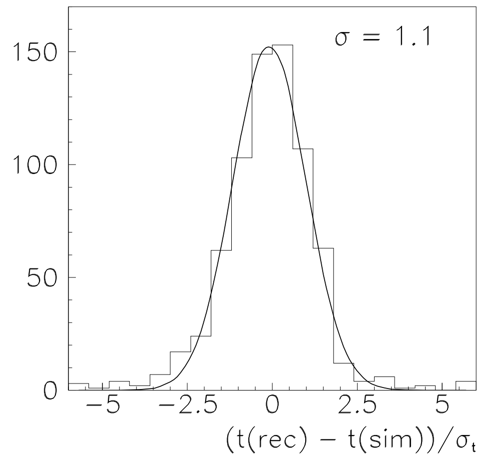

(a) Pull distribution of t(rec) for $\mathrm{B_s} \to \mathrm{D_s}X$.

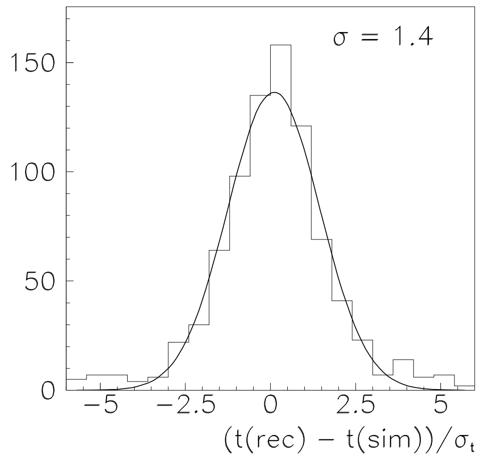

(b) Pull distribution of t(rec) for other $\mathrm{B} \to \mathrm{D_s}X$.

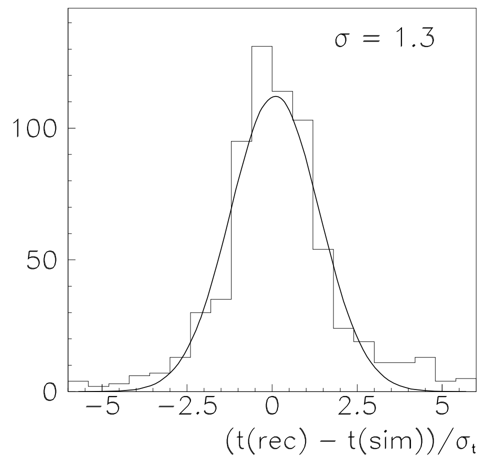

(c) Pull distribution of t(rec) for events in which the additional track originates from the fragmentation process.

Figure 4.8: *Difference between reconstructed and simulated proper time divided by the error σ_t, for the different sources of D_s mesons.*

We conclude that the proper $\mathrm{B_s}$ decay time is reconstructed on an event-by-event basis, with a high resolution of 0.17 ps. This result may be compared to the average B meson decay time, which is approximately 1.5 ps. The error on the decay time is also well understood.

4.4 D_s decay time reconstruction

The measurement of the average D_s decay time will be used as a crosscheck of the lifetime fitting procedure. Here, the algorithm used to reconstruct the D_s proper decay time is presented.

The momentum of the D_s meson is accurately known since the decay is fully reconstructed. The difference between the reconstructed and simulated momentum is distributed according to a Cauchy function with a resolution of 0.10 GeV/c, corresponding to a relative resolution of 1 %. The error on the momentum increases linearly as a function of the reconstructed momentum:

$$\sigma_p = -0.022 + 0.014 \cdot \mathrm{p}(\mathrm{D_s}) \tag{4.8}$$

where $\mathrm{p}(\mathrm{D_s})$ is the reconstructed D_s momentum in GeV/c. The resulting momentum has a pull distribution of width one.

All sources of D_s mesons will be included to measure the average D_s decay time. D_s mesons may originate from a B_s decay vertex, from another B hadron decay vertex, or from a $Z \to c\bar{c}$ decay. For all these sources, the production vertex is determined by intersecting the line of flight of the D_s meson with the additional lepton or hadron track.

The requirement of a positive D_s flight distance, as used in the selection of B_s decays, is dropped for the measurement of the D_s lifetime. The reconstructed flight distance in the xy plane has a pull distribution of width 1.6. Similar to the B_s case, the polar angle of the D_s meson is used to convert the two dimensional D_s flight distance and its error to three dimensions:

$$\begin{aligned} d(\mathrm{rec}) &= d(xy)/\sin\theta \\ \sigma_d &= 1.6 \cdot \sigma(xy)/\sin\theta \end{aligned}$$

The resolution of the flight distance d(rec) is 430 μm. It has a pull distribution of width one. The flight distance is reconstructed with less accuracy than that of the B_s meson, because here the production vertex is determined by the intersection of two relatively parallel lines, while the production vertex of the B_s meson is determined by using many charged tracks from the interaction point.

Although the flight distance resolution is worse for the D_s meson than for the B_s meson, the D_s momentum is reconstructed much more accurately. The result is a reconstructed D_s decay time that has a resolution of 0.17 ps, as shown in figure 4.9(a), which is similar to the resolution achieved for B_s decays. The pull distribution is of width one, as shown in figure 4.9(b).

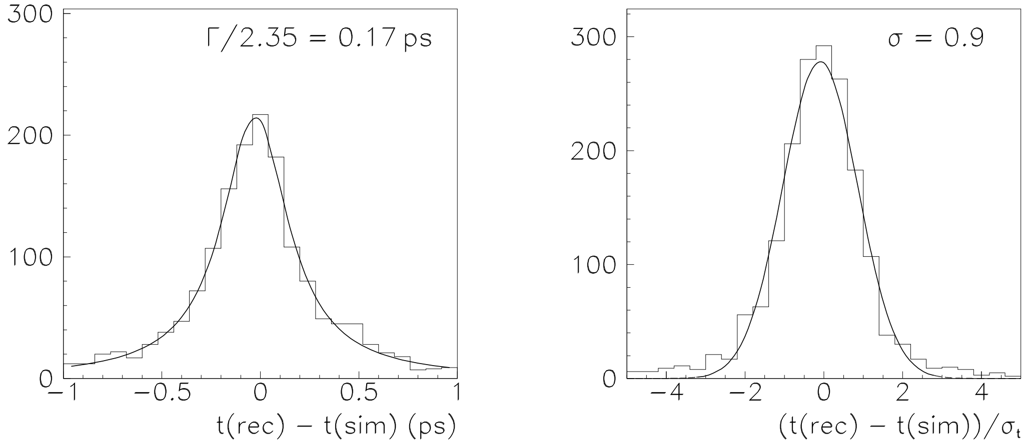

(a) Difference between reconstructed and simulated D_s proper time

(b) Difference between reconstructed and simulated D_s proper time, divided by the error.

Figure 4.9: *Quality of the reconstructed D_s proper decay time.*

Chapter 5

Measurement of the average B_s decay time

For each B_s candidate the proper decay time and its error are calculated using the methods described in the previous chapter. The resulting decay time spectra are used in this chapter to determine the average B_s decay time from an unbinned maximum likelihood fit.

5.1 The decay time spectra

In chapter 3, B_s decays were selected by the requirement that the reconstructed $KK\pi$ mass should be within the D_s peak:

	$KK\pi$ mass window
D_s peak	1.94 - 1.99 GeV/c^2

This corresponds to a window of two standard deviations around the center value of the Gaussian D_s resonance peak at 1.965 GeV/c^2. The total number of events that is selected in this window is indicated by N_T and consists of both D_s meson decays and combinatorial background events: $N_T = N_S + N_B$. The combinatorial background is not only present in the D_s selection window, but is distributed over the complete $KK\pi$ mass spectrum. The combinatorial background events in the selection window cannot be distinguished from D_s meson decays on an event-by-event basis. However, their number N_B can be obtained from a linear fit to the $KK\pi$ mass spectrum, as shown in figure 3.9.

An independent sample of events is collected from regions in the $KK\pi$ mass spectrum to the left and right of the D_s mass window:

	$KK\pi$ mass window
left sideband	1.70 - 1.80 GeV/c^2
right sideband	2.05 - 2.20 GeV/c^2

These "sideband" regions contain only combinatorial background events. The left sideband region is chosen such, that events from the $D^+ \rightarrow KK\pi$ resonance at 1.87 GeV/c^2

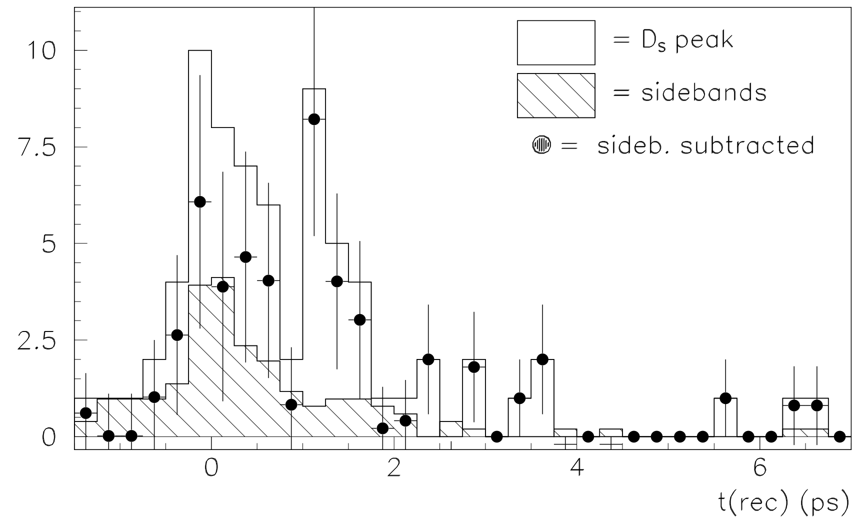

Figure 5.1: *Decay time spectrum of the selected D_s-lepton events.*

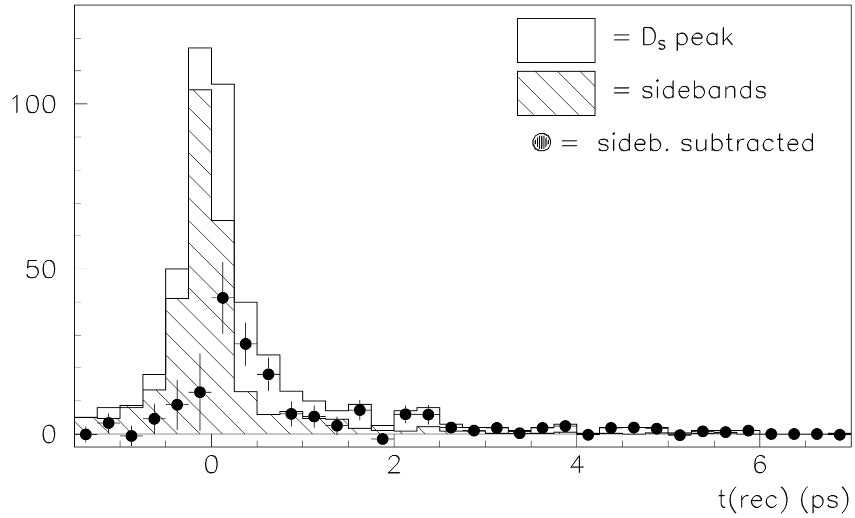

Figure 5.2: *Decay time spectrum of the selected D_s-hadron events.*

are not included. The total number of events collected in the sidebands is indicated by N'_B. Their decay time spectrum represents that of the combinatorial background events (N_B) in the D_s mass window.

The decay time spectra of the events from the D_s peak and from the sideband regions are shown in figures 5.1 and 5.2, for the D_s-lepton and D_s-hadron samples respectively. In these figures, the sideband time spectrum is normalized to the number N_B by multiplying the contents of each histogram bin with a factor $r = N_B/N'_B = 0.2$. This spectrum is subtracted from the decay time spectrum of the events in the D_s peak to yield the "combinatorial background subtracted" time distribution, as indicated by the points in figures 5.1 and 5.2.

The remaining signal (N_S) consists only of the three sources of D_s mesons: D_s mesons from B_s meson decays, D_s mesons from other B hadron decays and D_s mesons which are combined with an additional track from the fragmentation process. The following paragraphs describe the decay time spectra of these three sources of D_s mesons. To illustrate their shape, figures 5.3 and 5.4 show the decay time distributions for simulated events.

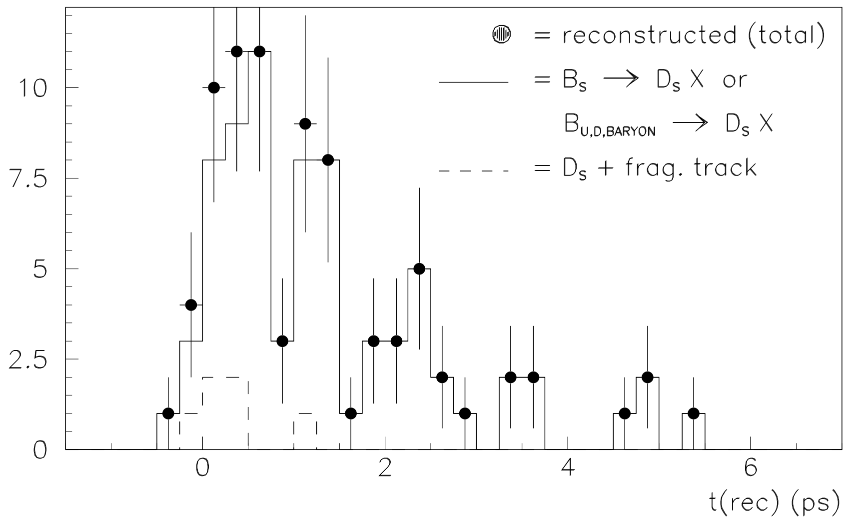

Figure 5.3: *Decay time spectrum of simulated D_s-lepton events, for all sources of D_s mesons.*

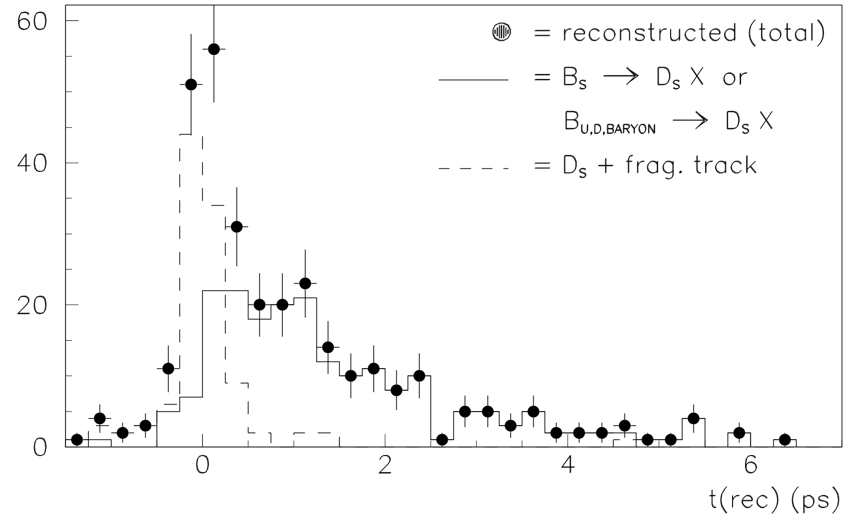

Figure 5.4: *Decay time spectrum of simulated D_s-hadron events, for all sources of D_s mesons.*

(1) $\mathbf{B_s \rightarrow D_sX}$:

The decay time spectrum of the signal from B_s decays is described by an exponential decay time function $\exp(-t/\tau)$ that is "smeared" by the experimental resolution. Here, τ is the average B_s decay time (or B_s lifetime), which is the object of our measurement. The probability of observing a measured time t_i with error σ_i is proportional to:

$$p(t_i, \sigma_i, \tau) \;=\; \frac{1}{\tau\sigma_i\sqrt{2\pi}} \int_{t=0}^{\infty} \exp(-t/\tau)\ \exp(-(t_i - t)^2/2\sigma_i^2)\ dt \qquad (5.1)$$

Equation (5.1) describes an exponential decay time distribution, that is folded with a Gaussian function which describes the experimental resolution.

Equation (5.1) can be rewritten as:

$$p(t_i, \sigma_i, \tau) \;=\; \frac{1}{2\tau} \cdot \exp\left[\frac{\sigma_i^2}{2\tau^2} - \frac{t_i}{\tau}\right] \cdot \operatorname{erf}\left[\frac{1}{\sqrt{2}}\left(\frac{\sigma_i}{\tau} - \frac{t_i}{\sigma_i}\right)\right] \qquad (5.2)$$

where $\operatorname{erf}(a) = \frac{2}{\sqrt{\pi}} \int_0^a \exp(-t^2) dt$.

(2) $B_{u,d,baryon} \rightarrow$ $\mathbf{D_sX}$**:**
D_s mesons from other B hadrons produce a decay time spectrum that is similar to the signal from B_s decays, source **(1)**, but with the average B meson lifetime $\tau(B) = 1.537 \pm 0.021$ ps [34]. The error on the proper time is larger for this type of decays, since the additional track often originates from an intermediate long-lived D meson. Therefore the error σ_i, which was tuned for B_s decays, is multiplied by a scaling factor $s_2 = 1.4$, as determined in section 4.3.

(3) $\mathbf{D_s}$ mesons combined with an additional track from the fragmentation process:
These background events consist of a D_s meson that is combined with a track from the primary vertex of the Z decay. When these tracks are intersected with the line of flight of the D_s meson, they produce decay times centered at $t = 0$. The experimental resolution "smears" these zero times according to a Gaussian distribution:

$$g(t_i, \sigma_i) = \frac{1}{\sigma_i\sqrt{2\pi}} \exp(-t_i^2/2\sigma_i^2) \tag{5.3}$$

This background is therefore concentrated as a Gaussian function around $t = 0$. At larger times the contribution of this background is negligible, as can be seen in figures 5.3 and 5.4. Its contribution in the D_s-lepton sample is small. Since the error σ_i is tuned for B_s decays, the error for this contribution has to be multiplied by a scaling factor $s_3 = 1.3$, as determined in section 4.3.

The integrals of the decay time probability functions p and g are normalized to one, when integrated over the time spectrum t_i from $-\infty$ to $+\infty$.

5.2 Result of the maximum likelihood fit

The average B_s meson decay time is determined by maximizing the following log likelihood function:

$$\mathcal{L} = \frac{N_S}{N_T}\left[\sum_{i=1}^{N_T} \log P(t_i, \sigma_i, \tau(B_s)) - r \cdot \sum_{i=1}^{N'_B} \log P(t_i, \sigma_i, \tau(B_s))\right] \tag{5.4}$$

where P is a probability density function, which will be given explicitly in the following paragraphs. The first part of eq.(5.4) is a sum over all events in the D_s peak N_T ($= N_S + N_B$) and the second part is a sum over all sideband events N'_B. The sideband contribution is multiplied by a normalization factor $r = N_B/N'_B$ and subtracted from the likelihood. The factor N_S/N_T allows the D_s-lepton and D_s-hadron samples to be combined with their appropriate statistical weight. Function minimization and error analysis is done with the MINUIT package [36].

Since the contribution of the combinatorial background events from the sidebands is subtracted from the contribution of the events in the D_s peak, the two contributions from combinatorial background events in the likelihood cancel. The remaining contribution to the likelihood is formed by the number of D_s decays in the D_s peak (N_S), and only the decay time spectra of the three sources of D_s mesons need to be described. Thus, the decay time spectrum of the combinatorial background events does not need to be parameterized[1].

The probability to observe a D_s-lepton/hadron combination with a reconstructed decay time t_i and error σ_i is given by the sum of all three sources of D_s mesons, as presented in the previous section:

$$A(t_i, \sigma_i, \tau(B_s)) = \begin{array}{rl} f(B_s) & p(t_i, \sigma_i, \tau(B_s))+ \\ f(B_{u,d,baryon}) & p(t_i, s_2\,\sigma_i, \tau(B))+ \\ f(\text{frag}) & g(t_i, s_3\,\sigma_i) \end{array} \tag{5.5}$$

The observation of measured decay times is limited to the interval $t_i \in [t_1, t_2]$, i.e. only events with reconstructed times between t_1 and t_2 will be accepted in the fit. Therefore, the probability density function is normalized by integrating over this time interval[2]:

$$P(t_i, \sigma_i, \tau(B_s)) = A(t_i, \sigma_i, \tau(B_s)) \Bigg/ \int_{t_1}^{t_2} A(t_i, \sigma_i, \tau(B_s))\, dt_i \tag{5.6}$$

The fractions $f(B_s)$, $f(B)$ and $f(\text{frag})$ indicate the contributions of the three sources of D_s mesons in the total data sample. Their values are different for the D_s-lepton and the D_s-hadron samples. The sum of these fractions is normalized to one. The ratios of B_s meson decays to other B hadron decays $f(B_s)/f(B)$ are 6.3 ± 1.7 and 2.1 ± 0.6, as determined in section 3.7, for the D_s-lepton and D_s-hadron samples, respectively. The fraction of D_s mesons combined with a fragmentation track $f(\text{frag})$ is expected to be 27.9 ± 3.4 % for the D_s-hadron sample and only 4.6 ± 2.1 % for the D_s-lepton sample (see table 3.8).

To achieve a better estimate of this background fraction for the D_s-hadron sample, $f(\text{frag})$ is determined directly from the selected data sample. This is done by initially leaving $f(\text{frag})$ as a free parameter in the fit, in addition to the B_s lifetime, while using the complete decay time spectrum ($t_1 = -1$ ps). $f(\text{frag})$ is thus measured to be 42 ± 10 %, compatible with the expected fraction of 27.9 ± 3.4 %. At higher times the contribution of this background quickly decreases, as can be seen from the dashed histogram in figure 5.4.

The upper time limit of the observation window is fixed at $t_2 = 7$ ps. The lower time limit t_1 is chosen differently for the D_s-lepton and D_s-hadron samples. For the D_s-lepton sample, the complete decay time spectrum, $t_1 = -1$ ps, is used. For the D_s-hadron sample, a higher lower time limit is chosen to reduce the systematic error due to the description of the background from the fragmentation process. Here, the lower time limit is set at $t_1 = 0.5$ ps, where the contribution of this background is expected to be only 5 %.

All input parameters to the fit are now fixed at their standard values and the most likely value of $\tau(B_s)$ is determined. Individual fits to the D_s-lepton and D_s-hadron event samples yield:

[1] This method has e.g. also been used to determine the lifetime of B_u and B_d mesons through decays into D–lepton combinations at DELPHI [37]

[2] $\int_{t_1}^{t_2} p(t, \sigma, \tau)dt = \frac{1}{2}\left[\exp(2\alpha x - \alpha^2) \cdot \text{erf}(x) + \text{erf}(x - \alpha)\right]_{x_1}^{x_2}$
where: $\alpha = \sigma/(\sqrt{2}\tau)$, $\quad x_k = \frac{1}{\sqrt{2}}[\sigma/\tau - t_k/\sigma] \quad (k = 1, 2)$ [35]

error source		range	$\Delta\tau(B_s)$ (ps)
D_s-lepton	$f(B_s)/f(B)$	6.3 ± 1.7	
D_s-hadron	$f(B_s)/f(B)$	2.1 ± 0.6	0.005
D_s-lepton	f(frag)	$4.6 \pm 2.1\%$	
D_s-hadron	f(frag)	$42 \pm 10\%$	0.100
$\tau(B)$		1.537 ± 0.021 ps	0.005
sideband normalization factor r		0.20 ± 0.04	0.090
scaling of all errors		1 ± 0.2	0.085
scaling factor s_2		1.4 ± 0.2	0.015
scaling factor s_3		1.3 ± 0.2	0.010
momentum reconstruction		0.4 GeV/c	0.045
$\Delta\Gamma(B_s)$		15 %	0.002

Table 5.1: *Contributions to the systematic error.*

$$\begin{aligned} D_s\text{-lepton}: &\quad \tau(B_s) = 1.50 \pm 0.41 \text{ ps} \quad (t_1 = -1 \text{ ps}) \\ D_s\text{-hadron}: &\quad \tau(B_s) = 1.57 \pm 0.44 \text{ ps} \quad (t_1 = 0.5 \text{ ps}). \end{aligned}$$

The two samples have similar statistical weights N_S/N_T, and contain a similar estimated number of $B_s \to D_sX$ decays. To profit optimally from the collected statistics and to allow for correlations in the systematic errors, the final result is obtained from a simultaneous fit to the D_s-lepton and D_s-hadron samples, yielding:

$$D_s\text{-lepton/hadron}: \quad \tau(B_s) = 1.54 \pm 0.31 \pm 0.15 \text{ ps}$$

where the first error is statistical. The second error is systematic and will be discussed in detail in the following section. The decay time distributions (combinatorial background subtracted), with the result of the fitted function overlayed, are shown in figures 5.5 and 5.6. The fitted function is not straightforward to present, because each event has its own individual error. Here, the fitted curve is produced by randomly generating events according to the probability density function, with the fitted value of $\tau(B_s)$, using the same error distribution as in the fit. The fitted contribution of the background from the fragmentation process is indicated by dashed lines.

5.3 Study of the systematic error

The systematic error is obtained by varying the input parameters to the fit by one standard deviation. Table 5.1 lists the variation of all error sources and their effect on the measured lifetime. The background fraction f(frag) and the ratio $f(B_s)/f(B)$ are varied simultaneously for the D_s-lepton and D_s-hadron sample. To account for possible differences between the real and simulated data, all errors σ_i on the proper time are scaled by ± 20 %. In addition only the error scaling factors s_2 and s_3 are varied.

Since the B_s meson decays are only partially reconstructed, the uncertainty of the B_s momentum reconstruction introduces a systematic error. Therefore, a possible difference in the momentum reconstruction for real and simulated events of ± 0.4 GeV/c

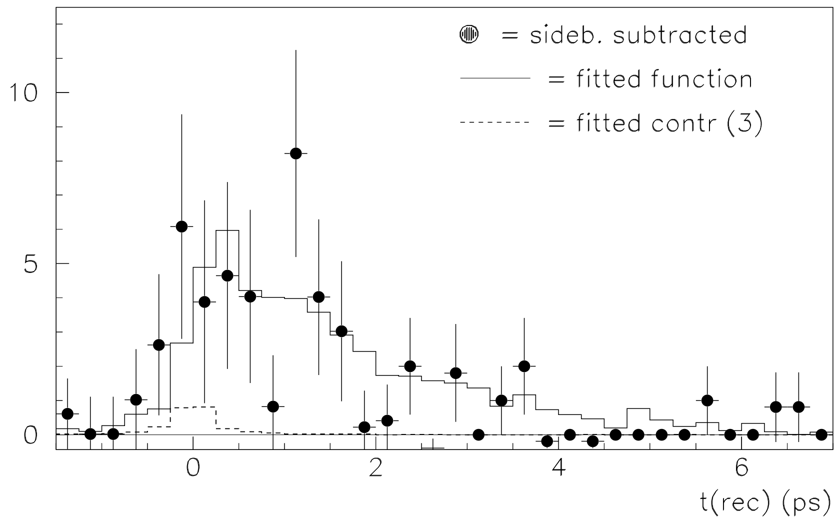

Figure 5.5: *Decay time spectrum of the D_s-lepton events, with the result of the fitted function overlayed.*

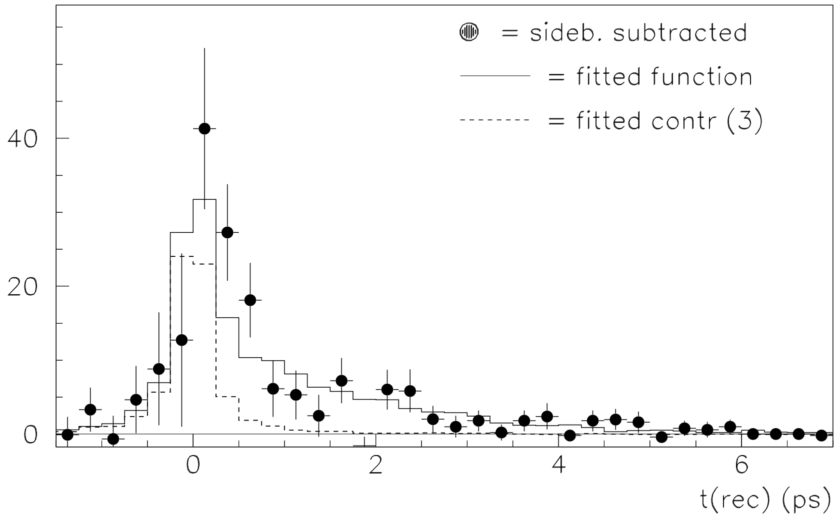

Figure 5.6: *Decay time spectrum of the D_s-hadron events, with the result of the fitted function overlayed.*

is taken into account, as described in section 4.1.3, see also figure 4.3(c). A possible lifetime difference of 15 % between the two CP eigenstates is included and is found to have a negligible effect on the lifetime. To account for possible correlations between the different error sources, they are all varied simultaneously around their central value, according to a Gaussian distribution. This is done in a random way and repeated 100 times. The distribution of the fitted lifetimes is shown in figure 5.7. The combined systematic error is obtained from the standard deviation of this distribution, which is determined to be 0.15 ps.

Relatively large systematic errors originate from the uncertainty in the contribution of background from the fragmentation process $f(\text{frag})$ and from the sideband normalization factor r. Since these quantities are determined directly from the data, they can be more accurately determined with increasing statistics.

Finally, we study the effect of varying the lower time limit in the D_s-hadron sample. The fitted lifetime as a function of the lower time limit is shown in figure 5.8, where the plotted errors are purely statistical. The dashed lines indicate the limits of the systematic error (± 0.15 ps) at $t_1 = 0.5$ ps. The fitted lifetime varies within the expected

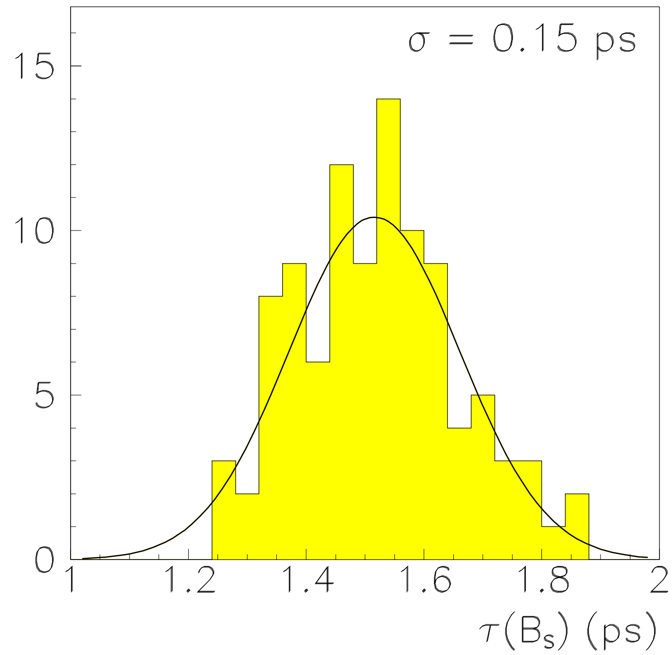

Figure 5.7: *Determination of the total systematic error.*

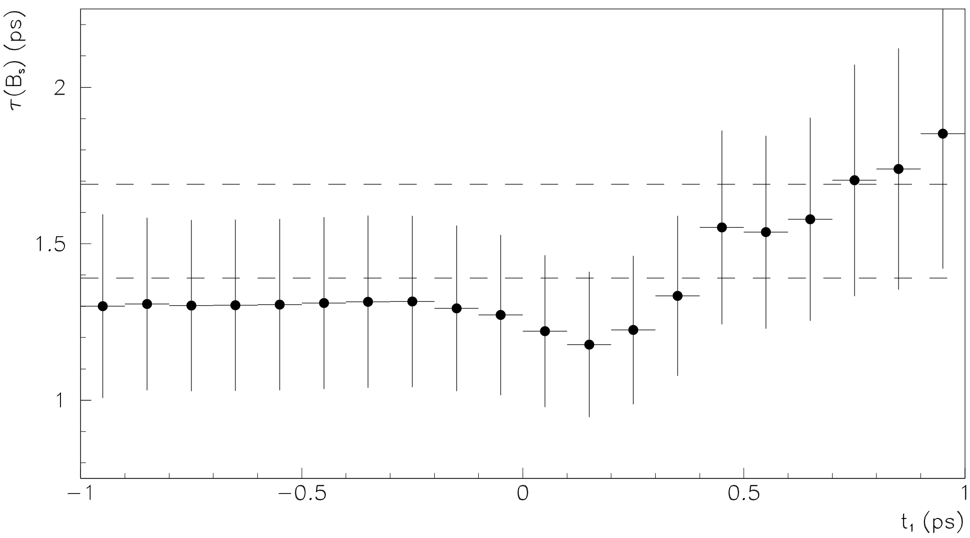

Figure 5.8: *Fitted lifetime as a function of the lower time limit.*

statistical and systematic errors. Below $t_1 = 0.5$ ps there is a large influence from the background from the fragmentation in the D_s-hadron sample and from statistical variations in the sideband sample. At limits t_1 above 0.5 ps, events with valuable lifetime information are lost and the statistical error increases. Note that the fitted lifetimes at different lower limits as shown in figure 5.8 are statistically correlated.

We conclude that the systematic error is 0.15 ps, a factor two smaller than the statistical error and that increasing statistics would allow this systematic error to decrease.

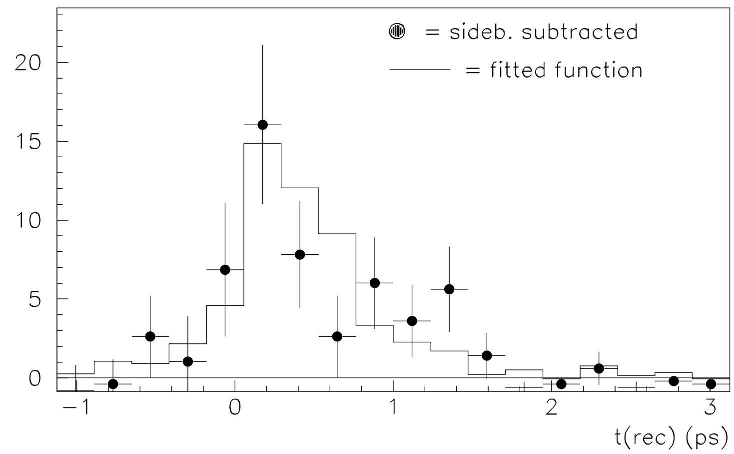

Figure 5.9: *Reconstructed D_s decay time, for D_s-lepton events.*

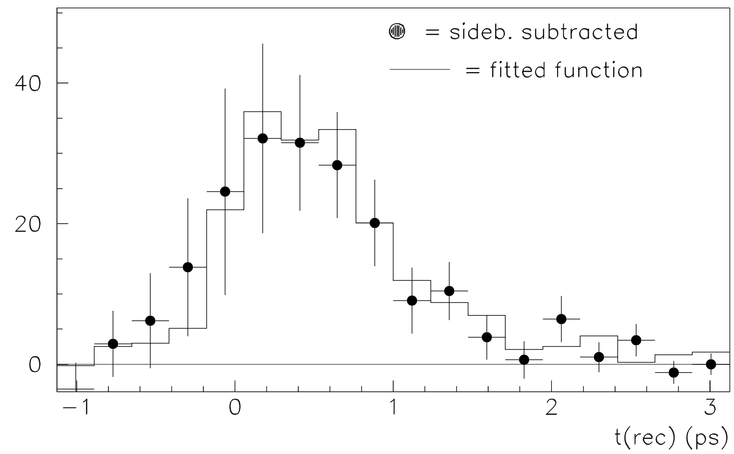

Figure 5.10: *Reconstructed D_s decay time, for D_s-hadron events.*

5.4 Measurement of the $\mathrm{D_s}$ lifetime

As a cross-check of the lifetime measurement, also the well-known $\mathrm{D_s}$ lifetime is measured. All sources of $\mathrm{D_s}$ mesons are used. The algorithm that is used to reconstruct the $\mathrm{D_s}$ decay times on an event-by-event basis is described in section 4.4. The $\mathrm{D_s}$ meson decay time spectra (combinatorial background subtracted) are shown in figures 5.9 and 5.10 for the $\mathrm{D_s}$-lepton and $\mathrm{D_s}$-hadron samples, respectively.

The probability density function consists of an exponential decay time function folded with a Gaussian resolution function. The average $\mathrm{D_s}$ decay time is measured to be:

$$\begin{aligned} \mathrm{D_s}\text{-lepton}: &\quad \tau(\mathrm{D_s}) = 0.43 \pm 0.10 \text{ ps} \\ \mathrm{D_s}\text{-hadron}: &\quad \tau(\mathrm{D_s}) = 0.54 \pm 0.10 \text{ ps} \\ \text{combined}: &\quad \tau(\mathrm{D_s}) = 0.49 \pm 0.07 \text{ ps} \end{aligned}$$

which is compatible with the measured world average value of 0.467 ± 0.017 ps [6].

experiment	reconstruction mode	τ (ps)	reference
DELPHI	D_s-lepton/hadron	$1.54 \pm 0.31 \pm 0.15$	this thesis
DELPHI	D_s-lepton, D_s-hadron, ϕX-lepton, D_sX	1.67 ± 0.14	[58]
ALEPH	D_s-hadron	$1.61^{+0.30}_{-0.29}{}^{+0.18}_{-0.16}$	[59]
ALEPH	D_s-lepton	$1.54^{+0.14}_{-0.13} \pm 0.04$	[60]
OPAL	D_s-lepton	$1.54^{+0.25}_{-0.21} \pm 0.06$	[61]
CDF	D_s-lepton	$1.42^{+0.27}_{-0.23} \pm 0.11$	[62]
CDF	$J/\psi\phi$	$1.34^{+0.23}_{-0.19} \pm 0.05$	[63]
world average B_s lifetime		$1.34^{+0.32}_{-0.27}$	PDG (1994) [6]
world average B_s lifetime		$1.61^{+0.10}_{-0.09}$	PDG (1996) [64]
world average B_d lifetime		1.56 ± 0.06	PDG (1996) [64]

Table 5.2: *Current status of the B_s lifetime measurement. When two errors are given the first error is statistical and the second error is systematic.*

5.5 Conclusions

Table 5.2 shows the current status of the B_s lifetime measurements. The measured lifetime presented in this thesis is compatible with the world average value. The large data samples recently collected at LEP and at the Tevatron (where B_s mesons are produced in $p\bar{p}$ collisions at $\sqrt{s} = 1.8$ TeV) have led to a great improvement of the measured B_s lifetime. The second DELPHI result listed in table 5.2 includes also two other decay channels that are not discussed here ($B_s \rightarrow D_sX$ and $B_s \rightarrow \phi$X-lepton). These reconstruction modes yield more statistics but are less pure in B_s decays.

The world average B_d lifetime is also listed. It is more accurately known than the B_s lifetime, since the relative production of B_d mesons is higher. The world average B_d and B_s lifetimes are equal at the level of 10 %. This is consistent with Heavy Quark Effective Theory, which predicts that this lifetime difference should be equal within 1 %. Given this accurate theoretical prediction, it is still up to the experiments to improve the accuracy of the lifetime measurements. Unfortunately, no more data will be taken at LEP at the energy of the Z resonance. The latest data were taken in 1995 and are not included in the present results. For DELPHI, this data will add approximately 0.7 million hadronic Z decays to the 3 million decays used here. Highly accurate lifetime measurements will become possible at future experiments, expected to start data-taking around the year 2000 [41], where an abundant number of B decays will be collected, e.g. at hadron colliders, allowing the use of full reconstruction methods.

Appendix A

The neutral B meson system

The neutral B meson is in general a superposition of B^0 and $\overline{\mathrm{B}^0}$ states, since oscillations between the two states may occur. There are two CP eigenstates, which may have different lifetimes. In this appendix the time evolution of these states is derived, and the subject of CP violation is briefly introduced, since it is, in the framework of the Standard Model, closely related to the oscillations. At LEP, measurements of CP violation are beyond reach, since the number of collected B decays is too small.

A.1 Time evolution

The state vector of a neutral B meson is in general a superposition of a B^0 and a $\overline{\mathrm{B}^0}$ particle:

$$|\psi(t)> = \psi_1(t)\,|\mathrm{B}^0> + \psi_2(t)\,|\overline{\mathrm{B}^0}> \tag{A.1}$$

This vector satisfies the Hamiltonian equation:

$$i\frac{\partial\,|\psi(t)>}{\partial t} = H\,|\psi(t)> \tag{A.2}$$

where the Hamiltonian is a 2×2 matrix in the B^0-$\overline{\mathrm{B}^0}$ base, with matrix elements:

$$\begin{array}{ll} H_{11} = <\mathrm{B}^0\,|H\,|\mathrm{B}^0> & H_{12} = <\mathrm{B}^0\,|H\,|\overline{\mathrm{B}^0}> \\ H_{21} = <\overline{\mathrm{B}^0}\,|H\,|\mathrm{B}^0> & H_{22} = <\overline{\mathrm{B}^0}\,|H\,|\overline{\mathrm{B}^0}> \end{array} \tag{A.3}$$

H can be decomposed into two Hermitian matrices M and Γ:

$$H\begin{pmatrix} \mathrm{B}^0 \\ \overline{\mathrm{B}^0} \end{pmatrix} = \begin{pmatrix} M_{11} - \frac{1}{2}i\Gamma_{11} & M_{12} - \frac{1}{2}i\Gamma_{12} \\ M_{21} - \frac{1}{2}i\Gamma_{21} & M_{22} - \frac{1}{2}i\Gamma_{22} \end{pmatrix}\begin{pmatrix} \mathrm{B}^0 \\ \overline{\mathrm{B}^0} \end{pmatrix} \tag{A.4}$$

CPT invariance requires $H_{11} = H_{22}$.

The physically observed mass eigenstates $|\mathrm{B_L}>$ and $|\mathrm{B_H}>$ satisfy the Schrödinger equations:

$$\begin{aligned} i\frac{d\,|\mathrm{B_L}>}{dt} &= M_L\,|\mathrm{B_L}> \\ i\frac{d\,|\mathrm{B_H}>}{dt} &= M_H\,|\mathrm{B_H}> \end{aligned} \tag{A.5}$$

To obtain the solutions of these eigenvalue equations, the Hamiltonian is diagonalized, which yields:

$$\begin{aligned} M_L &= H_{11} + iqp \\ M_H &= H_{11} - iqp \end{aligned} \tag{A.6}$$

p and q are defined as $p^2 = iH_{12}$ and $q^2 = iH_{21}$. The subscripts L and H denote respectively the light and heavy eigenstates:

$$\begin{aligned} |\,\mathrm{B_L}> &= \tfrac{1}{\sqrt{p^2+q^2}}\left(p\,|\,\mathrm{B^0}> + \,q\,|\,\overline{\mathrm{B^0}}>\right) \\ |\,\mathrm{B_H}> &= \tfrac{1}{\sqrt{p^2+q^2}}\left(p\,|\,\mathrm{B^0}> - \,q\,|\,\overline{\mathrm{B^0}}>\right) \end{aligned} \tag{A.7}$$

CP is the simultaneous operation of Charge conjugation and inversion of Parity. Charge conjugation converts a particle to its anti-particle and the parity operation performs a reflection in space. Neutral B mesons transform like a pseudoscalar under the parity operation P, which gives:

$$\begin{aligned} \mathrm{CP}\,|\,\mathrm{B^0}> &= \eta_{CP}\,|\,\overline{\mathrm{B^0}}> \\ \mathrm{CP}\,|\,\overline{\mathrm{B^0}}> &= \eta_{CP}\,|\,\mathrm{B^0}> \end{aligned} \tag{A.8}$$

Choosing the phase $\eta_{CP} = -1$, the eigenstates of the CP operator are:

$$\begin{aligned} |\,\mathrm{B_2^0}> &= \tfrac{1}{\sqrt{2}}\left(|\,\mathrm{B^0}> + \,|\,\overline{\mathrm{B^0}}>\right) \\ |\,\mathrm{B_1^0}> &= \tfrac{1}{\sqrt{2}}\left(|\,\mathrm{B^0}> - \,|\,\overline{\mathrm{B^0}}>\right) \end{aligned} \tag{A.9}$$

$$\begin{aligned} \mathrm{CP}\,|\,B_2^0> &= -\,|\,\mathrm{B_2^0}> \\ \mathrm{CP}\,|\,B_1^0> &= \quad |\,\mathrm{B_1^0}> \end{aligned} \tag{A.10}$$

which correspond to the mass eigenstates $|\,\mathrm{B_L}>$ and $|\,\mathrm{B_H}>$, in case of CP invariance. If $p \neq q$, CP is violated, i.e. the mass eigenstates $|\,\mathrm{B_L}>$ and $|\,\mathrm{B_H}>$ are no longer orthogonal:

$$<\mathrm{B_L}\,|\,\mathrm{B_H}> = \frac{p^2 - q^2}{p^2 + q^2} \neq 0 \tag{A.11}$$

To study the time evolution of the neutral B system, the state vector is rewritten as a superposition of the mass eigenstates $|\,\mathrm{B_L}>$ and $|\,\mathrm{B_H}>$:

$$|\,\psi(t)> = A_L(t)\,|\,\mathrm{B_L}> + A_H(t)\,|\,\mathrm{B_H}> \tag{A.12}$$

with amplitudes for the states $\mathrm{B_L}$ or $\mathrm{B_H}$ as a function of t:

$$\begin{aligned} A_L(t) &= A_L(0)e^{-(\Gamma_L/2 + iM_L)t} \\ A_H(t) &= A_H(0)e^{-(\Gamma_H/2 + iM_H)t} \end{aligned} \tag{A.13}$$

In the experiment the particles are produced in a pure $\mathrm{B^0}$ state or a pure $\overline{\mathrm{B^0}}$ state, because they originate from the production of a $b\bar{b}$ quark pair. At production time $t = 0$ the amplitudes must then be:

$$\begin{aligned} A_L(0) = \quad A_H(0) &= \tfrac{1}{2p} \quad \text{, for } |\,\psi(0)> = |\,\mathrm{B^0}> \\ A_L(0) = -A_H(0) &= \tfrac{1}{2q} \quad \text{, for } |\,\psi(0)> = |\,\overline{\mathrm{B^0}}> \end{aligned} \tag{A.14}$$

Combining equations A.7, A.12, A.13, and A.14 the time evolution of the states becomes:

$$\begin{array}{ll} |\psi(t)\!>= \frac{1}{2\sqrt{p^2+q^2}}[& g_+(t)\,|\mathrm{B}^0\!> \;+\; (q/p)g_-(t)\,|\overline{\mathrm{B}^0}\!>\;] \\ |\psi(t)\!>= \frac{1}{2\sqrt{p^2+q^2}}[& (p/q)g_-(t)\,|\mathrm{B}^0\!> \;+\; g_+(t)\,|\overline{\mathrm{B}^0}\!>\;] \end{array} \tag{A.15}$$

Where,

$$\begin{aligned} g_+(t) &= e^{-(\Gamma_L/2+iM_L)t} + e^{-(\Gamma_H/2+iM_H)t} \\ g_-(t) &= e^{-(\Gamma_L/2+iM_L)t} - e^{-(\Gamma_H/2+iM_H)t} \end{aligned} \tag{A.16}$$

If $\Gamma_L = \Gamma_H$:

$$\begin{aligned} g_+(t) &= e^{-\frac{1}{2}\Gamma t}e^{-iMt}\cos(\tfrac{1}{2}\Delta Mt)\cdot 2 \\ g_-(t) &= e^{-\frac{1}{2}\Gamma t}e^{-iMt}\sin(\tfrac{1}{2}\Delta Mt)\cdot 2i \end{aligned} \tag{A.17}$$

M is defined as $(M_H + M_L)/2$ and ΔM as $M_H - M_L$.

The lifetime τ is $1/\Gamma$ and the oscillation frequency x is defined as $x = \Delta M/\Gamma$. Starting at $t = 0$ from a meson in a pure $|\,B^0\!>$ state, the probabilities that it decays at time $t > 0$ as $|\mathrm{B}^0\!>$ or $|\overline{\mathrm{B}^0}\!>$, respectively, are (in the limit of $p = q$):

$$|\psi(0)\!> \;=\; |\mathrm{B}^0\!> \tag{A.18}$$

$$\begin{aligned} P(\mathrm{B}^0 \to \mathrm{B}^0) &= |\!<\mathrm{B}^0\,|\psi(t)\!>|^2 = \tfrac{1}{4}\,|g_+|^2 = e^{-t/\tau}\cos^2(xt/2\tau) \\ P(\mathrm{B}^0 \to \overline{\mathrm{B}^0}) &= |\!<\overline{\mathrm{B}^0}\,|\psi(t)\!>|^2 = \tfrac{1}{4}\,|g_-|^2 = e^{-t/\tau}\sin^2(xt/2\tau) \end{aligned} \tag{A.19}$$

where τ is the average B^0 meson lifetime.

A.2 CP violation

The neutral kaon system is the only place where CP violation has been observed [1]. Another space–time symmetry operator is time reversal T. Invariance of the laws of nature under the product CPT is a condition for most relativistic field theories and results in equal quantities for masses and lifetimes of particles and anti–particles. No evidence for CPT invariance has been observed [6].

The well-known neutral kaon system has proven to be a valuable tool in the understanding of fundamental topics such as the Quark Model, Quantum Mechanics, and CP violation. Some of the main differences with respect to the neutral B system will be discussed here. Unfortunately, theoretical calculations in the kaon system are complicated, as non-perturbative effects are much larger than in the heavy B system. Measurements in the kaon system are therefore more difficult to translate to measurements of CKM matrix elements.

In contrast to the heavy B meson decays, the phase space and the number of decay modes for kaon decays is limited. One of the main decay modes results in two pions,

[1] The observed matter-antimatter asymmetry in the universe is also thought to be a consequence of CP violating processes [39]. Assuming that the net baryon number was initially zero, then baryon number violating processes should have occurred, and CP violation would be necessary to ensure that the rates of the inverse processes are different.

system	τ (10^{-12} s)	$y = \Delta\Gamma/\Gamma$	Δm (ns^{-1})	$x = \Delta m/\Gamma$
K^0-$\overline{K^0}$	89 $\leftrightarrow$ 51700	~ 100 %	5.333 ± 0.027	
D^0-$\overline{D^0}$	0.415 ± 0.004	< 17 %	< 200	< 0.1
B^0_d-$\overline{B}^0_d$	~ 1.5	< 1 %	465 ± 20	0.7
B^0_s-$\overline{B}^0_s$	~ 1.5	~ 15 %	> 5000	> 7.5

Table A.1: *Comparison between the different neutral meson systems*

with a state of zero angular momentum, which transforms as a CP even state. If CP is not violated this decay mode is therefore only allowed for the K^0_1 state and the K^0_2 state is only allowed to decay into three particle states. Because the available phase space for three particle decays is very small, the K^0_2 state will have a much longer lifetime than the K^0_1 state. The observed lifetime difference is indeed very large, which has led to the names 'short' and 'long' for the K^0_1 and K^0_2 states respectively. In 1964 it was discovered that a small fraction 2×10^{-3} of the long lived (CP odd) kaons does decay into a (CP even) charged pion pair [38].

This CP violating effect is related to the oscillation of neutral kaons. In terms of the B system, it would cause a transition from $|\,B^0>$ to $|\,\overline{B^0}>$ to be different from a transition from $|\,\overline{B^0}>$ to $|\,B^0>$. In the notation of the previous section this would imply: $p \neq q$. This effect is referred to as indirect CP violation. It is expected to be very small for oscillations in the B system, and may therefore be neglected in measurements of oscillation.

The Standard Model can accommodate a violation of CP, since the 3 dimensional CKM matrix may contain an imaginary phase. In fact, the existence of a third family of quarks was originally proposed to offer an explanation for the observed CP violation [3]. The CP symmetry may then be violated through the interference between box diagrams or decay diagrams, since the presence of an imaginary phase for a CKM matrix element leads to different transition probabilities for matter and anti-matter mesons.

Contrary to the kaon system the available phase space for B decays is large and the lifetimes of the two CP eigenstates are approximately equal. Recent calculations predict a lifetime difference < 1 % for the B_d system and the lifetime difference in the B_s system is expected to be about 15 % [13]. Therefore, one cannot distinguish experimentally between a short and a long-lived state. Instead the $|\,B^0>$ and $|\,\overline{B^0}>$ states are determined at production time from the flavor of a co-produced b quark.

The third neutral meson system is that of the charmed D^0 meson. D^0-$\overline{D^0}$ mixing in the Standard Model is strongly suppressed. The heaviest quark to which the charmed quarks can couple in the process of $D^0 \rightarrow \overline{D^0}$ is the b quark, but this coupling is not Cabibbo favored. The currently measured limit on the mass difference is $\Delta m_D <$ 200 ns^{-1} (or $< 1.3 \times 10^{-4}$ eV). A summary of different neutral meson systems is given in table A.1.

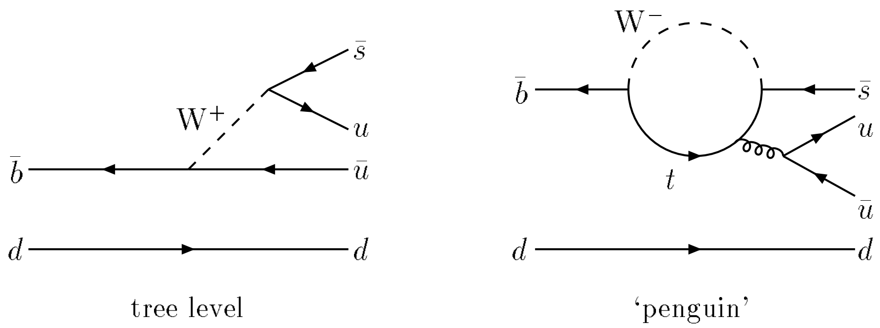

Figure A.1: *A tree level diagram and a higher level diagram for the decay* $B_d^0 \to K^+\pi^-$.

Direct CP violation

The existence of a complex phase in the CKM matrix of the Standard Model predicts that there should also be direct CP violation in the *decay* of mesons, originating from the interference of tree level diagrams with higher level decay diagrams. In kaon decays, this direct CP violation is expected to be three orders of magnitude smaller than the indirect CP violation in the mixing process, and has not been conclusively observed experimentally. The measurement of direct CP violation at the expected rate would be a great success of the Standard Model. Even more interesting, measurements of CP violation deviating from the Standard Model predictions would indicate new physics.

B decays offer an excellent possibility for measuring direct CP violation. One may choose to study a B decay mode of which the branching ratio at tree level is small. The interference with a higher order decay diagram can then be large [40]. Figure A.1 shows an example of a tree level decay diagram and a higher level decay diagram that lead to the same final state. Since the branching ratios are small, the study of such effects requires a large number of B decays to be studied. The interesting prospect of measuring direct CP violation in the B system will be addressed in a new generation of experiments, which are expected to start data-taking around the year 2000. They include asymmetric e^+e^- machines at the $\Upsilon(4S)$ resonance, a fixed target experiment, and high energy pp collisions that produce B mesons abundantly [41].

Appendix B

$\mathrm{B_s}$ branching fractions

Measurements of the $\mathrm{B_s}$ branching fractions have become available only recently, using their production at the Z resonance, and still contain relatively large errors. In contrast, many branching fractions of the $\mathrm{B_u}$ and $\mathrm{B_d}$ mesons have been measured accurately at the $\Upsilon(4S)$ resonance, where no $\mathrm{B_s}$ mesons are produced.

This appendix first discusses the expected $\mathrm{B_s}$ branching fractions and then gives a complete list of measurements of processes that produce $\mathrm{D_s}$ mesons. These results are used in section 3.7 to determine the event sample composition.

Expected branching fractions

The expected branching ratios of some $\mathrm{B_s}$ decays are listed in table B.1 [42–44]. This table also includes the measured branching ratios of subsequent decays of intermediate resonances that would allow a full reconstruction of the decay. The following two examples would result in final states with charged particles only:

$$\begin{array}{lclclcl} \mathrm{BR}(\mathrm{B_s} \to \mathrm{D_s}\pi) & \times & \mathrm{BR}(\mathrm{D_s} \to \phi\pi) & \times & \mathrm{BR}(\phi \to K^+K^-) & \simeq & (4-8)\cdot 10^{-5} \\ \mathrm{BR}(\mathrm{B_s} \to J/\psi\phi) & \times & \mathrm{BR}(J/\psi \to \mu^+\mu^-) & \times & \mathrm{BR}(\phi \to K^+K^-) & \simeq & 4\cdot 10^{-5} \end{array}$$

Since the products of these branching ratios are small, only a small fraction of the decays can be fully reconstructed. This method of full reconstruction has been used succesfully by the LEP experiments and has yielded the first measurement of the $\mathrm{B_s}$ mass [28]. It is also used to reconstruct $\mathrm{B_s}$ decays produced in $p\bar{p}$ collisions at the Tevatron [45].

When more statistics are needed, $\mathrm{B_s}$ meson decays may be tagged by the presence of a $\mathrm{D_s}$ meson. This is an efficient way of tagging $\mathrm{B_s}$ mesons since the majority of the decays proceeds through the spectator diagram, resulting in a $\bar{c}s$ combination (see chapter 1, figure 1.3(a)). This can be a $\mathrm{D_s}$, $\mathrm{D_s^*}$ or a $\mathrm{D_s^{**}}$ meson. The $\mathrm{D_s^*}$ always produces a $\mathrm{D_s}$ meson through the decay $\mathrm{D_s^*} \to \mathrm{D_s}\gamma$. Only a small portion ($\sim 4\%$) of the orbitally excited $\mathrm{D_s^{**}}$ mesons produce a $\mathrm{D_s}$ meson, since most are expected to decay to other D mesons through the decay $\mathrm{D_s^{**}} \to \mathrm{DK}$ [47].

The production of $\mathrm{D^{**}}$ mesons in semileptonic decays of non–strange B mesons is measured to be [46]:

$$\mathrm{BR}(\mathrm{B} \to \mathrm{D^{**}}l\nu)/\mathrm{BR_{sl}} = 17 \pm 4\%$$

BR($B_s \to D_s^- \pi^+$)	$2.8 \cdot 10^{-3}$, $5.5 \cdot 10^{-3}$, $5 \cdot 10^{-3}$	[42], [43], [44]
BR($B_s \to D_s^{*-} \pi^+$)	$2.8 \cdot 10^{-3}$, $4.1 \cdot 10^{-3}$, $2 \cdot 10^{-3}$	[42], [43], [44]
BR($B_s \to J/\psi\phi$)	$(1.4 \pm 0.4) \cdot 10^{-3}$, $1.3 \cdot 10^{-3}$	[42], [43]
BR($D_s \to \phi\pi^+$)	3.5 ± 0.4 %	[6]
BR($D_s \to K^{*0}K$)	3.3 ± 0.5 %	[6]
BR($D_s \to K^+K^-\pi^+$)	4.8 ± 0.7 %	[6]
BR($\phi \to K^+K^-$)	49.1 ± 0.9 %	[6]
BR($K^*(892) \to K^+\pi^-$)	~ 66 %	[6]
BR($J/\psi \to e^+e^-$)	5.99 ± 0.25 %	[6]
BR($J/\psi \to \mu^+\mu^-$)	5.97 ± 0.25 %	[6]

Table B.1: *Predicted branching ratios of B_s decays and the measured branching ratios of subsequent decays of the intermediate resonances that allow a full reconstruction of the decay.*

From this, the branching ratio of the semileptonic decay $B_s \to D_s l^- \nu$ may be derived with the assumption that the production of the D_s^{**} in B_s decays is similar:

$$\mathrm{BR}(B_s \to D_s l\nu X)/\mathrm{BR}_{sl} = 85 \pm 5\%$$

In non-leptonic decays this portion of the decays is expected to be equally large [29]:

$$\mathrm{BR}(B_s \to D_s X) = 86^{+8}_{-13}\%$$

Measurements of D_s production

Table B.2 shows a list of measured branching fractions of processes that produce D_s mesons. These measurements are used to derive the branching ratios $B1$-$B4$ as used in section 3.7 to determine the event sample composition. Most measurements are normalized to the decay rate of $D_s \to \phi\pi$.

The branching ratios for the semi-leptonic decay $B_s \to D_s l\nu$ and the inclusive decay $B_s \to D_s X$ have been measured by the LEP experiments ALEPH, DELPHI and OPAL. The results are combined into the ratios $B1$ and $B3$ respectively. These measurements still have large errors but are consistent with the expected branching fractions.

The production of D_s mesons in B_u or B_d decays has been well measured at the $\Upsilon(4S)$ resonance by the ARGUS and CLEO experiments, and is summarized in $B2$.

To determine the probability that a c quark hadronizes into a D_s meson, measurements of these same experiments are used which are obtained from the $e^+e^- \to q\bar{q}$ continuum spectrum near the $\Upsilon 4(S)$ resonance. Part of the data used here is also recorded at the $\Upsilon 4(S)$ resonance, in which case D_s mesons from B decays need to be excluded. To exclude these D_s mesons from the measurement, the momentum of the

B1a	$2R_{b\bar{b}}$ BR($b \to \mathrm{B_s} \to \mathrm{D_s}X\mu\nu$)			
	$\times$BR($\mathrm{D_s} \to \phi\pi$)	=	$(18 \pm 8) \times 10^{-5}$	DELPHI [48]
B1b	BR($b \to \mathrm{B_s} \to \mathrm{D_s}Xl\nu$)$\times$BR($\mathrm{D_s} \to \phi\pi$)	=	$(3.9 \pm 1.1 \pm 0.8) \times 10^{-4}$	OPAL [49]
B1c	BR($b \to \mathrm{B_s} \to \mathrm{D_s}Xl\nu$)	=	$(0.82 \pm 0.09^{+0.13}_{-0.14}) \times 10^{-2}$	ALEPH [50]
B1	BR($b \to \mathrm{B_s} \to \mathrm{D_s}l$)$\times$BR($\mathrm{D_s} \to \phi\pi$)	=	$(0.031 \pm 0.005) \times 10^{-2}$	combined
B2a	BR($\mathrm{B_{u,d}} \to \mathrm{D_s^+}X$)			
	$\times(3.7 \pm 0.9$ %)/BR($\mathrm{D_s^+} \to \phi\pi^+$)	=	$(11.81 \pm 0.43 \pm 0.94)$ %	CLEO [52]
B2b	BR($\mathrm{B_{u,d}} \to \mathrm{D_s^+}X$)$\times$BR($\mathrm{D_s^+} \to \phi\pi^+$)	=	$(2.92 \pm 0.5) \times 10^{-3}$	ARGUS [53]
B2	BR($\mathrm{B_{u,d}} \to \mathrm{D_s}X$)$\times$BR($\mathrm{D_s} \to \phi\pi$)	=	$(0.366 \pm 0.022) \times 10^{-2}$	combined
B3a	BR($b \to \mathrm{B_s} \to \mathrm{D_s}X$)$\times$BR($\mathrm{D_s} \to \phi\pi$)	=	$(5.9 \pm 1.9 \pm 1.1) \times 10^{-3}$	OPAL [49]
B3b	BR($b \to \mathrm{B_s} \to \mathrm{D_s}X$)$\times$BR($\mathrm{D_s} \to \phi\pi$)	=	$(6.1 \pm 1.9 \pm 1.2) \times 10^{-3}$	DELPHI [54]
B3c	BR($b \to \mathrm{B_s} \to \mathrm{D_s}X$)	=	$0.088 \pm 0.020 \pm 0.020$	ALEPH [55]
B3	BR($b \to \mathrm{B_s} \to \mathrm{D_s}X$)$\times$BR($\mathrm{D_s} \to \phi\pi$)	=	$(0.39 \pm 0.09) \times 10^{-2}$	combined
B4a	$\sigma(e^+e^- \to \mathrm{D_s}X)$$\times$BR($\mathrm{D_s} \to \phi\pi$)	=	$6.5 \pm 0.5 \pm 0.3$ pb	CLEO [56]
B4b	$\sigma(e^+e^- \to \mathrm{D_s}X)$$\times$BR($\mathrm{D_s} \to \phi\pi$)	=	$7.5 \pm 0.8 \pm 0.7$ pb	ARGUS [53]
B4c	$\sigma(e^+e^- \to q\bar{q})$ at $\sqrt{s} = 10.5$ GeV	=	$3 \times (0.85 \pm 0.04)$ nb	ARGUS [46]
B4	BR($c \to \mathrm{D_s}X$)$\times$BR($\mathrm{D_s} \to \phi\pi$)	=	$(3.2 \pm 0.4) \times 10^{-3}$	combined

Table B.2: *Measured branching ratios of decays producing* $\mathrm{D_s}$ *mesons. Branching ratios to leptons are given as the sum of the electron and muon channels divided by two.*

$\mathrm{D_s}$ meson is now required to be large, since for high momenta, the origin can only be an $e^+e^- \to c\bar{c}$ interaction.

The measured quantity is the production rate of $\sigma(e^+e^- \to \mathrm{D_s} \to \phi\pi)$, which is used to determine the branching ratio BR($c \to \mathrm{D_s}$) in the following way:

$$\sigma(e^+e^- \to \mathrm{D_s} \to \phi\pi) = \sigma(e^+e^- \to c\bar{c}) \times 2 \times \mathrm{BR}(c \to \mathrm{D_s}) \times \mathrm{BR}(\mathrm{D_s} \to \phi\pi)$$

In the $q\bar{q}$ continuum, at the energy of the $\Upsilon(4S)$ resonance, the production of charm quarks constitutes 40 % of the total hadronic production:

$$\sigma(e^+e^- \to c\bar{c}) = \frac{4/9}{\sum_i Q_i^2}\,\sigma(e^+e^- \to q\bar{q}) = 40\ \% \times \sigma(e^+e^- \to q\bar{q})$$

where Q_i is the charge of the quark, and the sum is over all quark pairs that may be produced. The result is summarized in the ratio $B4 = \mathrm{BR}(c \to \mathrm{D_s}X) \times \mathrm{BR}(\mathrm{D_s} \to \phi\pi)$.

Bibliography

[1] O. Nachtmann, *"Elementary Particle Physics, Concepts and Phenomena"* Springer-Verlag New York Berlin Heidelberg, 1990.

[2] N. Cabibbo, *"Unitary symmetry and leptonic decays"*, Phys. Rev. Lett. **10** (1963) 531.

[3] M. Kobayashi and T. Maskawa, *"CP-Violation in the Renormalizable Theory of Weak Interaction"*, Prog. Th. Phys.**49** (1973) 652.

[4] L. Wolfenstein, *"Parametrization of the Kobayashi-Maskawa Matrix"*, Phys. Rev. Lett. **51** (1983) 1945.

[5] A. Ali, D. London, *"CP violation and Flavour Mixing in the Standard Model"*, DESY 95-148, Presented as the 6th International Symposium on Heavy Flavour Physics, Pisa, June 6-10 (1995).

[6] The Particle Data Group, *"Review of Particle Properties"*, Phys. Rev. **D50** (1994) 1173.

[7] N. Isgur, M.B. Wise, *"Heavy Quark Symmetry"*, in [8].

[8] *"B decays"*, ed. S. Stone, revised 2nd edition, World Scientific (1994).

[9] T.E. Browder, K. Honscheid, *"B mesons"*, UH 511-816-95, OHSTPY-HEP-E-95-010, to appear in *Progress in Nuclear and Particle Physics* Vol. 35.

[10] I. Bigi *et al.*, *"Non-leptonic decays of beauty hadrons – from phenomenology to theory"*, in [8].

[11] M. Neubert and C.T. Sachradja, *"Spectator Effects in Inclusive Decays of Beauty Hadrons"*, CERN-TH/96-19 (1996), submitted to Nucl. Phys. **B**.

[12] S. Malvezzi, *"Charm lifetime"*, talk presented at the 6th International Symposium on Heavy Flavour Physics, Pisa, June 1995.

[13] R. Aleksan *et al.*, *"Estimation of $\Delta\Gamma$ for the $B_s - \bar{B}_s$ system. Exclusive decays and the parton model."*, Phys. Lett. **B316** (1993) 567.

[14] J. Liu and L. Wolfenstein, *"Superweak contribution to B^0-$\bar{B}^0$ mixing"*, Phys. Lett. **B197** (1987) 536.
L. Wolfenstein, *"Superweak interactions"*, Comments Nucl.Part.Phys. **21** (1994) 275.

[15] ed. G. Altarelli, *"Z physics at LEP 1"*, CERN 89-08, 1989.

[16] LEP design report, vol I, *"The LEP injector chain"*, CERN-LEP/TH/83-29, 1983.

[17] LEP design report, vol II, *"The LEP main ring"*, CERN-LEP/TH/84-01, 1984.

[18] P. Aarnio *et al.*, *"The DELPHI detector at LEP"*, Nucl. Instrum. Methods **A303** (1991) 233.

[19] P. Abreu *et al.*, *"Performance of the DELPHI detector"*, CERN-PPE/95-194, to be published in Nucl. Instrum. Methods .

[20] W. Blum, L. Rolandi, *"Particle Detection with Drift Chambers"*, Springer-Verlag (1993).

[21] C. Bourdarios *et al.*, *"User guide of the HADIDENT/RICH software"*, internal DELPHI manual, 1995.

[22] P. Abreu *et al.*, *"Inclusive measurements of the $K^{\pm}$ and $p/\bar{p}$ production in hadronic Z^0 decays"*, Nucl. Phys. **B 444** (1995) 3.

[23] W. Adam *et al.*, *"Analysis Techniques for the DELPHI Ring Imaging Cherenkov Detector"*, ICHEP contributed paper, Glasgow, 1994.

[24] S. Haider, *"B_s^0 mixing at the Z^0 resonance determined with the RICH technique"*, Ph.D. thesis for the University of Leiden, 1995.

[25] *"DELANA User's Guide"* DELPHI 89-44 PROG 137.

[26] T. Sjöstrand, *"The LUND Monte Carlo program"*, Computer Physics Commun. **39** (1986) 347.
T. Sjöstrand and M. Bengtsson, *"The LUND Monte Carlo program for jet fragmentation and e^+e^- physics: JETSET version 6.3; an update"*, Computer Physics Commun. **43** (1987) 367.

[27] *"DELSIM, Users guide"*, DELPHI 89-15 PROG 130 (1989).
"DELSIM, Reference manual", DELPHI 89-68 PROG 143 (1989).

[28] D. Buskulic *et al.*, The ALEPH collaboration, *"First measurement of the B_s meson mass"*, Phys. Lett. **B311** (1993) 425 + erratum **B316** (1993) 631.
P. Abreu *et al.*, The DELPHI collaboration, *"A measurement of the B_s^0 meson mass"*, Phys. Lett. **B324** (1994) 500.
R. Akers *et al.*, The OPAL collaboration, *"Observation of Exclusive Decays of B mesons at LEP"*, Phys. Lett. **B337** (1994) 196.

[29] M. Suzuki, *"F-meson production rate in bottom-meson decays"*, Phys. Rev. **D31** (1985) 1158.

[30] I. Siccama, *"Prospects for direct measurement of time–integrated B_s mixing"* , NIKHEF 94/21 (1994).

[31] The LEP Collaborations ALEPH, DELPHI, L3, OPAL, and the LEP Electroweak Working Group, *"A Combination of Preliminary LEP Electroweak Measurements and Constraints on the Standard Model"*, CERN-PPE/95-172 (1995).

[32] H. Albrecht *et al.*, The ARGUS collaboration, *"Observation of inclusive D_s production in B meson decay*, Phys. Lett. **B187** (1987) 425.

[33] P. Billoir *et al.*, *"Report on Global Track and Vertex Fitting in the DELPHI detector"* DELPHI 86-99 PROG 61.
DELPHI Analysis Software Task Groups, *"DST Analysis Libraries Writeup"*, internal DELPHI manual.

[34] LEP B lifetimes working group, "Averaging lifetimes for B hadron species at LEP", DELPHI note 94-164 PHYS 467 (1994).

[35] H. Yamamoto *et al.*, The DELCO Collaboration, *"Measurement of D^0 lifetime in e^+e^- annihilation at high energy"*, Phys. Rev. **D32** (1985) 2901.

[36] F. James, *"MINUIT, Function Minimization and Error Analysis"*, Reference manual, CERN Program Library Long Writeup D506.

[37] P. Abreu *et al.*, The DELPHI Collaboration, *"A measurement of B meson production and lifetime using Dl^- events in Z^0 decays"* Z. Phys. **C57** (1993) 181.

[38] J.H. Christenson *et al.*, *"Evidence for the 2π decay of the K_2^0 meson"*, Phys. Rev. Lett. **13** (1964) 138.

[39] A.D. Sakharov, *"Violation of CP invariance, C asymmetry, and baryon asymmetry of the universe"*, JETP lett. **5** (1967) 24.

[40] Y. Nir, H. R. Quinn, *"CP violation in B physics*, Annu. Rev. Nucl. Part. Sci. **42** (1992) 211.

[41] The BELLE collaboration, *"Letter of intent for the study of CP violation in B meson decays"*, KEK report 94-2 (1994).
The BaBar collaboration, *"Letter of intent for the study of CP violation and heavy flavor physics at PEP-II"*, SLAC-443 (1994)
"BABAR Technical Design Report", SLAC-R-95-457 (1995).
The HERA-B collaboration, *"HERA-B, An Experiment to Study CP Violation in the B system Using an Internal Target at the HERA Proton Ring"*, Design Report, DESY-PRC 95/01 (1995).
The LHC-B collaboration, *"LHC-B Letter of Intent"*, *"A dedicated LHC Collider Beauty Experiment for Precision Measurements of CP-Violation"*, CERN/LHCC 95-5 (1995).

[42] A. Deandrea *et al.*, *"Two body non–leptonic decays of B and B_s mesons"*, Phys. Lett. **B318** (1993) 549.

[43] J. Bijnens and F. Hoogeveen, *"Two–body Decays of B_s mesons"*, Phys. Lett. **B283** (1992) 434.

[44] P. Blasi *et al.*, *"Phenomenology of B_s decays"*, Phys. Rev. **D49** (1994) 238.

[45] F. Abe *et al.*, The CDF collaboration, *"Observation of the decay $B_s^0 \to J/\psi\phi$ in $p\bar{p}$ collisions at $\sqrt{s}$ = 1.8 TeV"*, Phys. Rev. Lett. **71** (1993) 1685.
F. Abe *et al.*, The CDF collaboration, *"Measurement of the B_s meson lifetime"*, Phys. Rev. Lett. **74** (1995) 4988.
F. Abe *et al.*, The CDF collaboration, *"Measurement of the lifetime of the* $\mathrm{B_s^0}$ *meson using the exclusive decay mode* $\mathrm{B_s^0} \to J/\psi\phi$*"*, FERMILAB-PUB-96-101-E, to be published in Phys. Rev. Lett. .

[46] A. Nau, *"Measurement of Inclusive Semileptonic B Decays with the ARGUS Detector"*, Ph.D. thesis, DESY 93-005 (1993).

[47] A. Stocchi, *"Mesures de la production et de la duree de vie du meson B_s^0 avec le detecteur DELPHI a LEP"*, Ph.D. thesis, LAL 93-10 (1993).

[48] P. Abreu *et al.*, The DELPHI collaboration, *"Evidence for B_s^0 meson production in Z^0 decays"*, Phys. Lett. **B289** (1992) 199.

[49] P.D. Acton *et al.*, The OPAL collaboration, *"Evidence for the Existence of the Strange b-flavoured Meson B_s^0 in Z^0 Decays"*, Phys. Lett. **B295** (1992) 357.

[50] D. Buskulic *et al.*, The ALEPH collaboration, *"Measurement of the B_s^0 lifetime and production rate with $D_s^- l^+$ combinations in Z decays*, to be published in Phys. Lett. **B**.

[51] D. Buskulic *et al.*, The ALEPH collaboration, *"Study of the B_s^0-$\overline{B_s^0}$ oscillation frequency using $D_s^- l^+$ combinations in Z decays"*, CERN-PPE/96-30, to be published in Phys. Lett. **B**.

[52] T. Bergfeld *et al.*, The CLEO collaboration, *"Measurements of $B \to D_s^+ X$ decays"*, CLEO-CONF 94-9, Glasgow (1994).

[53] H. Albrecht *et al.*, The ARGUS collaboration, *"Production of D_s^+ mesons in B decays and determination of f_{D_s}"*, Z. Phys. **C54** (1992) 1.

[54] P. Abreu *et al.*, The DELPHI collaboration, *"Production Rate and Decay Lifetime Measurements of B_s^0 mesons at LEP energies using D_s and ϕ mesons"*, Z. Phys. **C61** (1994) 407.

[55] D. Buskulic *et al.*, The ALEPH collaboration, *"Measurement of* $\mathrm{D_s^+}$ *meson production in* Z *decays and of the* $\overline{\mathrm{B}}_\mathrm{s}^0$ *lifetime"*, CERN-PPE/95-092, to be published in Z. Phys. **C**.

[56] W.Y. Chen *et al.*, The CLEO collaboration, *"Measurement of D_s decay modes"*, Phys. Lett. **B226** (1989) 192.

[57] D. Bortoletto *et al.*, The CLEO collaboration, *"Charm production in nonresonant e^+e^- annihilations at $\sqrt{s} = 10.55\ GeV$"*, Phys. Rev. **D37** (1988) 1719.

[58] P. Abreu *et al.*, The DELPHI collaboration, *"Mean lifetime of the* $\mathrm{B_s^0}$ *meson"*, CERN-PPE/96-32, to be published in Z. Phys. **C**.

[59] D. Buskulic *et al.*, The ALEPH collaboration, *"Measurement of* $\mathrm{D_s^+}$ *meson production in* Z *decays and of the* $\mathrm{B_s^0}$ *lifetime"*, CERN-PPE/95-092, to be published in Z. Phys. **C**.

[60] D. Buskulic *et al.*. The ALEPH collaboration, *"Measurement of the* $\mathrm{B_s^0}$ *lifetime and production rate with* $\mathrm{D_s^-} l^-$ *combinations in* Z *decays"*, CERN-PPE/95-125, to be published in Phys. Lett. **B**.
D. Buskulic *et al.*, The ALEPH collaboration, *"Study of the* $\mathrm{B_s^0\overline{B}_s^0}$ *oscillation frequency using* $\mathrm{D_s^-} l^-$ *combinations in* Z *decays"* CERN-PPE/96-30, to be published in Phys. Lett. **B**.

[61] R. Akers *et al.*, The OPAL collaboration, *"An improved measurement of the* $\mathrm{B_s}$ *lifetime"*, CERN-PPE/95-020, to be published in Phys. Lett. **B**.

[62] F. Abe *et al.*, The CDF collaboration, *"Measurement of the* $\mathrm{B_s}$ *Meson Lifetime"*, Phys. Rev. Lett. **74** (1995) 4988.

[63] F. Abe *et al.*, The CDF collaboration, *"Measurement of the lifetime of the* $\mathrm{B_s^0}$ *meson using the exclusive decay mode* $\mathrm{B_s^0} \to J/\psi\phi$*"*, FERMILAB-PUB-96-101-E, to be published in Phys. Rev. Lett. .

[64] L. Montanet *et al.*, The Particle Data Group, Phys. Rev. **D50** (1994) 1173, and 1995 off-year partial update for the 1996 edition available on the PDG WWW pages (URL:http://pdg.lbl.gov/).

Summary

This thesis presents a measurement of the B_s lifetime using 3 million hadronic Z decays collected by the DELPHI detector at LEP from 1991 to 1994. The large number of B hadrons produced in hadronic Z decays provides a good opportunity to study the various B meson species. Due to the low relative production rate of B_s mesons compared to the production of B_d and B_u mesons, the properties of the B_s meson are still largely unknown. More accurate decay time measurements are needed to test the predictions of Heavy Quark Effective Theory and to allow a better determination of the CKM matrix element V_{cb}. They are also an important tool for the measurement of B_s-$\overline{B}_s$ oscillations.

Decays of B_s mesons are tagged by the reconstruction of a $D_s^- \rightarrow \phi\pi^-$ or $D_s^- \rightarrow K^{*0}K^-$ decay (including the charge conjugate states of these decay modes). Both decay modes result in a final state with one charged pion and two charged kaons. The RICH plays an important role in the identification of these two kaons. In addition to the charged pion and the charged kaons, a high momentum particle of opposite charge to the D_s meson is added for the B_s reconstruction. This additional particle may be an identified lepton (muon or electron), in which case a pure sample of semi-leptonic B_s decays is obtained. The selected additional particle may also be a charged hadron (pion or kaon), which allows the collection of an additional pure sample of hadronic B_s decays.

The background consists of combinatorial background, as well as two other sources of D_s mesons: $B_{u,d,baryon} \rightarrow D_sX$ decays and $Z \rightarrow c\bar{c} \rightarrow D_sX$ decays. The sample of hadronic B_s decays contains more background than the semi-leptonic sample. This additional background originates mainly from the fragmentation process and is therefore concentrated at small reconstructed decay times of the B_s. At larger decay times, a pure sample of hadronic B_s decays is obtained, with a similar number of events as in the D_s-lepton sample.

The decay time is obtained by reconstructing both the B_s momentum (with a resolution of 10 %) and the B_s flight distance (with a resolution of 200 μm). The result is an accurately reconstructed decay time with a resolution of 0.17 ps. The average B_s decay time is obtained from a maximum likelihood fit, that describes the decay time spectra of the signal from B_s decays and the two other sources of D_s mesons. The combined result for the D_s-lepton and D_s-hadron samples is:

$$\tau(B_s) = 1.54 \pm 0.31 \pm 0.15 \text{ ps}$$

where the first error is statistical and the second is systematic. This result is in agreement with the world average. The world average B_d and B_s lifetimes are currently measured to be equal at the level of 10 %. This is consistent with Heavy Quark Ef-

fective Theory, which predicts that this lifetime difference should be equal within 1 %. Given this accurate theoretical prediction, it is still up to the experiments to improve the accuracy of the lifetime measurements. But since no more data will be taken at the Z resonance at LEP, this improvement will have to wait for future experiments.

It has been shown that the decay time can be accurately reconstructed at LEP using the high precision of the silicon vertex detectors. A measurement of the sofar unobserved $\mathrm{B_s}$ oscillation frequency is, however, still limited by statistics. The increase in statistics which is obtained by adding a pure sample of hadronic $\mathrm{B_s}$ decays to a sample of semi-leptonic decays, as described in this thesis, is therefore of great value to a measurement of the oscillation frequency. With the present statistics and decay time resolution, the LEP experiments can hope, in a combined effort, to be able to measure a value of the oscillation frequency x_s up to an upper limit of 15 (or $\Delta m_s = x_s/\tau(\mathrm{B_s}) \approx 10\ \hbar\mathrm{ps}^{-1}$), which corresponds to the most likely value predicted by the Standard Model. Experimental confirmation of this value would be a first step towards a deeper understanding of CP violation.

Samenvatting

De natuur zoals wij die kennen wordt gekenmerkt door een grote verscheidenheid aan materie. De sterke vooruitgang van de wetenschap in de afgelopen eeuw heeft ons het inzicht gegeven dat al deze materie is opgebouwd uit slechts drie elementaire deeltjes: het electron en twee soorten quarks. Hierbij behoort nog een vierde elementair deeltje: het neutrino. Deze deeltjes worden elementair genoemd, omdat zij op hun beurt niet uit nog kleinere elementen lijken te bestaan. De elementaire-deeltjesfysica zoekt naar en bestudeert deze elementaire bouwstenen en beschrijft de interacties of krachten ertussen. Met behulp van deeltjesversnellers, die onderzoek mogelijk maken bij hoge energie en kleine details, is ontdekt dat er nog twee andere "families" van elk vier elementaire deeltjes bestaan. De meerderheid van deze deeltjes vervalt snel tot deeltjes van de eerste familie.

Dit proefschrift beschrijft een meting van de gemiddelde vervaltijd van het B_s meson, een deeltje dat is opgebouwd uit twee quarks: een b ("beauty" of "bottom") quark en een s ("strange") quark, respectievelijk uit de derde en tweede familie. Deze quarks worden gebonden door de sterke interacties. Het verval van het B_s meson vindt plaats via de zwakke interactie.

De eigenschappen van het B_s meson zijn nog grotendeels onbekend. Voor de meting van deze eigenschappen biedt de LEP deeltjesversneller een goede mogelijkheid. Het is de eerste versneller waarbij het B_s meson direct waargenomen is. LEP is gebouwd bij CERN, het Europese onderzoekscentrum voor elementaire deeltjesfysica, op de grens van Frankrijk en Zwitserland nabij Genève. De versneller bevindt zich in een ondergrondse tunnel met een omtrek van 27 kilometer. In deze tunnel bevindt zich een vacuum pijp, met ongeveer de diameter van een standaard bierflesje, waarin bundels van electronen en positronen in tegengestelde richting tot hoge energie worden versneld. Op vier punten in de ring kruisen de bundels en vinden botsingen plaats. Een botsing tussen een electron en een positron produceert daarbij een Z deeltje dat vrijwel direct vervalt. Om de vervalprodukten te registreren zijn om de vier interactiepunten heen detectoren gebouwd. Eén van deze detectoren is DELPHI. Een Z verval kan op diverse manieren verlopen en vele vervallen dienen bestudeerd te worden om een nauwkeurige beschrijving van de interacties te verkrijgen. De meting in dit proefschrift maakt gebruik van ongeveer 3 miljoen Z vervallen geregistreerd door de DELPHI detector tussen 1991 en 1994.

Een aanzienlijk deel van de Z bosonen vervalt in een paar van b quarks. Op deze manier produceert de LEP versneller een groot aantal B hadronen (deeltjes die een b quark bevatten) waaronder het B_s meson. De produktie van het B_s meson vormt echter slechts 13 % van de totale B hadron produktie. Om het verval van een B_s meson van andere B hadronen te onderscheiden dienen de vervalprodukten geïdentificeerd te worden. Hierin speelt de Ring Imaging Cherenkov detector van DELPHI een belangrijke rol. Omdat bij LEP de B hadronen met grote impuls geproduceerd worden leggen zij gemiddeld een afstand van ongeveer 1.5 mm in de bundelpijp af, alvorens te vervallen. De vervalsafstand kan worden gereconstrueerd met behulp van de silicium Vertex Detector, die de positie van de sporen van de vervalsprodukten met grote precisie vastlegt. Dit maakt de meting van levensduren mogelijk.

Omdat de meerderheid van de B_s mesonen vervalt in een D_s meson is de reconstructie van een D_s meson een effectieve manier om een B_s meson verval te onderscheiden. Voor de reconstructie van het B_s meson wordt verder nog één spoor toegevoegd, dat evenals het D_s meson direct van het B_s vervalpunt afkomstig is. Dit deeltje dient een grote impuls en tegengestelde lading tot het D_s meson te hebben. Helaas kunnen slechts weinig D_s mesonen volledig gereconstrueerd worden waardoor het totale aantal gereconstrueerde B_s vervallen van de orde van 100 is. D_s mesonen worden ook in vervallen van andere B hadronen geproduceerd en in $Z \to c\bar{c}$ interacties. Deze bronnen geven een achtergrond voor het signaal van B_s mesonen.

Wanneer het toegevoegde spoor is geïdentificeerd als een lepton (electron of muon) wordt een verzameling van gebeurtenissen verkregen die bijzonder rijk is aan semi-leptonische B_s vervallen. De analyse in dit proefschrift laat zien dat ook met toegevoegde hadron sporen (pion of kaon) een rijke verzameling verkregen kan worden, hetgeen een vergelijkbaar aantal gereconstrueerde, hadronische vervallen oplevert. Hoewel de hadronische vervallen meer achtergrond bevatten is deze achtergrond voornamelijk geconcentreerd bij kleine vervaltijden en voor een meting van de gemiddelde vervaltijd dus relatief gemakkelijk in rekening te brengen.

De vervaltijd wordt verkregen door zowel de impuls van het B_s meson (met een resolutie van 10 %) als de vervalsafstand (met een resolutie van 200 μm) te reconstrueren. Dit resulteert in een nauwkeurig gereconstrueerde vervaltijd met een resolutie van 0.17 ps. De gemiddelde vervaltijd van de verzamelde gebeurtenissen volgt uit een 'maximum likelihood fit' die zowel het vervaltijdspectrum van de B_s vervallen als dat van de andere twee bronnen van D_s mesonen beschrijft. Het gecombineerde resultaat van de D_s-lepton en D_s-hadron verzamelingen is:

$$\tau(B_s) = 1.54 \pm 0.31 \pm 0.15 \text{ ps}$$

waar de eerste fout statistisch is en de tweede systematisch. Dit resultaat is in overeenstemming met de gemiddelde B_s levensduur zoals die bij andere LEP detectors is gemeten als ook met metingen van de levensduur verricht bij een $p\bar{p}$ botsingsexperiment. De momenteel gemeten gemiddelde B_s en B_d levensduren zijn gelijk binnen de experimentele nauwkeurigheid van 10 %. Dit is consistent met de theoretische verwachting, welke voorspelt dat deze levensduren gelijk zijn tot op 1 %. Gegeven deze nauwkeurige theoretische voorspelling is het dus nog steeds de beurt aan de experimenten om de nauwkeurigheid van de gemeten waarden te verbeteren. Deze verbetering zal moeten wachten op toekomstige experimenten bij hadron versnellers en op een nieuwe generatie van experimenten die zich specifiek zal richten op de produktie van grote aantallen B hadronen.

De meting van de vervaltijd is een essentiële stap op de weg naar een meting van de B_s-$\overline{B}_s$ oscillatie-frequentie, welke tot nog toe niet gemeten is. Van het B_d meson is de oscillatie-frequentie lager en deze is daardoor wel reeds gemeten. Zoals mede in dit proefschrift gedemonstreerd, wordt de vervaltijd door de LEP detectoren zeer nauwkeurig gereconstrueerd. Een meting van de oscillatie-frequentie wordt echter nog steeds beperkt door de relatief geringe hoeveelheid gereconstrueerde B_s vervallen. De toevoeging van de reconstructie van hadronische vervallen tot de semi-leptonische vervallen zoals beschreven in dit proefschrift zal daarom van groot nut zijn in de meting van de B_s oscillatie-frequentie. Met behulp van de verzamelde statistiek en de verkregen resolutie zullen de gecombineerde LEP experimenten in staat zijn een frequentie x_s te meten tot een waarde van 15 (of $\Delta m_s = x_s/\tau(B_s) \simeq 10\ \hbar ps^{-1}$). Deze waarde correspondeert met de meest waarschijnlijke theoretische voorspelling van het Standaard Model.

Acknowledgements

Many friends and colleagues at NIKHEF and at CERN, in Amsterdam and Geneva, have contributed to the work presented in this thesis. Important driving forces behind this work have been promotor Jos Engelen and co-promotor Werner Ruckstuhl. My special thanks to Werner for teaching me the tricks of the trade of physics analysis and of cheese fondue, and for being a mentor in every way. I thank Jan Timmermans for introducing me to DELPHI and for coming to the rescue on many occasions when thunderstorms roared over Geneva and the Inner Detector was adrift.

At NIKHEF, the help of Marcel Merk was essential to this analysis. His coffee bar was always open and my personal record in tennisball soccer has greatly improved since knowing Marcel. I would further like to thank Bert Koene for his continuous support, Dick Holthuizen and Niels Kjaer. Jan van Eldik maintained a sophisticated UNIX script, an essential tool in the data analysis and I thank him for always meeting the requirements of its demanding users. Great help has come from the other students at the DELPHI White Room at CERN through their friendship and support: Nicolo de Groot, Nichol Brummer, Erwin Agasi, Martin 'alle remmen' Los, and I will never forget all the good laughs I shared with Stefan Haider, who also taught me everything I know about the RICH.

It has been a great pleasure to work with Achille Stocchi, Patrick Roudeau, Wilbur Venus, Oleg Kuznetsov, Fabrizio Parodi, Michela Canepa and the rest of the DELPHI B physics team. I also thank the computer groups at CERN and NIKHEF for their support. Many spelling errors in this thesis were corrected thanks to the advice of Paul Kooijman.

Many friends have supported me over the last years of which I would like to mention Alan Tam, Olaf Steinkamp, Esther Merk, Ujjwal Vikas, Richard van den Bergh and Jiri Hoogland. I want to thank Magali for her love and support. My sincere thanks to Hoite Tolsma for helping me to survive harsh winter weekends when food was scarce at NIKHEF. Marc, thanks for keeping me sharp with surprise attacks.

I thank PoiLing for her love and encouragement, my father Jan-Geert, my mother Louise, Katjoesja, Sandhya and Clint. Finally, I would like to thank my gang of six cats: Speedy, Jokey, Kareltje, Gini, Ziggi and big boss Faak-Tjai, for being there and always making me laugh.